NEUTRON POLARIZATION FROM THE $D(d,n)^3He$ REACTION

AND

ANALYZING POWERS OF $T(\vec{p},d)D$ AND $T(p,p)T$

by

Robert Allen Hardekopf

Department of Physics
Duke University

Date : _____

Approved :

_____
Richard L. Walter, Supervisor

_____

_____

_____

_____

A dissertation submitted in partial fulfillment of
the requirements for the degree of Doctor of
Philosophy in the Department of Physics
in the Graduate School of Arts and
Sciences of Duke University

1971

ABSTRACT

(Physics)

NEUTRON POLARIZATION FROM THE $D(d,n)^3He$ REACTION

AND

ANALYZING POWERS OF $T(p,d)D$ AND $T(p,p)T$

by

Robert Allen Hardekopf

Department of Physics
Duke University

Date : _____

Approved :

_____

Richard L. Walter, Supervisor

_____

_____

_____

_____

An abstract of a dissertation submitted in partial fulfillment of the requirements for the degree of Doctor of Philosophy in the Department of Physics in the Graduate School of Arts and Sciences of Duke University

1971

Abstract

NEUTRON POLARIZATION FROM THE $D(d,n)^3He$ REACTION AND ANALYZING POWERS OF $T(p,d)D$ AND $T(p,p)T$

by

Robert Allen Hardekopf

The neutron polarization from the $D(d,n)^3He$ reaction has been measured at 45 degrees c. m. for incident deuteron energies between 16 and 22 MeV. In addition, a polarization angular distribution was measured at 18 MeV. The results show that the 45 degree c. m. polarization remains above 0.35 in this energy range, but the peak polarization has shifted to near 40 degrees c. m. The usefulness of $D(d,n)^3He$ as a source of 16 to 22 MeV polarized neutrons is discussed.

Accurate angular distributions of the analyzing power in the $T(p,d)D$ reaction were measured at eight energies from 6.7 to 14.7 MeV. By reciprocity, these distributions are the same as the proton polarizations of the $D(d,p)T$ reaction from 2.0 to 14.0 MeV. Comparisons are made with the polarizations from the mirror reaction $D(d,n)^3He$, and good agreement is found when the reactions are compared at the same exit channel energies. The implications of this are discussed in the light of other recent comparisons which suggest that differences in these mirror reactions may be a violation of charge inde-

pendence of nuclear forces.

Very accurate polarizations in T(p,p)T elastic scattering were obtained in conjunction with the T(p,d)D measurements. Single energy complex phase shift parameterizations were made at five energies from 9.4 to 14.7 MeV. No resonance structure was seen for any of the phase shifts in this energy range.

ACKNOWLEDGMENTS

I wish to express my appreciation to Professor R. L. Walter for his continuing interest and support during the course of these investigations. I would like to thank Professor T. B. Clegg for his indispensable aid with the polarized ion source and the polarized beam measurements and for his advice on the analysis. Professor J. M. Joyce assisted with the neutron polarization measurements, and for this I am grateful.

Appreciation is due Dr. G. A. Bissinger for his assistance with the polarized ion source and Mr. George Spalek for his work in the design and installation of the neutron polarimeter. Discussions with Dr. Thomas Stammbach on analysis of neutron polarization data and with Dr. John Taylor on computer programs and hardware are gratefully acknowledged.

I would especially like to thank Mr. T. C. Rhea and Mr. P. W. Lisowski for helping to maintain the polarized ion source and the neutron polarimeter and for the many hours they spent taking data. I am indebted to Dr. F. O. Purser for his assistance with the cyclotron and Professor N. R. Roberson for the design of the computer interface.

Appreciation is due Professor W. J. Thompson and Professor R. Y. Cusson for fruitful discussions on the interpretation of the data. I am grateful to Dr. T. R. Donoghue for his advice on the tritium target.

I would like to express appreciation to my parents for their many years of encouragement. Finally, a very special thanks to my wife Priscilla for her patience and understanding, and to Catherine, David, and Kenneth, who missed the presence of their father on many evenings and weekends.

This work was supported in part by the U. S. Atomic Energy Commission.

R. A. H.

CONTENTS

ABSTRACT iii

ACKNOWLEDGMENTS v

LIST OF FIGURES ix

LIST OF TABLES xi

I. INTRODUCTION 2

PART I. NEUTRON POLARIZATION FROM THE $D(d,n)^3He$ REACTION

II. EXPERIMENTAL PROCEDURE 6

A. Neutron Polarimeter, 6
B. Electronics, 8
C. Data Acquisition, 12

III. REDUCTION OF DATA 14

A. Analysis of Spectra, 14
B. Analyzing Power of Polarimeter, 18
C. Error Analysis, 19

IV. RESULTS AND CONCLUSIONS 22

PART II. ANALYZING POWERS OF T(p,d)D AND T(p,p)T

V. EXPERIMENTAL PROCEDURE 31

A. Lamb Shift Polarized Ion Source, 31
B. Scattering Chamber, Target, and Polarization Monitor, 35

C. Electronics, 37
D. Data Acquisition and Reduction, 39
E. Error Analysis, 45

VI. T(p,d)D RESULTS AND ANALYSIS 50

A. Polarization - Asymmetry Relation, 50
B. Results and Fits to Data, 51
C. Comparison with D(d,n)^{3}He Data and Conclusion, 61

VII. T(p,p)T RESULTS AND ANALYSIS 70

A. Results and Comparison to Other Data, 70
B. Theory of Spin 1/2 on Spin 1/2 Scattering, 76
C. Phase Shift Analysis, 83

APPENDIXES 94

A. Programs for Data Acquisition and Analysis in Polarization Experiments, 95
B. The Computer Code CPHASE, 107

LIST OF REFERENCES 110

LIST OF FIGURES

1. Schematic Diagram of Neutron Polarimeter 7

2. Block Diagram of Neutron Polarization Electronics 9

3. Typical Summed Spectrum and Fit for $D(d,n)^3He$ 17

4. Polarization Distribution and Fit for $D(d,n)^3He$ at 18 MeV 24

5. Polarization Near 45 Degrees c.m. for $D(d,n)^3He$ 26

6. Sources of Polarized Neutrons 28

7. Schematic Diagram of Polarized Ion Source 33

8. Schematic Diagram of Scattering Chamber and Polarization Monitor 36

9. Block Diagram of Mass Identification Electronics 38

10. Typical Mass Spectrum for T + p 40

11. T(p,d)D Analyzing Power Data and Fits 52

12. Comparisons of T(p,d)D and D(d,p)T Data 56

13. Comparisons of D(d,p)T and $D(d,n)^3He$ Polarizations at Same Bombarding Energies 63

14. Comparison of Associated Legendre Coefficients for D(d,p)T and $D(d,n)^3He$ 65

15. Comparisons of D(d,p)T and $D(d,n)^3He$ Polarizations at Same Exit Channel Energies 66

16. Comparisons of T(p,p)T and $^{3}He(n,n)^{3}He$ Polarization Data 68

17. T(p,p)T Analyzing Power Data and Fits 71

18. Comparisons with Other T(p,p)T Data Near 10.7 and 13.4 MeV 77

19. T(p,p)T Phase Shifts; S and P Waves 90

20. T(p,p)T Phase Shifts; D Waves and Mixing Parameters 91

21. Flow Diagram of Control Subroutine for Neutron Polarization Data Acquisition 103

LIST OF TABLES

1. Polarization Data for $D(d,n)^3He$ 23

2. Analyzing Power Data for T(p,d)D 53

3. Associated Legendre Coefficients for D(d,p)T 60

4. Analyzing Power Data for T(p,p)T 72

5. Starting Phase Shift Sets for T(p,p)T Analysis 86

6. Phase Shifts for T(p,p)T 88

NEUTRON POLARIZATION FROM THE $D(d,n)^3He$ REACTION

AND

ANALYZING POWERS OF $T(p,d)D$ AND $T(p,p)T$

Chapter I

INTRODUCTION

The information about nuclear forces needed to solve a problem in nuclear physics depends on the energy of the system under investigation and on the number of nucleons in that system. The study of few nucleon systems has played an important role in endeavors to understand the nuclear interaction. Precise nucleon-nucleon scattering data is one of the primary sources of information about nuclear forces. However, there are some features of the nuclear interaction that require a study of more than a two nucleon system. Systems composed of many particles, in general, cannot be treated exactly, and one is bound to introduce some model. Nuclear spectroscopy and nuclear reactions involving heavy nuclei therefore display only the effective nuclear interaction. Consequently, simple nuclear systems appear as more appropriate objects to test the basic principles of nuclear physics. The study of systems composed of only a few nucleons thus gains a particularly important place in nuclear physics.

Advances in experimental techniques have permitted the acquisition of more extensive and more accurate data to aid theoretical studies of light nuclei. The use of polarized beams and polarized targets has given added impetus to polarization measurements, allowing more thorough investigations of spin-dependent effects in the nuclear interaction.

The experimental work reported here was undertaken with three objectives in mind. First, to obtain accurate polarization measurements for reactions in the mass-4 system to aid theoretical studies of light nuclei. Second, to investigate whether differences previously reported for the polarizations in the mirror reactions $D(d,n)^3He$ and $D(d,p)T$ are real. Third, to determine the usefulness of the $D(d,n)^3He$ reaction as a source of medium energy polarized neutrons.

Part I describes the measurement of the neutron polarization from the $D(d,n)^3He$ reaction from 16 to 22 MeV. The polarizations obtained at 45 degrees in the center-of-mass are considerably higher than previous measurements in this energy range (Alekseev et al., 1964) and show that this reaction is a good source of polarized neutrons here. A polarization angular distribution at 18 MeV shows little change in shape from lower energy data (Spalek et al., 1970) but indicates that the peak in the polarization is shifting slightly to smaller angles.

Part II describes analyzing power measurements obtained by bombarding tritium with a polarized proton beam at eight energies from 6.7 to 14.7 MeV. The analyzing powers in the T(p,d)D reaction are equated to the proton polarizations in the D(d,p)T reaction by time reversal invariance. This data can therefore be used to compare the polarizations in the mirror reactions $D(d,n)^3He$ and $D(d,p)T$. On the basis of charge independence of nuclear forces, one might expect that these polarizations should be the same after corrections are made for Coulomb effects. Previous comparisons (Barschall, 1966; Porter and Haeberli, 1967; Spalek et al., 1970), however, have shown the proton polarizations to be larger than the neutron polarizations over a broad energy range. These comparisons have been made for the same deuteron bombarding energies in the two reactions.

The present data show that the difference between the polarizations is real when compared at the same entrance channel energies, but there is close agreement when compared at the same exit channel energies. The implications of this are discussed in Chapter VI.

Accurate analyzing powers in the elastic scattering T(p,p)T are also obtained, and single energy phase shift parameterizations are presented. Dodder (1971) at Los Alamos is making multi-channel phase shift fits to these and other mass-4 system data in an attempt to decrease the ambiguity of single channel analyses.

The appendixes contain brief descriptions of data acquisition and analysis programs written for both neutron and charged particle polarization experiments. There is also a description of the complex phase shift search program used for the T(p,p)T analysis.

PART I

NEUTRON POLARIZATION FROM THE $D(d,n)^3He$ REACTION

Chapter II

EXPERIMENTAL PROCEDURE

A. Neutron Polarimeter

The neutron polarimeter used in the $D(d,n)^3He$ measurements has been described previously (Meier, 1969; Taylor, 1971). A schematic of the setup is shown in Figure 1. Deuterons from the Cyclo-Graaff bombarded a gas target containing 5 atm deuterium gas. The beam entered and exited the target through 6.3 μm foils[1] and was stopped 7 cm downstream in a tantalum end cap. Neutrons from the reaction were incident on a helium scatterer after passing through a high current solenoid whose axial magnetic field precessed their spins clockwise or counterclockwise. The helium was contained at 130 atm in a high pressure scintillation cell which permitted measurement of the helium recoil energies. The construction and preparation of the helium cell is described by Morgan and Walter (1968) and by Taylor (1971). The neutrons which scattered from the helium through an analyzing angle θ_2 were detected by two $5 \times 7.5 \times 15\ cm^3$ plastic scintillators, placed at a distance of 19 cm in the vertical scattering plane. A long tapered collimator in the solenoid and a flight path of 110 cm gave an angular resolution of about 2 degrees. The energy spread in

[1] The foils were of a high tensile strength cobalt alloy (HAVAR) sold by Hamilton Watch Company, Lancaster, Pennsylvania.

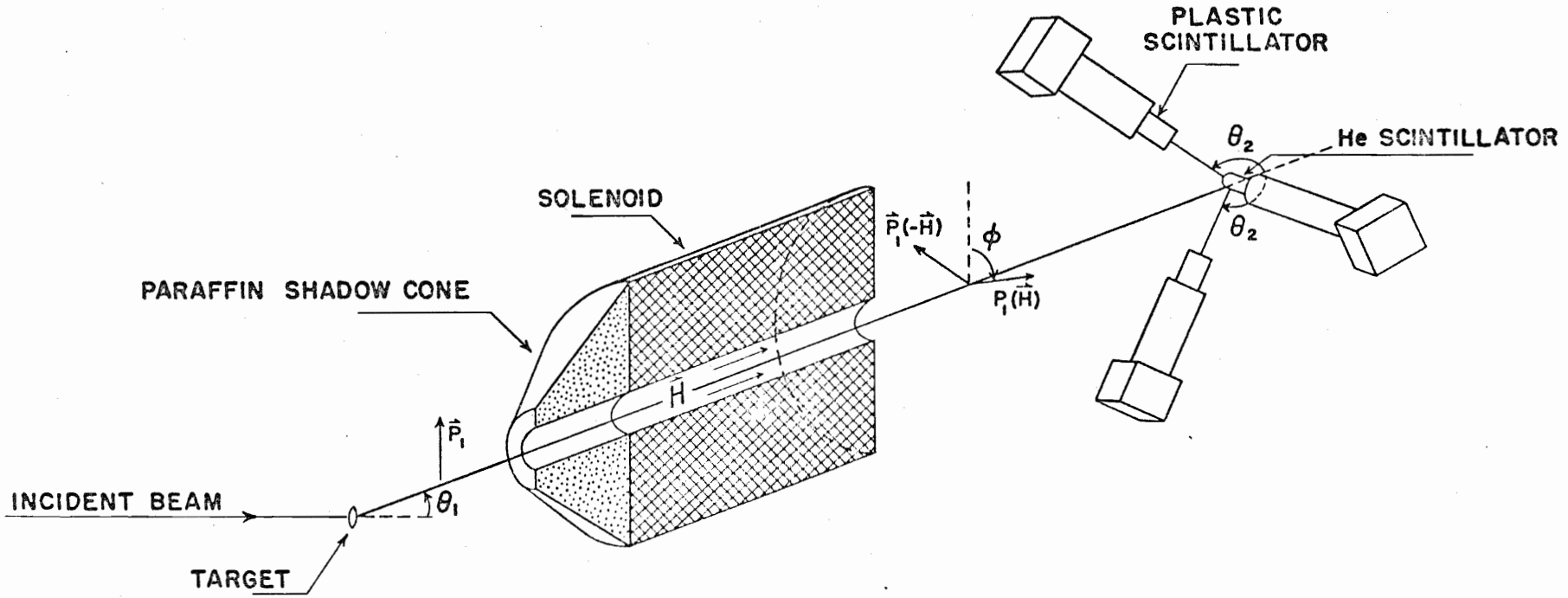

Figure 1. Schematic Diagram of Neutron Polarimeter

the deuterium target was about 120 keV.

RCA 6810 photomultiplier tubes viewed each of the side detectors and the helium cell through tapered light pipes. The phototubes were shielded both electrostatically and magnetically as described by Purser (1966). The magnetic shields reduced the effects of the solenoid fringe field to a negligible amount, thus preventing false asymmetries due to reversing of the solenoid field.

B. Electronics

A simplified block diagram of the neutron polarization electronics used is shown in Figure 2. Fast signals from the phototube anodes triggered fast discriminators to produce logic signals which were fed to a strobed coincidence unit. Accidental coincidences were obtained simultaneously by inserting 80 ns delays between the UP and DOWN discriminators and the strobed coincidence. Eighty ns was chosen because this is the period of the deuteron beam bursts from the cyclotron (rf = 12.5 MHz). This assured that the time correlation between random coincidences and the beam bursts would be properly accounted for. A coincidence between either of the direct signals or the delayed signals with the helium strobe produced an output at the appropriate terminal of the coincidence unit. These signals, representing "true" or "accidental" coincidences,were sent through logic shapers (not shown) to the router.

The output of the helium discriminator was also used as the start signal for a time-to-amplitude converter (TAC). The stop signal came from a zero-crossing discriminator on the cyclotron rf. A single channel analyzer (SCA) was used to set a window on the peak

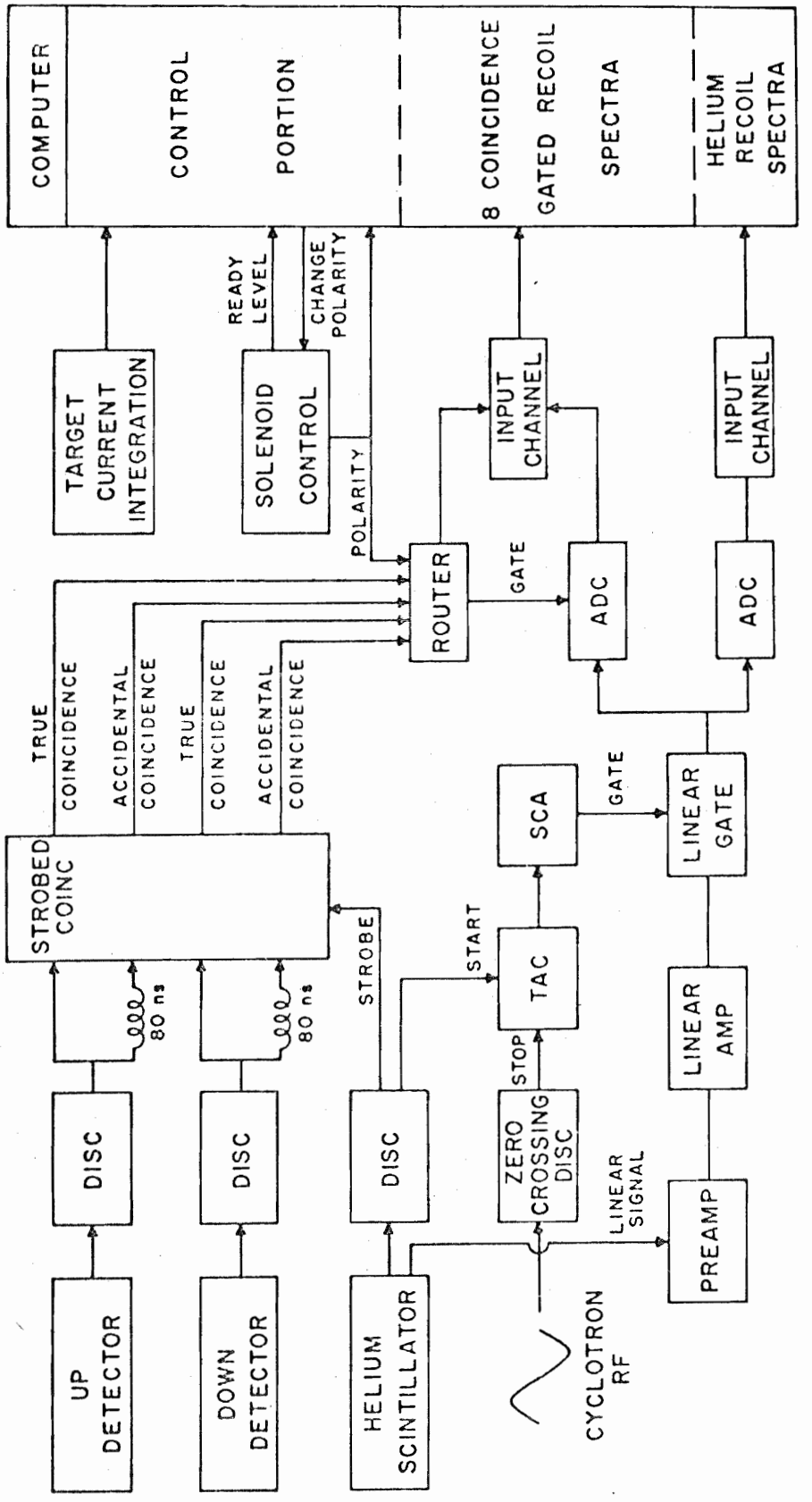

Figure 2. Block Diagram of Neutron Polarization Electronics

corresponding to direct neutrons from the $D(d,n)^3He$ reaction in the time spectrum. This output was then used to open a linear gate. The slow signal from the helium cell phototube was suitably amplified and used as the linear input to the linear gate. The linear signals sent to the analog-to-digital converter (ADC) were thus limited to those that had the correct time correlation with the beam bursts. The routing pulses from the true and accidental coincidences and a signal denoting solenoid polarity were used to store the helium pulse height signal from the ADC in one of eight 128 channel spectra, corresponding to its combination of side detector, spin precession, and true or accidental coincidence.

The resolving time of the cyclotron time-of-flight setup described above was not sufficient to discriminate completely against events other than the direct neutrons desired. This was due to several factors: First, the flight path between target and helium cell was only 110 cm. Secondly, the beam intensity required from the cyclotron necessitated using large extraction slits. Several turns were probably being extracted, resulting in a larger energy (and therefore time) resolution than normal. Nevertheless, many of the neutrons resulting from the D(d,np)D breakup reaction were gated out, as well as a significant amount of low energy background events. This substantially improved both the total recoil and the coincidence gated recoil spectra.

The simultaneous accumulation of accidental coincidences along with the true coincidences enabled accurate accidental coincidence background subtraction, but care had to be taken to insure that the coincidence "windows" had the same width. These windows were set as follows: The output of the helium discriminator was used as the start signal to a TAC with a 50 ns range. The stop signal was from each of the side detector discriminators alternately. The resulting time spectrum was accumulated in a 100 channel

block of a multichannel analyzer (MCA). It was necessary at these high deuteron energies to gate the MCA with a single channel analyzer output set about halfway down from the recoil edge on the helium linear signal. This eliminated most of the accidental counts in the TAC spectrum and allowed the neutron peak to stand out above the background. A second 100 channel block of the MCA was then used to store the TAC spectrum, but this time gated with the true coincidence output from the strobed coincidence unit. The resulting "window" in the TAC spectrum was made to coincide with the neutron peak from the previous spectrum by adjusting nanosecond delay cables between the discriminator and coincidence unit. The width of this window was adjusted by changing the width of the discriminator output going to the coincidence unit. A typical width (or resolving time) used in this experiment was 10 ns. The background window was checked in a similar manner by gating with the accidental coincidence output from the coincidence unit. In this case, no attempt was made to make the window coincide with the neutron peak, but the width was noted. If this window width were different than the foreground width (due possibly to loss of amplitude of the discriminator signal in the delay cable) a correction was made in the off-line analysis of the spectra. For some of the later runs, another discriminator was placed after the delay cable to provide a separate width adjustment for this window. This eliminated the need for further corrections to the data. Both the UP and the DOWN detector coincidence windows were set in this manner, and they were checked whenever the neutron energy changed substantially.

C. Data Acquisition

The principles underlying neutron polarization measurements are similar to those discussed in Chapter V with regard to charged particle measurements with a polarized ion source. Since polarized neutrons cannot be produced in an ion source and accelerated, however, a traditional double scattering experiment is required. The polarization produced in the first scattering (or reaction) is being measured, and the analyzing power in the second scattering from ^{4}He can be calculated from known phase shifts. Care must be taken to avoid false asymmetries due to neutron backgrounds and the proximity of the spin precession solenoid to the detectors. An excellent discussion of these principles is given by Meier (1969) and will not be reproduced here.

The program NPOL was written by the author for data acquisition and control in neutron polarization experiments. The coincidence data were sent to the computer on a high interrupt level while the recoil spectrum was accumulated simultaneously on a lower interrupt level. In addition to these spectra, a SUM spectrum was continuously calculated and displayed. This spectrum is the sum of the four true coincidence spectra (UP forward, DOWN forward, UP reverse, DOWN reverse) minus the corresponding four accidental coincidence spectra. Asymmetries were calculated between light-penned points in the SUM spectrum and displayed on the oscilloscope to provide constant monitoring of the data. The control section sequenced the acquisition for a data point through short sequences of equal accumulated charge, reversing the solenoid polarity approximately every fifteen minutes. At the end of each sequence, scalers recording the charge accumulated and the number of coincidence and background counts from each detector were typed out. At the end of each group (forward, reverse, reverse, forward sequences), the accumulated data

were dumped on magnetic tape and the asymmetries typed out. The number of FRRF groups accumulated for each data point is a typewriter input. Most of the data reported here were obtained near the cross section minimum in the $D(d,n)^3He$ reaction, and six to eight groups were required to obtain the desired statistics. At the end of a run, the spectra were transferred to an analysis block for further analysis while accumulating the next data point. Operations performed included output of the spectra on the line printer, line printer plots, and channel-by-channel asymmetries. This early analysis was useful in spotting any problems and in determining the course of the experiment. In addition, runs were taken for each data point with the deuterium gas cell evacuated to determine the foil background. The analysis block was used to subtract these background spectra from the $D(d,n)^3He$ neutron spectra. A more detailed description of program NPOL may be found in Appendix A.

Chapter III

REDUCTION OF DATA

A. Analysis of Spectra

Preliminary analysis was done in a manner similar to that described in the last section. The program NPOL-α was used off-line to examine the data and make corrections to the accidental backgrounds if required by a difference in coincidence windows. The gas-out runs, which were usually taken for one-half the accumulated charge as the gas-in runs, were smoothed before subtracting the necessary number of times. In addition to the on-line analysis, channel-by-channel asymmetry plots were made to assist in the analysis.

Asymmetry calculations are derived in Chapter V with particular application to polarized ion source measurements. The only difference in the equations derived there and those used in the neutron polarization experiment is one of nomeclature. Here, the detectors are UP and DOWN and the different spin precessions are clockwise (Forward polarity) and counterclockwise (Reverse polarity). The asymmetry is given in the present notation by

$$\epsilon = \frac{r-1}{r+1} \qquad (1)$$

where

$$r = \sqrt{\frac{N_U(F) \times N_D(R)}{N_D(F) \times N_U(R)}} \qquad (2)$$

In this equation, $N_U(F)$ stands for the net number of counts in coincidence with the UP detector with the solenoid having forward polarity, etc. The net number of counts is obtained by summing the appropriate foreground spectrum between channels corresponding to light-penned points in the SUM spectrum and subtracting the accidental background between the same channels. A significant difference with the charged particle spectra should be noted, however, in the handling of the background counts. In principle this background, which is due to random coincidences, should be unpolarized. Since the number of background counts in the region of interest is usually small and thus exhibits poor statistics, less error is introduced into the asymmetry calculation by constraining the background to be unpolarized. This is accomplished by averaging the UP(F) and UP(R) backgrounds, then subtracting this average from both the UP(F) and UP(R) foregrounds, and similarly for the DOWN spectra. With this constraint, the effect of the background is only to dilute the asymmetry value. The error calculation is changed slightly from Chapter V, the result being

$$\Delta\epsilon = \frac{r}{(r+1)^2}\sqrt{\sum_{i=1}^{4} \frac{S_i + B_i/2}{(S_i - B_i)^2}} \qquad (3)$$

Although the neutron peak from the $D(d,n)^3He$ reaction was very clean, a small non-subtracting background remained after all the above corrections were made. Inspection showed this background to be unpolarized as might be expected from gamma-ray and room

scattered neutron coincidences. To properly subtract this background, the data were analyzed using the search program ASP of Taylor (1971). The final spectra (with smoothed gas-out spectra subtracted) were combined into a LEFT spectrum and a RIGHT spectrum in NPOL - α according to

$$N_{left}(I) = 2\sqrt{N_{UF}(I) \times N_{DR}(I)}$$
$$N_{right}(I) = 2\sqrt{N_{UR}(I) \times N_{DF}(I)} \qquad (4)$$

where I runs from 1 to 128. $N_{uf}(I)$ stands for the net number of UP-forward counts in channel I, etc. The net number of counts is obtained in the same manner as previously described for the sums, i. e., the accidental backgrounds are averaged before subtracting. Also generated was a spectrum containing the information on backgrounds (both accidental and gas-out) which were used to correct the original spectra. This last spectrum was used to provide the correct weighting factors for the search program and to retain the background information in the error calculation. A discussion of the fitting of neutron spectra with Gaussian line shapes and a description of the program ASP is given by Taylor (1971). A typical SUM spectrum from the data reported here is shown in Figure 3. The line through the points is from the fit to the data of a Gaussian peak on a linear background.

Either a linear or a quadratic background was used under the Gaussian in all cases, and its effect was studied carefully. Limits could be assigned by examining the channel-by-channel asymmetries and by optimizing the chi-square values from the search. Within reasonable variations, the backgrounds changed the calculated asymmetries by less than the statistical error of the data point. No additional error was assigned for this small

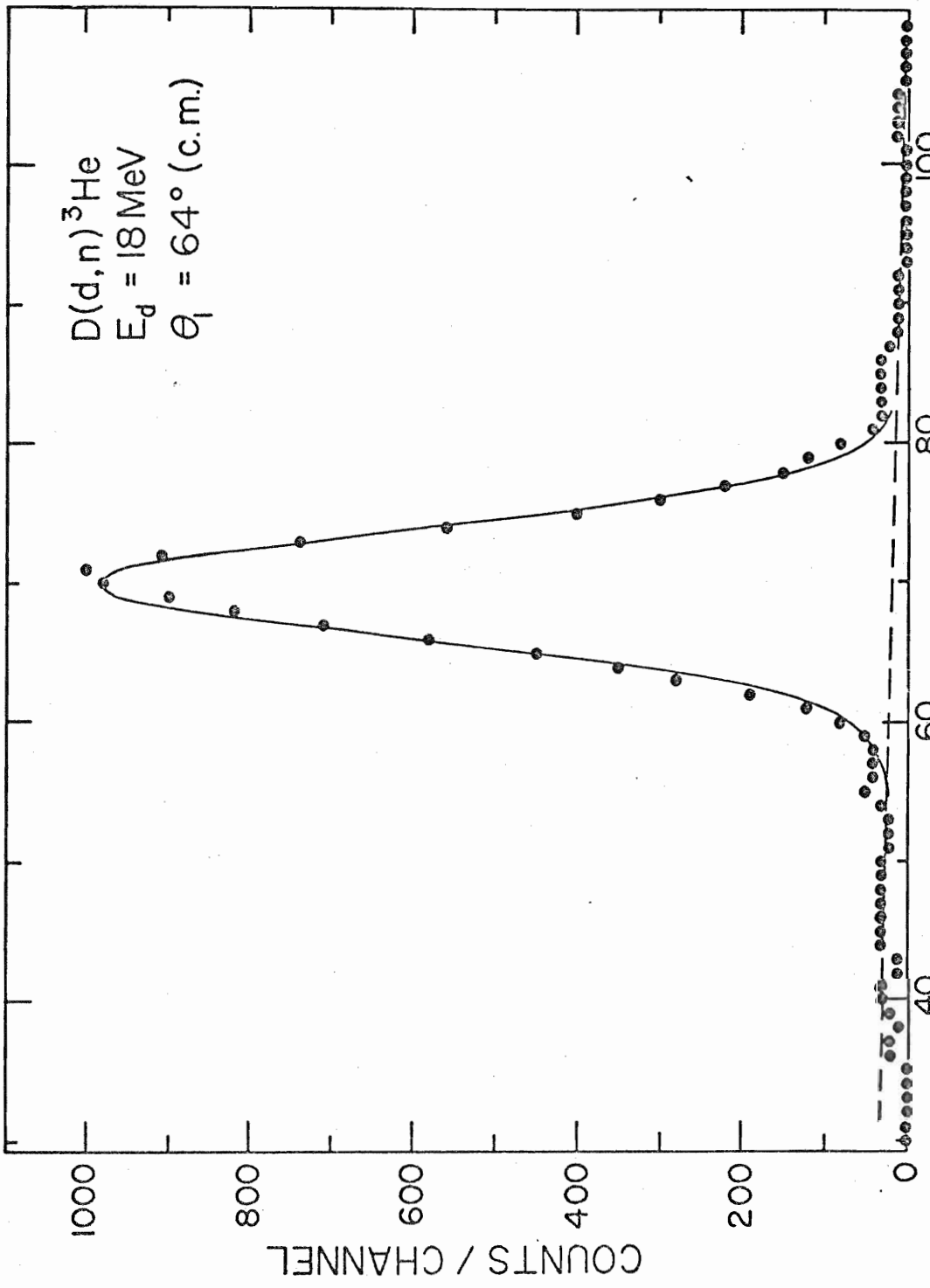

Figure 3. Typical Summed Spectrum and Fit for $D(d,n)^3He$

uncertainty. Several consistency checks were made between asymmetries calculated in NPOL (corrected for background) and ASP with good agreement. A test case was also run with the more powerful fitting program, PROMETHEUS, of Thomason (1969), and good agreement was obtained with the ASP results.

B. Analyzing Power of Polarimeter

For the neutron energies encountered in this experiment, the solenoid was not able to precess the spins through 90 degrees. For this case, the polarization P_1 produced in the reaction is related to the asymmetry by

$$\epsilon = P_1 \bar{P}_2 \sin\varphi \tag{5}$$

The angle through which P_1 is precessed φ is calculable and is proportional to the integrated field in the solenoid and the neutron time-of-flight through it. The calibration of the spin precession solenoid is discussed in the next section. The average analyzing power $\bar{P}_2$ was calculated by averaging the neutron-^{4}He analyzing power over the experimental geometry using the Monte Carlo scattering program MOCCASINS of Sawers (1966) and Stammbach (1970). In addition to the geometry correction, the calculations include effects due to neutron absorption in all three detectors, energy dependence of the side detector efficiencies, and double scattering effects. The side detectors were placed at a mean distance of 19 cm from the helium cell, subtending an angle of about 15 degrees in the θ_2 direction. For most of the measurements, the mean angle θ_2 was chosen to be 115 degrees in the laboratory system. The phase shifts of Hoop and Barschall (1966) and Stammbach

and Walter (1971) were used for the n-^{4}He analyzing power calculations. The difference in the predictions of these two phase shift sets is discussed in the next section.

C. Error Analysis

Statistical error. --The statistical errors were generated in ASP as follows: A statistical weight was assigned to each channel included in the search by summing the number of counts in the channel, the background counts (including gas-out background) which had been subtracted in that channel, and background counts from the linear or quadratic background. The search routine for the left and right Gaussian amplitudes then generated an amplitude error from the inverted matrix used to solve the simultaneous equations. This error included the statistical error from the weights assigned the channels of interest plus an error related to the quality of the fit (the usual chi-square value). For chi-square values near 1.0, which was the case for most of the D(d,n)^{3}He data reported here, this reduces to purely statistical error. Comparison of the errors generated in ASP with those calculated by NPOL (Equation 3) showed the ASP errors to be slightly larger. This is to be expected, since ASP accounts for subtraction of gas-out runs and linear background under the peak.

The uncertainty in the calculation of $\overline{P}_2$ by the Monte Carlo code may be made as small as desired consistent with the computer time available. For this analysis, 4000 passes were used for the single scattering (geometry) correction and 1000 passes for double scattering. For the geometry corrections of approximately -0.090, this gives a statistical error of ±0.0016. The double scattering corrections were very small (on the order of

-0.004) for gaseous helium at these high neutron energies, and the error in their calculation is less than ±0.0004. Both of these errors are much smaller than either the statistical error in the asymmetry or the uncertainty in the n-^{4}He phase shifts, and they were therefore neglected in the final error.

Spin precession angle. --The uncertainty in the spin precession angle introduces a negligible error in the correction for precession angles near 90 degrees. For a precession of 80 degrees, for example, a one degree uncertainty gives an error in the polarization of only 0.3 per cent. At a neutron energy of 21.1 MeV, however, the spin precession was only about 56 degrees. An uncertainty of one degree in the precession angle here gives an error of 1.2 per cent in the polarization. Thus it was necessary to calibrate the solenoid rather precisely. This was done in two ways. First, the magnetic field was measured over the length of the solenoid with an accurately calibrated Hall probe. This was done for solenoid currents of 100, 200, and 300 amps, and no saturation effects were observed. The spin precession was calculated using the relativistically correct formula

$$\varphi = \frac{2\mu_n}{\beta\gamma c\hbar} \int_{z_{min}}^{z_{max}} B\, dz \qquad (6)$$

For the maximum current of 300 amps, the integrated B field measured will rotate the spin of an 8.3 MeV neutron by 90 degrees. Second, a solenoid calibration was done using low energy polarized neutrons. Three MeV neutrons from the $^{12}C(d,n)^{13}N$ reaction had their spins precessed through angles from zero to about 180 degrees by increasing the current in the solenoid in steps. The asymmetries were measured in the manner described earlier. The resulting asymmetry versus solenoid current was fitted with a sine curve, and the period of the curve was used to calculate the solenoid current for 90 degree spin precession at any

energy. The neutron energy for 90 degree precession at 300 amps was calculated from this to be 8.65 MeV. Since all of the neutron energies encountered in this experiment were greater than 10 MeV, the maximum current of 300 amps was used and φ was calculated from Equation (6). The difference between the two calibrations gives an uncertainty in the spin precession factor of only 0.9 per cent at 14 MeV and 1.4 per cent at 20 MeV. The calibration based on the $^{12}C(d,n)^{13}N$ neutron precession was used for the values reported here.

Neutron-^{4}He analyzing power. --The uncertainty in the n-^{4}He analyzing power at various energies is graphically displayed by Rhea et al. (1970). This paper shows that the analyzing powers on the back angle peak calculated from different sets of phase shifts at 18 MeV differ by as much as 0.10. Both the Hoop and Barschall (1966) phase shifts and the Stammbach and Walter (1971) phase shifts were used to calculate $\overline{P}_2$ for most of the data reported here. Since the H-B phases predict the highest values for P_2 at the back angle peak and the S-W phases predict the lowest, the differences in these predictions may be taken as the uncertainty in the n-^{4}He analyzing power in this energy range. This uncertainty was not included in the error reported for the data, since additional n-^{4}He polarization data and future analyses should resolve the question.

Chapter IV

RESULTS AND CONCLUSIONS

The results of the $D(d,n)^3He$ polarization measurements from 16 to 22 MeV are tabulated in Table 1. The energies listed are mean energies in the target, having been corrected for the energy loss of the deuteron beam in the entrance foil and the gas of the target. The spin precession factor SPF is seen from Equation (5) to be $1/\sin\varphi$ for converting measured asymmetries to polarizations. Values are listed for both the Hoop and Barschall (1966) phase shifts (H-B) and for the Stammbach and Walter (1971) phase shifts (S-W).

Figure 4 shows the angular distribution obtained at 18 MeV. Only the forward angles were measured, since the identity of the particles in the entrance channel requires the polarization to be antisymmetric about 90 degrees in the center of mass. The line through the data is derived from an associated Legendre polynomial fit to $P(\theta)\sigma(\theta)$ calculated from this data (using H-B phase shifts) and the cross section Legendre coefficients of Dietrich et al. (1970). The $P\sigma$ values calculated from this fit were divided by σ values calculated from the cross section coefficients to obtain the curve shown. The data and fit indicate that the polarization peaks at about 40 degrees c. m., although it is difficult to estimate precisely the magnitude of the polarization at the peak from the present data.

Table 1

Polarization Data for $D(d,n)^3He$

E_d (MeV)	θ_1 c.m. (deg)	E_n (MeV)	Asymmetry	SPF	P_2 (Hoop-Barschall phase shifts)	$\overline{P}_2$ (Hoop-Barschall phase shifts)	Polarization (Hoop-Barschall phase shifts)	P_2 (Stammbach-Walter phase shifts)	$\overline{P}_2$ (Stammbach-Walter phase shifts)	Polarization (Stammbach-Walter phase shifts)
16.0	45.0	16.3	0.317 ± 0.013	1.10	0.970	0.880	0.396 ± 0.015	0.910	0.815	0.428 ± 0.017
18.0	15.0	20.2	0.008 ± 0.008	1.17	0.921	0.832	0.012 ± 0.012	0.778	0.696	0.014 ± 0.014
	25.4	19.7	0.050 ± 0.011	1.16	0.955	0.867	0.067 ± 0.015	0.798	0.714	0.081 ± 0.019
	34.3	19.0	0.241 ± 0.020	1.15	0.960	0.871	0.318 ± 0.025	0.823	0.737	0.376 ± 0.031
	45.0	17.9	0.307 ± 0.011	1.13	0.967	0.876	0.396 ± 0.014	0.862	0.773	0.450 ± 0.016
	54.5	16.7	0.197 ± 0.011	1.11	0.970	0.879	0.249 ± 0.014	0.898	0.805	0.272 ± 0.016
	64.3	15.4	0.137 ± 0.012	1.09	0.953	0.870	0.170 ± 0.014	0.932	0.836	0.177 ± 0.015
	75.2	13.8	0.115 ± 0.015	1.06	0.961	0.863	0.141 ± 0.018	0.961	0.863	0.141 ± 0.018
20.0	45.0	19.5	0.280 ± 0.016	1.16	0.957	0.868	0.374 ± 0.022	0.805	0.721	0.450 ± 0.026
22.0	45.0	21.1	0.257 ± 0.020	1.19	0.942	0.852	0.358 ± 0.028	0.744	0.664	0.460 ± 0.036

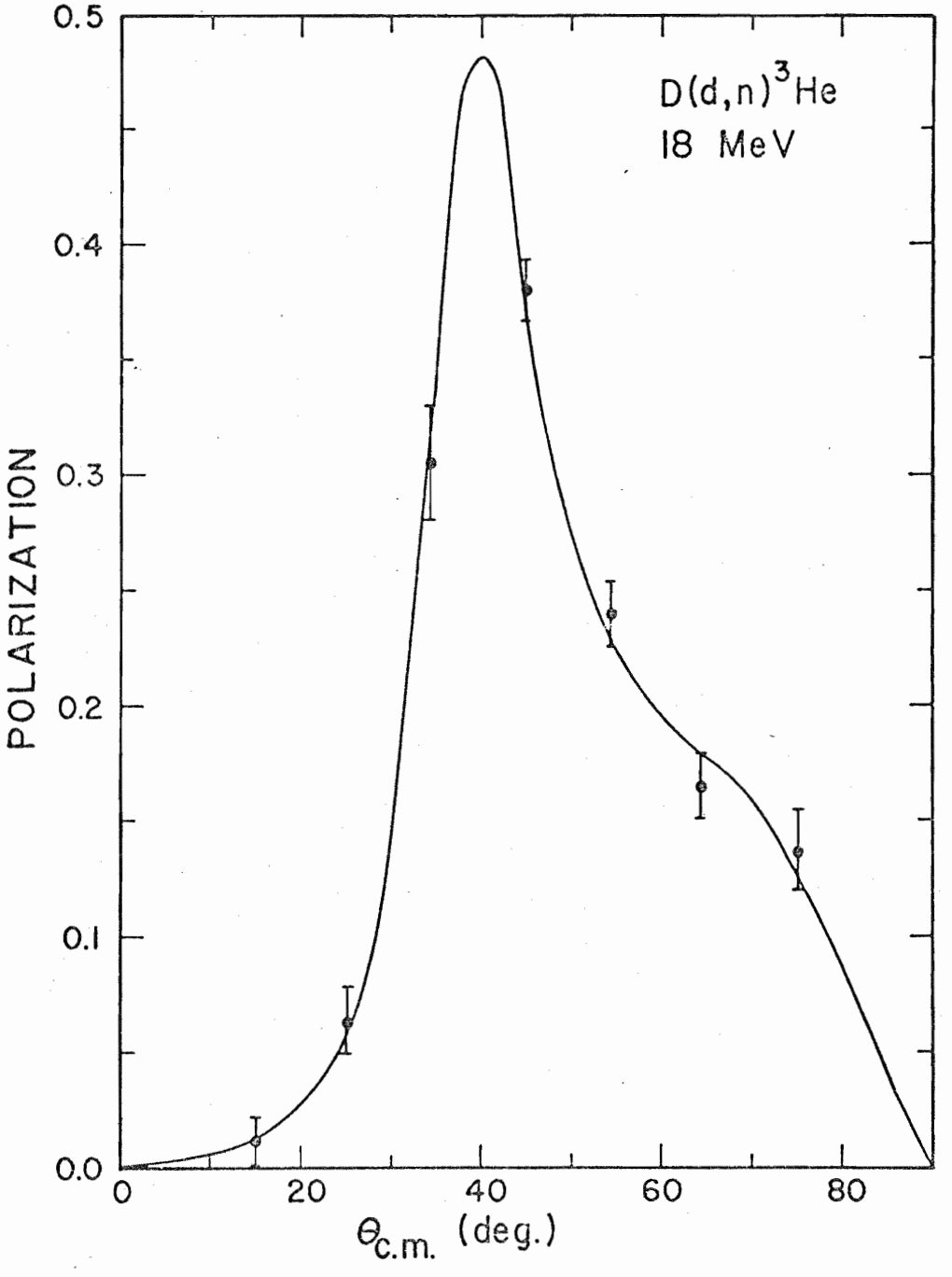

Figure 4. Polarization Distribution and Fit for $D(d,n)^3He$ at 18 MeV

Figure 5 shows the polarization at 45 degrees c.m. as a function of energy. For the data below 14 MeV, the uncertainty in the n-^{4}He analyzing power is small. The most recent D(d,n)^{3}He polarizations from 6 to 14 MeV (Spalek et al., 1970) used the S-W phase shifts. The present data is plotted for both the S-W phases (solid diamonds) and the H-B phases (open diamonds). The divergence in the predictions of the n-^{4}He analyzing power from the two sets is readily apparent. Recent n-^{4}He cross section and polarization data (Broste et al., 1971) support the predictions of the S-W phases. It is believed, therefore, that the D(d,n)^{3}He polarizations above 14 MeV lie closer to the values obtained using the S-W phases. The solid line below 14 MeV is drawn through the maxima of the calculated polarizations obtained by Spalek et al. (1970) from associated Legendre polynomial fits to their data. Above 14 MeV, the lines are guides to the eye through the values obtained using S-W phases (solid line) and H-B phases (broken line).

The D(d,n)^{3}He polarization at 45 degrees thus remains high in the energy range from 14 to 22 MeV. Moreover, since the peak is shifting to smaller angles as shown by the solid curve in Figure 4, the values obtained here are somewhat less than the expected maximum polarizations. A more precise determination of the maximum polarizations awaits more complete angular distributions and a better knowledge of the n-^{4}He analyzing power in this region. The theoretical implications of the D(d,n)^{3}He polarization and comparisons with D(d,p)T polarizations are presented in Chapter VI.

The D(d,n)^{3}He reaction is one of the best known means to produce a polarized neutron beam of neutron energies between 10 and 22 MeV. In spite of the large polarizations found, however, this reaction has some undesirable characteristics as a source of polarized neutrons at the higher energies. First, the polarization peaks near the minimum

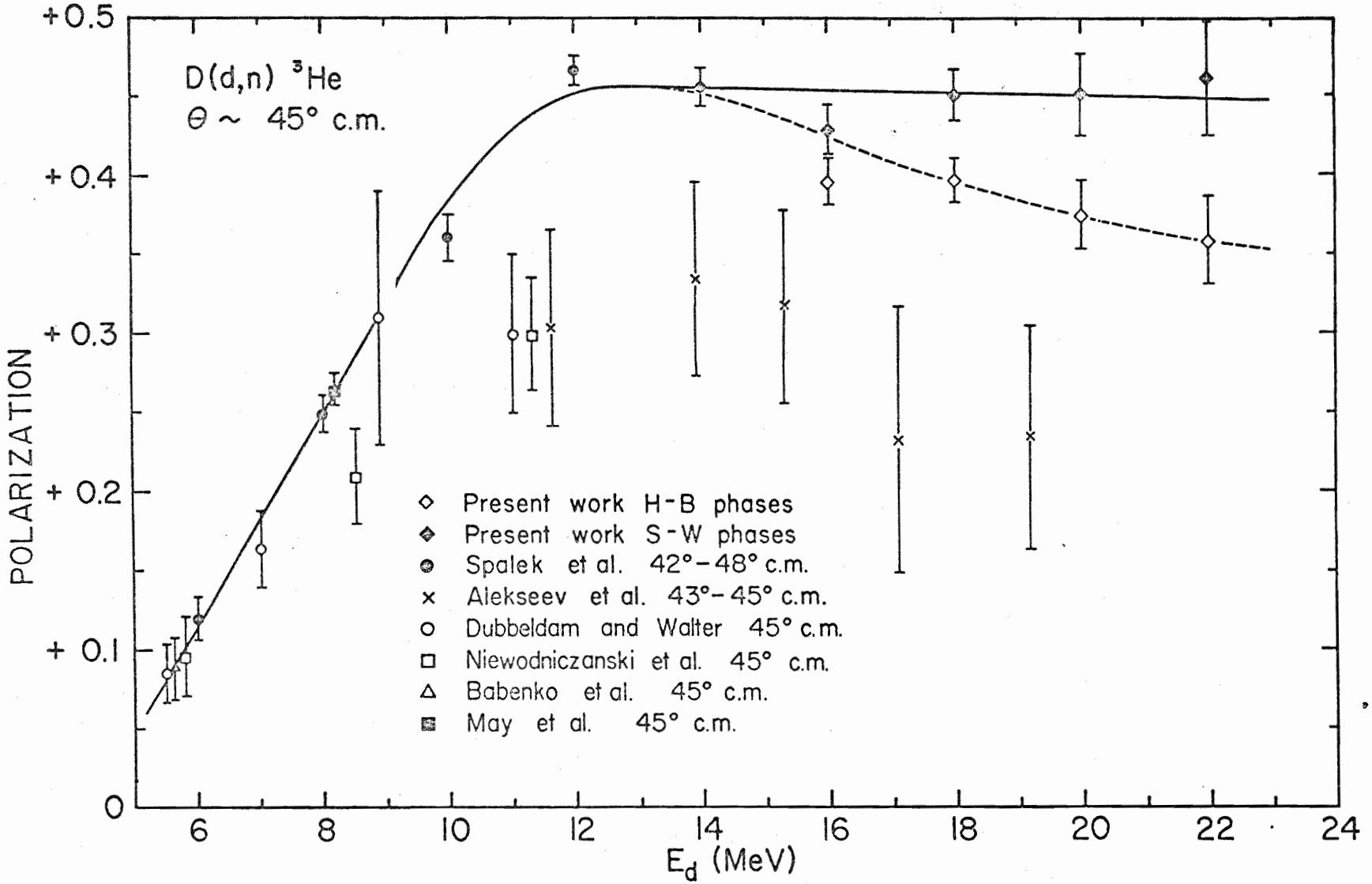

Figure 5. Polarization Near 45 Degrees c.m. for $D(d,n)^3He$

in the cross section. At 18 MeV the cross section is down from a maximum of 48 mb/sr at zero degrees to 2.5 mb/sr at 40 degrees. In order to get a reasonable flux of neutrons, therefore, a large beam current of high energy deuterons is required. This makes room background and shielding problems particularly acute. In the present experiment, with about 3 μa of deuterons on target, the neutron radiation level in the target room was greater than 2000 mrem/hr, and levels in the computer room (through 6 ft of concrete) were 2 to 4 mrem/hr. Care must be taken to keep counting rates from this large target room background from saturating the electronics. The second drawback is the increase in intensity of neutrons from the D(d,np)D breakup at these energies. These neutrons form a broad peak with a cross section of about 80 mb/sr and a mean energy of 11 MeV at zero degrees for 19 MeV deuterons incident (Rybakov, 1961). They not only contribute to the total background level as discussed above, but good energy resolution is required to separate the direct neutrons. Methods such as the time-of-flight gating used here or the associated particle method (Schuster and Hagengruber, 1970) are useful to reduce this background.

The maximum accuracy in a polarization measurement by scattering that is available in a minimum amount of time is proportional to the product of the neutron production cross section and the square of the reaction polarization. This product can be divided by the energy loss in the target to standardize flux comparisons. Figure 6 (adapted from Walter, 1970) shows a comparison of sources of polarized neutrons using reactions with unpolarized beams incident. The cross hatched line for the $D(d,n)^3He$ reaction was based on earlier data (Alekseev et al., 1964) above 14 MeV. The results from the present data (using S-W phase shifts) are indicated by a continuation of the vertical hatched line. This figure shows that the $D(d,n)^3He$ reaction is the only useful source of this type for

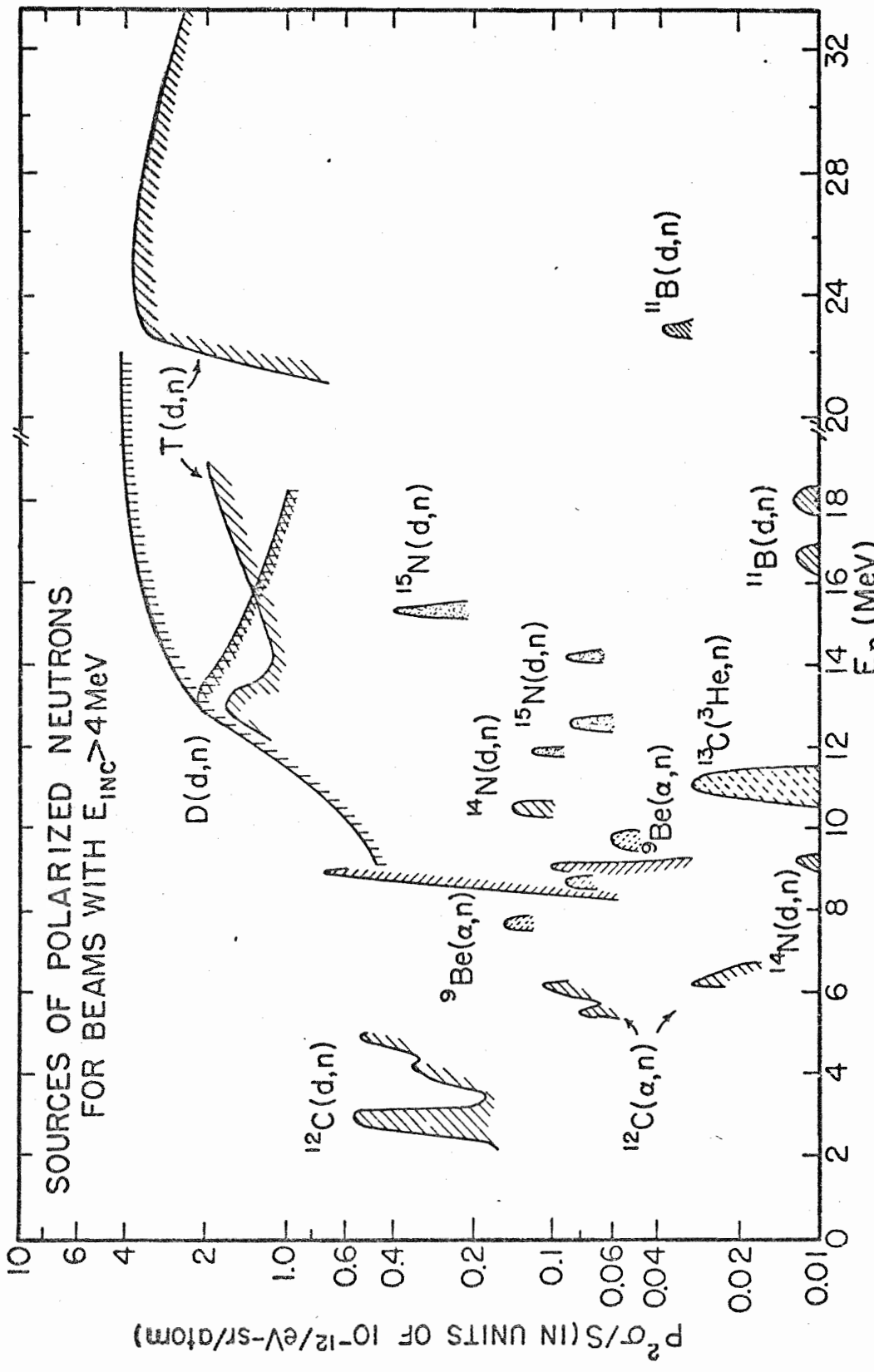

Figure 6. Sources of Polarized Neutrons

neutron energies between about 18 and 22 MeV. The $D(\vec{d},n)^3He$ reaction at zero degrees with polarized deuterons incident has recently been shown (Simmons et al., 1971) to be one of the best sources of polarized neutrons if at least 20 na of highly polarized deuterons are available. Neutrons of 18 to 22 MeV from this source require beam energies of 15 to 20 MeV.

PART II

ANALYZING POWERS OF T(p,d)D AND T(p,p)T

Chapter V

EXPERIMENTAL PROCEDURE

A. Lamb-Shift Polarized Ion Source

The acquisition of accurate polarization data has been greatly aided in the last few years by the development of polarized ion sources. The use of polarized beams, even of low intensity, represents a great advantage over double scattering methods for polarization measurements. Although several different types of sources are in use, the Lamb-Shift source has proven to be most attractive for producing negative polarized beams, i.e., for tandem accelerators. This type of source utilizes the metastable 2S state of the hydrogen (or deuterium) atom, which was shown to be non-degenerate with the short-lived $2P_{\frac{1}{2}}$ state by Lamb and Retherford (1950). The radio-frequency corresponding to the $2S-2P_{\frac{1}{2}}$ separation is about 1060 MHz, the 2S state shifted higher by this amount. The long lifetime of the 2S state depends on the fact that spontaneous transitions to the lower excited $2P_{\frac{1}{2}}$ and to the ground 1S states are rare. The transition to the $2P_{\frac{1}{2}}$ state has a lifetime on the order of 20 years due to the small difference in energy (1060 MHz corresponds to about 4.4×10^{-6} eV). For transitions to the ground state, E1 radiation is forbidden by parity, M1 transitions have a lifetime of about 2 days, and E2 and all other higher multipole transitions are forbidden by angular momentum conservation. The principal decay

mode turns out to be the simultaneous emission of two photons which has a lifetime of 0.14 second (Sakurai, 1967). This lifetime is extremely long compared to the lifetime of the $2P_{\frac{1}{2}}$ state, 1.6×10^{-9} second..

The methods used to utilize the metastable 2S state to produce a beam of polarized protons or deuterons are well documented in the literature (Haeberli, 1967; Cesati et al., 1969; Donnally, 1970; Ohlsen, 1970). Only a brief description will be given below, particularly as it applies to polarized proton beams from the TUNL source. Figure 7 shows a schematic diagram of the Lamb-Shift source used for the measurements reported here. A duoplasmatron of conventional design produces an intense beam of protons which are decelerated to 550 eV prior to entering a cesium charge exchange canal. At this energy the cross section for electron capture into the n=2 states by protons in cesium is large, and about 30 per cent of the atoms formed can be obtained in the metastable state. Deflection plates following the cesium canal deflect the remainder of the charged beam. The atomic beam enters the main coil region where a magnetic field produces Zeeman splitting of the atomic energy levels. At a magnetic field of about 535 gauss, the $m_j = -\frac{1}{2}$ levels of the 2S state have nearly the same energy as the $m_j = +\frac{1}{2}$ levels of the $2P_{\frac{1}{2}}$ state. A transverse electric field of about 10 v/cm is sufficient to mix the two levels via the Stark effect, and the metastable atoms having $m_j = -\frac{1}{2}$ decay quickly to the ground state. The metastable atoms remaining thus have 100 per cent electron polarization ($m_j = +\frac{1}{2}$) but zero nuclear polarization (equal numbers of $m_I = +\frac{1}{2}$ and $m_I = -\frac{1}{2}$). In the TUNL Lamb-Shift source, nuclear polarization is obtained by a spin-filter system similar to that developed at Los Alamos. This method uses a combination of a longitudinal rf field together with the transverse DC field to quench selectively one of the remaining m_I states,

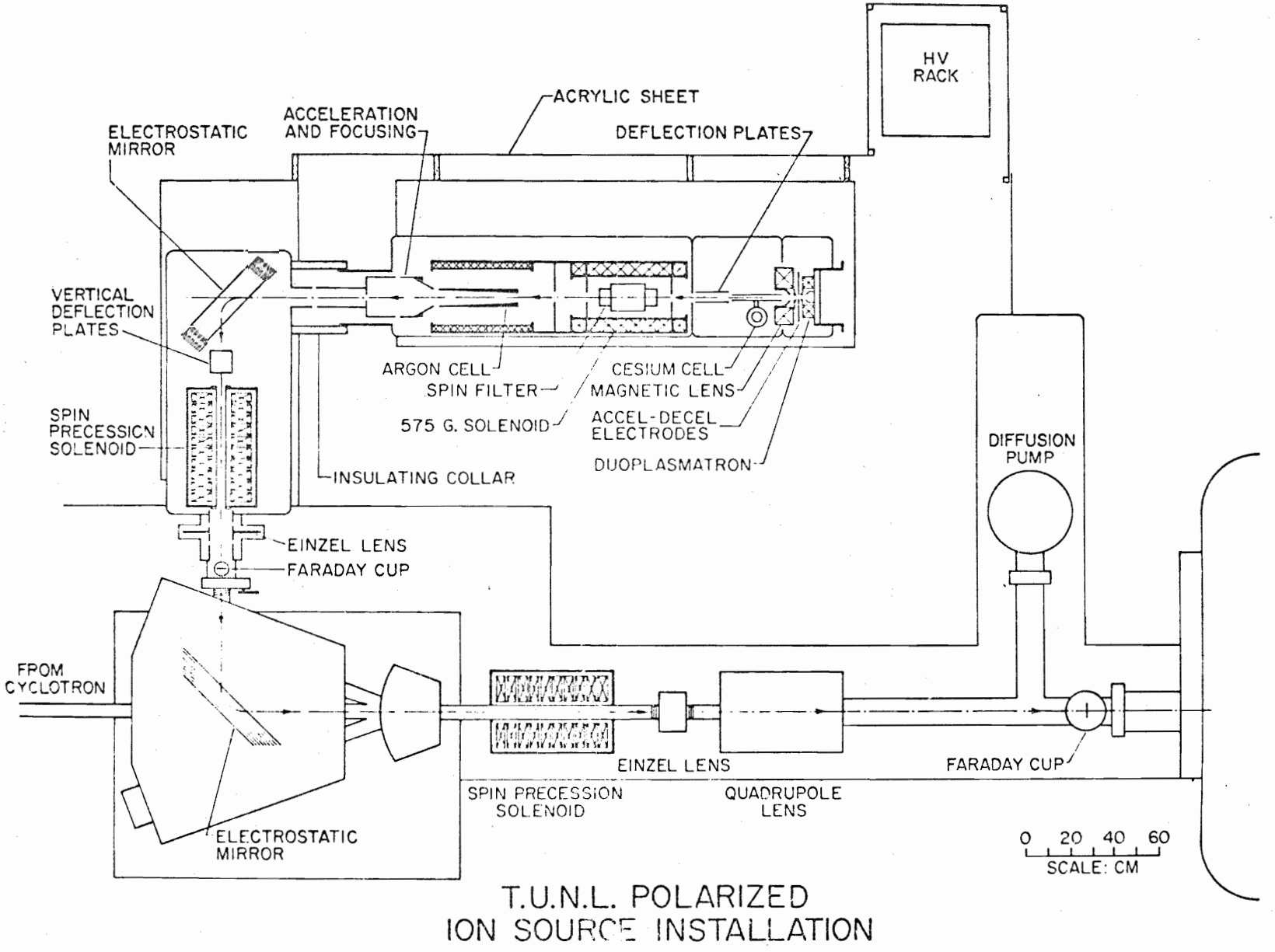

Figure 7. Schematic Diagram of Polarized Ion Source

leaving only metastable atoms with the same nuclear spin. This process makes use of the three-level interaction discovered by Lamb and Retherford (1951) and described in detail by Ohlsen and McKibben (1967). The atomic beam with nuclear polarization then enters an argon charge exchange region where the metastable atoms are selectively ionized, producing a negative beam of polarized hydrogen ions. Ionization of ground state hydrogen atoms (which are unpolarized) in this region will contribute a small background, reducing somewhat the theoretical 100 per cent beam polarization. An axial magnetic field in the argon charge exchange region (in the same direction as the main coil) defines the quantization axis of the beam.

The polarized ion source is operated at about minus 45 kV to provide the necessary injection energy for the beam entering the tandem accelerator. After accelerating to ground potential, the beam is deflected 90 degrees by an electrostatic mirror. The spin quantization axis is then perpendicular to the beam direction and can be rotated to a vertical position (either UP or DOWN) by a spin precession solenoid. Another electrostatic mirror then deflects the beam 90 degrees into the tandem accelerator beam tube. The focusing and acceleration of the beam, stripping of the electrons, and deflection by the analyzing magnet do not change the direction of the spin quantization axis. Thus, reversal of the spin precession solenoid at the source can provide either a spin UP or a spin DOWN polarized beam at the target. This feature can be used to cancel instrumental asymmetries as described later.

B. Scattering Chamber, Target, and Polarization Monitor

After acceleration, energy analysis, and focusing, the protons bombarded a self-supporting titanium-tritium foil at the center of a 60 cm diameter scattering chamber. Figure 8 shows a schematic of the scattering chamber and polarization monitor. The beam axis was defined by 5.1 x 7.6 mm collimators 130 cm from the target, and 1.5 x 3.0 mm chamber slits 10 cm from the target. The chamber slits were connected to an automatic steering system which held the beam centered on the target. A pair of detector telescopes were placed in the scattering chamber at equal angles to the left and right of the beam axis. These utilized 50 μ ΔE and 1500 μ E surface barrier detectors for most of the measurements. For the three lowest energy distributions (6.7, 7.4, and 8.0 MeV proton bombarding energy) 20 μ ΔE detectors were used. Rectangular collimators 1.6 x 3.2 mm placed before the detectors at a distance of 12.7 cm from the target gave an angular acceptance of 0.7 degrees in the laboratory frame.

After leaving the scattering chamber, the beam entered a polarization monitor 53 cm behind the target through a 0.25 μ HAVAR foil and a 2.5 x 6.4 mm entrance slit. The monitor contained 5 atm of ^{4}He gas and two 1000 μ rectangular surface barrier detectors. The monitor collimating system consisted of 1.6 x 19 mm slits placed 17.5 mm apart such that protons scattered at a mean angle of 112.2 degrees were counted with the right and left detectors. The body of the monitor was insulated and connected to a current integrator for beam current measurement and integration.

The 5 μ titanium-tritium foil was obtained commercially from the NUKEM Company of West Germany and was mounted between two target rings. Energy loss for protons in the foil ranged from about 100 keV at 6.7 MeV to 50 keV at 14.7 MeV.

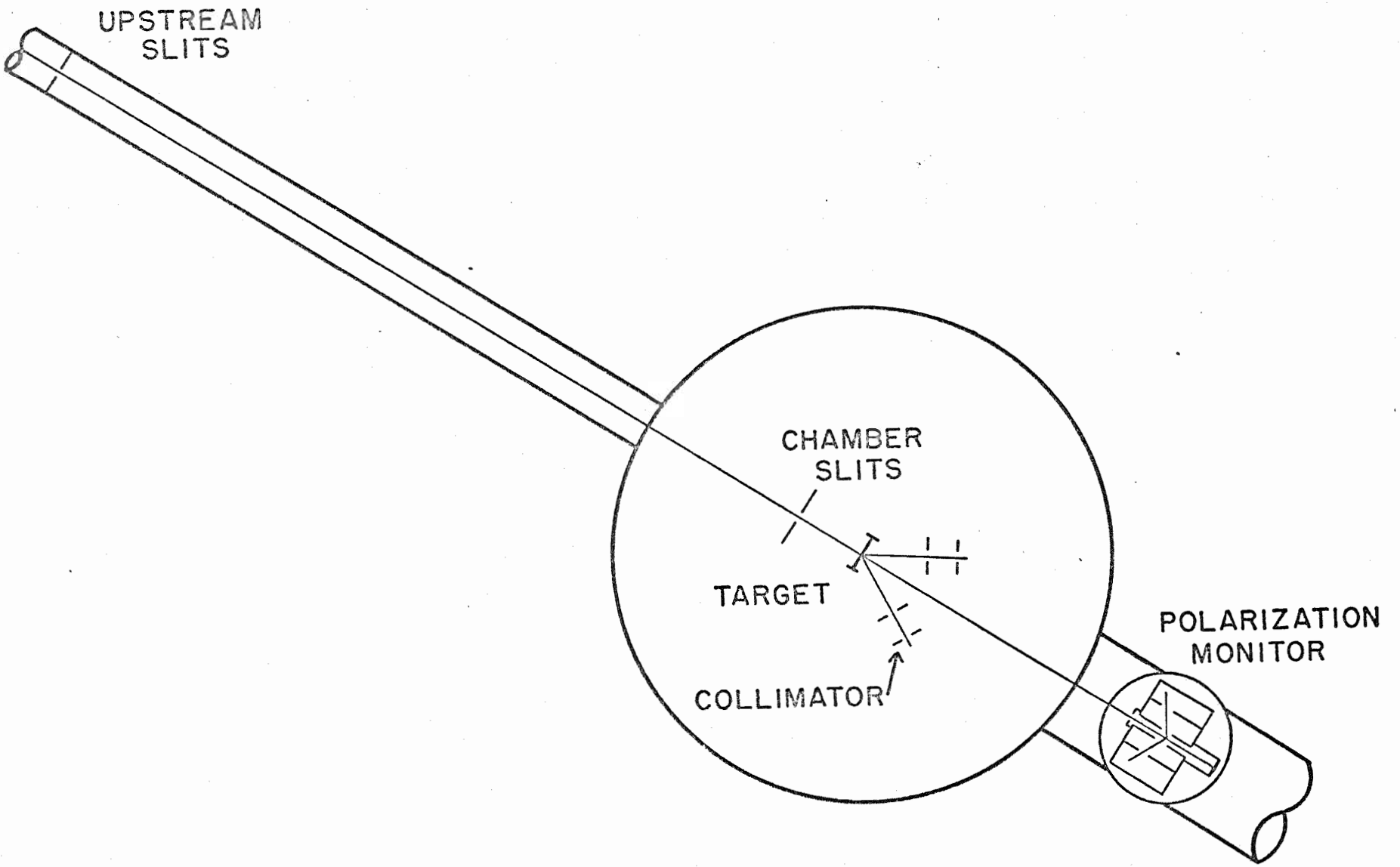

Figure 8. Schematic Diagram of Scattering Chamber and Polarization Monitor

C. Electronics

Charged reaction products resulting from protons incident on the Ti-t foils at the energies of this experiment were primarily elastic protons from the tritium and titanium, deuterons and helions from the T(p,d)D and T(p,^{3}He)n reactions, and recoil tritons from the elastic scattering. The kinematics of the reactions and scattering show that the deuterons and recoil tritons have nearly the same energy over the angular range of interest in this experiment. Therefore, mass identification was necessary to separate these reaction products. This was accomplished by using the particle telescopes and the on-line computer to calculate the mass of the detected particles.

Figure 9 is a block diagram of the electronics used. Pulses from the ΔE and E detectors were sent through preamplifiers to linear amplifiers. The prompt output from each amplifier went to a single channel analyzer (SCA) to develop slow logic pulses which were sent to a coincidence unit for each E-ΔE pair. The output of the coincidence units were used to open linear gates for the delayed outputs of the respective amplifiers. The outputs of all four linear gates (E and ΔE, right and left telescopes) were summed and sent through a biased amplifier to the "E+ΔE" analog-to-digital converter (ADC). The ΔE signals were also summed separately and sent to the "ΔE" ADC. Information on right or left telescope was retained by using the output of the coincidence units to route the signals from the ADC's. The outputs of the two ADC's and the router were combined to form a single 24 bit word which was stored in the computer via a direct memory access channel. This word contained all the information for the computer to calculate the mass of the particle (E+ΔE and ΔE) as well as the total energy (E+ΔE) and identification of the right or left telescope (routing bits). For each pair of coincident pulses, the computer calculates the function

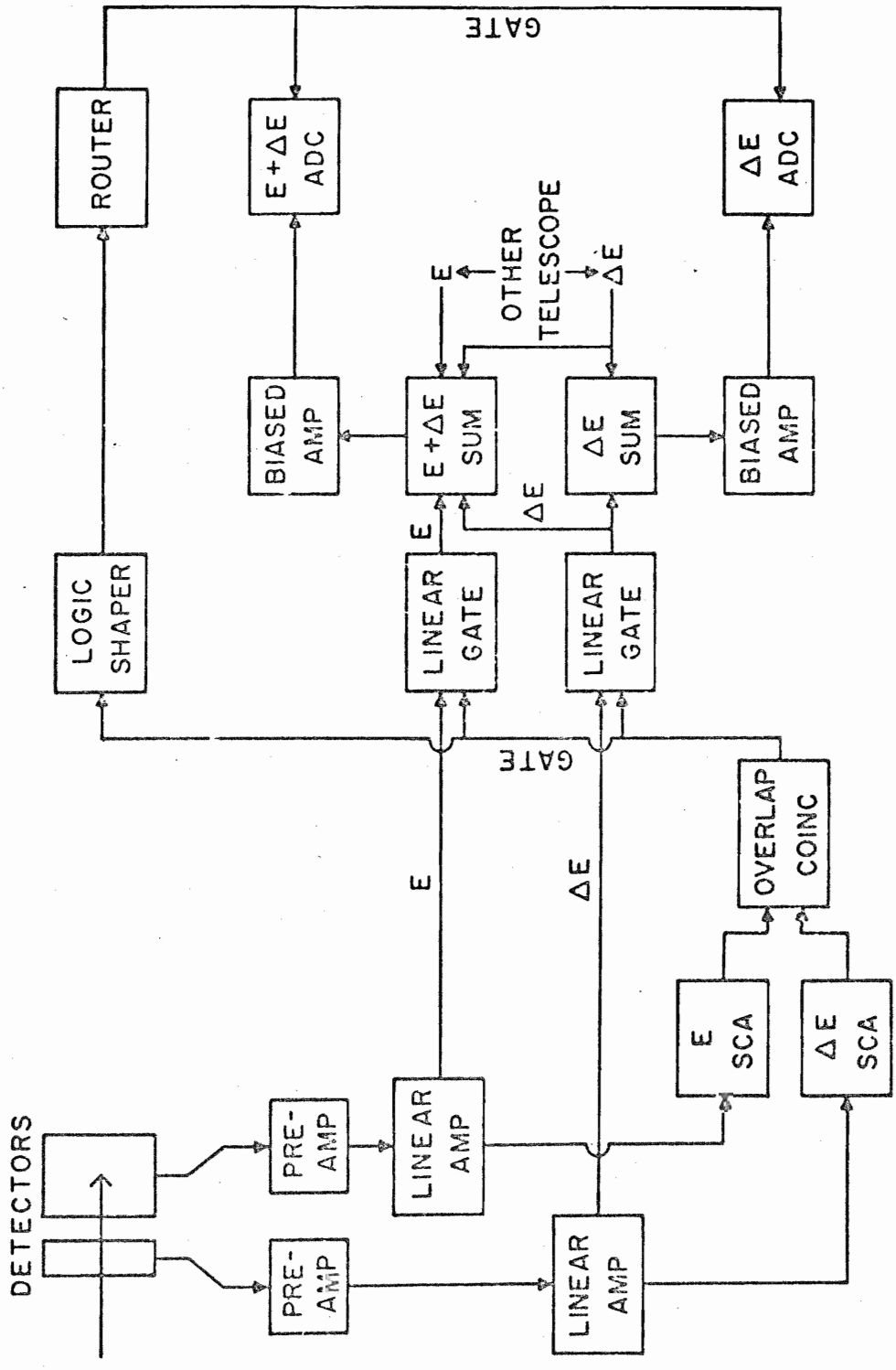

Figure 9. Block Diagram of Mass Identification Electronics

$(E+\Delta E)^{1.73} - E^{1.73}$ which is proportional to the mass of the detected particle for a given charge. Initially the computer is programmed to store the mass function for each detector telescope. The resulting mass spectra are displayed on the oscilloscope and the peaks from the masses identified. Acceptance windows for two of the particles are set with a light pen. A typical mass spectrum is shown in Figure 10. The scale has been expanded to show only the mass peaks corresponding to protons, deuterons, and tritons, since these were of primary interest in this experiment. The good mass separation between deuterons and tritons ensured that false asymmetries did not arise from overlapping peaks. The fluctuations in the proton peak arise from the low energy loss for these particles in the ΔE detectors and the integer arithmetic used in the mass identification calculation.

After selection of the mass windows, the program mode is changed to store the energy spectra. In this mode the computer stores and displays the total energy for pulses which satisfy either of the mass windows. The program APOL (see Appendix A) could store four 512 channel spectra, allowing data accumulation for two particles with two detector telescopes. For most of the runs these particles were deuterons and tritons. For the forward angle T(p,p)T data, protons were stored instead of tritons.

D. Data Acquisition and Reduction

Several computer programs were written by the author for data acquisition and reduction of polarization data. A description of their general features may be found in Appendix A. The basic procedure for obtaining asymmetry data, however, is general and will be discussed briefly below.

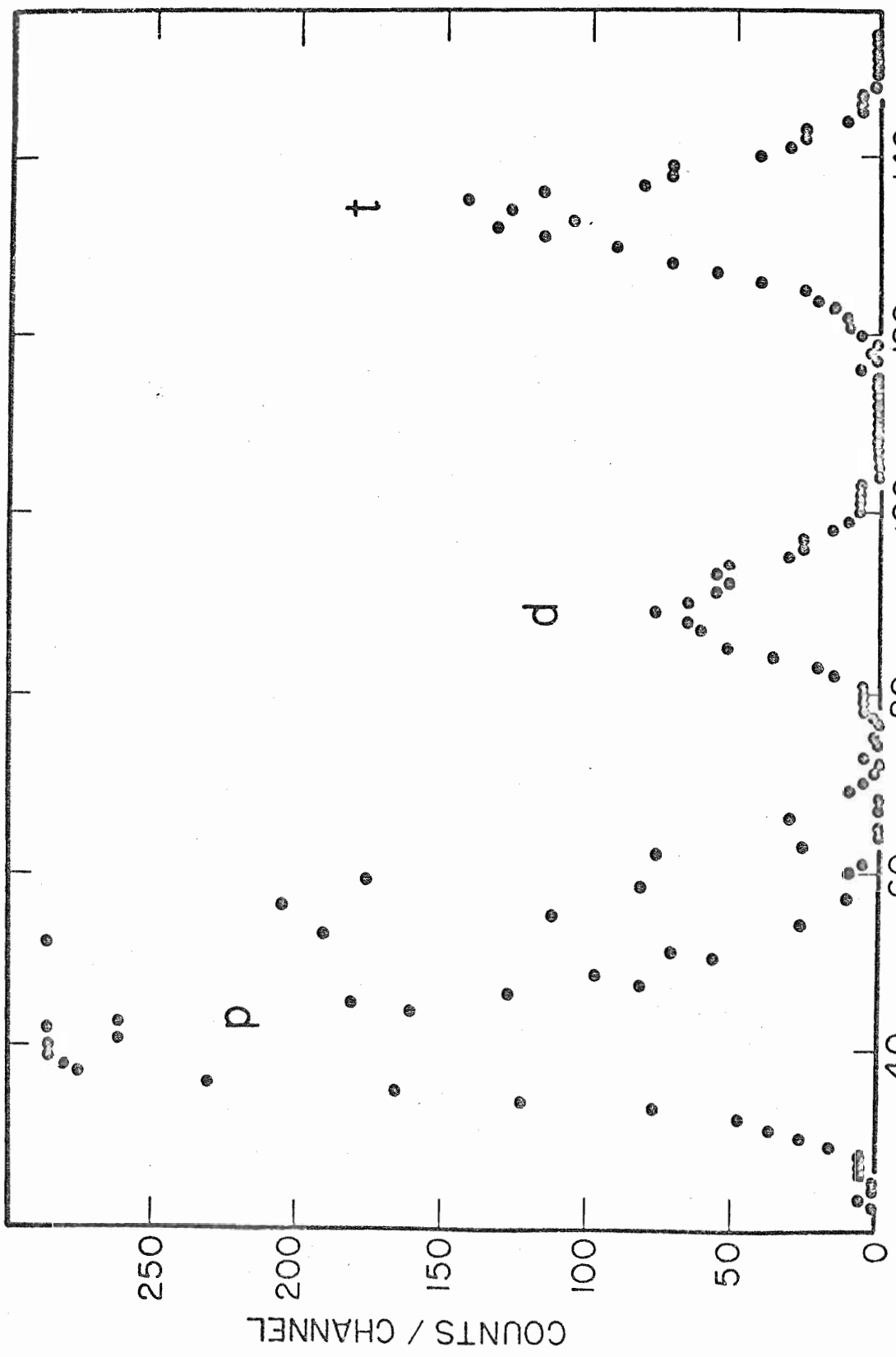

Figure 10. Typical Mass Spectrum for T + p

For nuclear reactions induced by spin 1/2 particles it can be shown from general invariance principles (Wolfenstein, 1956) that the cross section depends on the polarization in the following way:

$$\sigma(\theta,\varphi) = \sigma_o(\theta)\left[1 + \vec{P}_b \cdot \vec{A}(\theta)\right] \tag{7}$$

where $\vec{P}_b$ is the polarization of the incident beam and $\vec{A}(\theta)$ is the analyzing power of the reaction. We choose a cartesian reference frame with the incoming beam direction $\vec{k}_{in}$ as the +z axis and the normal to the reaction plane $\vec{k}_{in} \times \vec{k}_{out}$ as the +y axis (Basel Convention, 1960). Then for incident spin UP, $\varphi=0$ corresponds to a scattering to the left and $\varphi=\pi$ corresponds to a scattering to the right. Equation (7) gives for the two cases

$$\begin{aligned} \sigma_L &= \sigma(\theta,0) = \sigma_o(\theta)\left[1 + P_y A_y(\theta)\right] \\ \sigma_R &= \sigma(\theta,\pi) = \sigma_o(\theta)\left[1 - P_y A_y(\theta)\right] \end{aligned} \tag{8}$$

where P_y is the vertical (+y) component of the beam polarization. Solving for $A_y(\theta)$ gives

$$A_y(\theta) = \frac{1}{P_y}\left[\frac{\sigma_L - \sigma_R}{\sigma_L + \sigma_R}\right] \tag{9}$$

In practice, σ_L and σ_R are obtained by counting for a length of time with incident spin

UP, then reversing the polarity of the spin precession solenoid and counting for the same time with spin DOWN. This effectively interchanges the left or right position of the detector without physically moving it. In addition, if one uses both right and left detectors simultaneously, the effect of different counting times for spin UP and spin DOWN can be cancelled as well as the instrumental asymmetry due to different solid angles or efficiencies of the detectors. This is done by taking a geometrical average as follows.

Equation (9) can be written for the two cases of spin UP and spin DOWN as

$$A_y(\theta) = \frac{1}{P_y}\left[\frac{\sigma_L/\sigma_R - 1}{\sigma_L/\sigma_R + 1}\right] = \frac{1}{P_{-y}}\left[\frac{\sigma_R/\sigma_L - 1}{\sigma_R/\sigma_L + 1}\right] \tag{10}$$

Define

$$r = \sqrt{\frac{\sigma_L(UP) \times \sigma_R(DN)}{\sigma_R(UP) \times \sigma_L(DN)}} \tag{11}$$

where r is the effective ratio of left to right cross sections. If the magnitude of the beam polarization P_b is the same for the UP and DOWN runs we have

$$A_y(\theta) = \frac{1}{P_b}\left[\frac{r-1}{r+1}\right] \tag{12}$$

Now the cross sections may be written as

$$\sigma_L(UP) \propto K_b(UP)\, K_g(L)\, N_L(UP) \tag{13}$$

where $N_L(UP)$ is the number of counts in the left detector with incident spin UP, K_g is a solid angle (geometry) factor, and K_b is a beam integration factor. Obviously K_b is identical for both detectors on a run with the spin in one direction. Also K_g is identical for a given detector with the spin in either direction provided the beam position on the target does not change between an UP and a DOWN run. Combining expressions like Equation (13) for each cross section in the definition for r (Equation 11), it is seen that the beam integration and solid angle factors cancel. Thus r may be written as

$$r = \sqrt{\frac{N_L(UP) \times N_R(DN)}{N_R(UP) \times N_L(DN)}} \tag{14}$$

The analyzing power calculated from this expression for r in Equation (12) is independent of both beam integration and instrumental asymmetry.

During each run, the product of $A_y(\theta)$ and P_b called the asymmetry ϵ is output using the oscilloscope numerical display for each detector pair and for the monitor. Also output on the typewriter are the asymmetry errors, the ratio of left detector to right detector counts, and the number of counts in each peak, as well as the sum for each particle. The ratio of left to right counts, which is an indication of the relative efficiency of the two detectors (or the instrumental asymmetry) is calculated by

$$L/R = \sqrt{\frac{N_L(UP) \times N_L(DN)}{N_R(UP) \times N_R(DN)}} \qquad (15)$$

In this equation, the beam integration factor cancels as in Equation (14). This ratio should be relatively constant (and ideally near 1.0) for a series of runs with the same detector geometry. For on-line analysis the sums are computed between light-penned channels with no background subtraction. For off-line analysis using program VPOL backgrounds can be subtracted from the sums. The factor r (Equation 14) is then calculated using the net sum (total sum minus background) for each peak. The asymmetry in the polarization monitor is used to determine the beam polarization for each run through the relation

$$\epsilon = P_b A_Y(\theta) \qquad (16)$$

The analyzing power of the monitor $A_y(\theta)$ is known from previous calibration as discussed later. The value of P_b for the run is then used to determine $A_y(\theta)$ from the asymmetries calculated for the other spectra. The statistical and other errors arising from this method are discussed in the next section.

E. Error Analysis

The errors that contribute to the uncertainty of the polarization values arise from several sources. A discussion of these sources, estimation of errors, and methods used to minimize the errors follows.

Summing the peaks and background subtraction. --Errors that might arise from summing the peaks were minimized by summing between the same channels for the UP and DOWN runs for each detector. In addition, the same channels were used for the monitor sums for all runs at the same energy. The deuteron and triton spectra from protons on the Ti-t target were very clean and corrections due to backgrounds were negligible. The proton spectra from the Ti-t target and the monitor spectra had sizeable backgrounds, and care was taken to subtract these in a reasonable and consistent manner. The method used for averaging background points is discussed in Appendix A under program VPOL. There was no constraint that the background be unpolarized but, within statistics, that was the case for both the scattering chamber and monitor spectra. The maximum background effect occurred in the monitor spectra, where it resulted in an asymmetry change of about 0.02 from the asymmetry calculated with no background subtraction. In view of the good definition of this background and the consistent way in which it was summed, there was no need to assign an error due to its uncertainty. The statistical error from the background subtraction is discussed below.

Statistical errors. -- The asymmetry error is calculated by combining the statistical error from each sum and background in the standard way:

$$(\Delta\epsilon)^2 = \sum_{i=1}^{4} \left[\left(\frac{\partial\epsilon}{\partial S_i}\right)^2 \Delta S_i^2 + \left(\frac{\partial\epsilon}{\partial B_i}\right)^2 \Delta B_i^2 \right] \qquad (17)$$

where the S_i are the total sums for each peak (UP left, UP right, DOWN left, and DOWN right) and the B_i are the respective backgrounds. ΔS_i and ΔB_i are equal to the square root of the number of counts in the sum and background. Using Equations (12) and (14) in which the N's are the net counts in a peak (i.e., $N_i = S_i - B_i$) the expression for the asymmetry error is

$$\Delta\epsilon = \frac{r}{(r+1)^2}\sqrt{\sum_{i=1}^{4}\frac{S_i + B_i}{(S_i - B_i)^2}} \tag{18}$$

This equation was programmed in VPOL to calculate the statistical error for each of the asymmetries. The monitor asymmetry and error were then divided by the analyzing power of the monitor to obtain the beam polarization and its error. These were then used to calculate the final analyzing powers and statistical errors:

$$A_y(\theta) = \frac{\epsilon}{P_b} \tag{19}$$

and

$$\Delta A_y^2 = \left(\frac{\partial A_y}{\partial \epsilon}\right)^2 \Delta\epsilon^2 + \left(\frac{\partial A_y}{\partial P_b}\right)^2 \Delta P_b^2 \tag{20}$$

which reduces to

$$\Delta A_y = \frac{\epsilon}{P_b}\sqrt{\frac{\Delta\epsilon^2}{\epsilon^2} + \frac{\Delta P_b^2}{P_b^2}} \tag{21}$$

The total number of counts in the monitor peaks was usually on the order of 250,000. Thus the statistical error in measuring the beam polarization was very small (about 0.002) and contributed little to the final errors. For low ΔP_b Equation (21) reduces to

$$\Delta A_y = \frac{\Delta \epsilon}{P_b} \tag{22}$$

The low beam polarization (0.50 to 0.70) for many of the measurements, therefore, nearly doubled the statistical errors in the analyzing powers reported here. Since the asymmetry error is to a first approximation inversely proportional to the square root of the number of counts, it is seen that increasing the beam polarization by 0.20 would give the same reduction in error as counting for about twice the time. The importance of this fact in polarized source development should not be overlooked.

Polarization monitor average analyzing power. -- Accurate phase shifts for proton scattering from ^{4}He have led to a high degree of reliability in the analyzing power for energies up to 20 MeV. In particular, Plattner and Bacher (1971) give three calibration points below 20 MeV where the analyzing power is exactly 1.00. The polarization monitor used in this experiment was calibrated in two ways. First, the analyzing powers calculated from the phase shifts of Schwandt et al. (1971) were averaged over the slit geometry of the monitor using numerical integration techniques. The values obtained ranged from 0.935 to 0.950 over the energy range of this experiment (proton energies from 6.5 to 14.7 MeV). Secondly, the monitor was calibrated against a good geometry setup in the scattering chamber at 12.3 MeV, $\theta_{Lab} = 112$ degrees, which is one of the calibration points given by Plattner and Bacher (1971). Poor polarized source performance during this calibration precluded an accurate measurement, but the mean value of the 12 data points obtained was consistent with the calculated value of 0.950 here. The calculated analyzing powers of the monitor were therefore used for the data reported in Chapters VI and VII. The error in this calibration must be assigned as ± 0.02 until a better calibra-

tion is made. This gives an overall normalization error of 2 per cent to the data. Thus, the maximum normalization error of the analyzing powers in T(p,d)D is ±0.01 near the maximum. This is within the statistical error for these points.

Alignment of the scattering chamber and beam variations. -- The scattering chamber slit system and the polarization monitor were aligned optically to within ±0.1 mm. The angular scale on the scattering chamber was checked and found to be accurate to within ±0.05 degrees, which was also the precision with which it could be set. The 1.5 mm wide chamber slits were located 10 cm from the target and the beam was kept centered on these slits by the automatic slit control system. The slit geometry used allowed a maximum variation of the beam axis of ±0.12 degrees. Thus the maximum movement of the beam spot center on target was ±0.2 mm. The beam polarization direction was changed by reversing the spin precession solenoid current at the polarized source. Although this affected the beam steering at the low energy end of the accelerator, the slit control system prevented movement of the axis or position of the beam on target between UP and DOWN runs. False asymmetries introduced due to alignment and beam steering are thus considered negligible.

Another potential source of error was the variation in beam polarization during the runs. Although every effort was made to stabilize the polarized ion source, there was still a considerable fluctuation in both beam intensity and polarization during some of the measurements. Changes in beam intensity with accompanying changes in beam integration efficiency and dead time did not affect the measurements because of the symmetrical detector arrangement used. Although the polarization changes during a run may have been as much as 0.05 for a few of the runs, the polarization monitor provided a continuous monitoring and thus averaged over fluctuations during an UP or a DOWN run. However, the

calculation of the analyzing power in Equation (12) assumes the same beam polarization for the UP and DOWN runs. To assess the error introduced by variation in beam polarization between UP and DOWN runs, several hypothetical cases were calculated explicitly. It was found that for a beam polarization change of 0.05 between an UP and a DOWN run, the error introduced in measuring the analyzing power using the method described above was less than 0.0003. Even for a change in beam polarization of 0.10, the error introduced was only about 0.001. It is concluded that the continuous monitoring of beam polarization as done for these measurements will give accurate results, even with a fluctuating beam polarization. In fact, continuous monitoring of the beam polarization is seen to be a very powerful addition to any polarization experiment.

Chapter VI

T(p,d)D RESULTS AND ANALYSIS

A. Polarization - Asymmetry Relation

According to the polarization - asymmetry theorem, the analyzing power from a nuclear reaction induced by polarized spin 1/2 particles equals the polarization of the particles produced in the inverse reaction at the same center of mass energy. This was shown by Satchler (1958) to be valid for interactions involving spin polarization moments of any order (with possible sign changes) provided time reversal invariance is satisfied. Biedenharn (1959) has shown that the theorem is true for the more general situation where the interaction obeys reciprocity and not time-reversibility. This distinction is important in a scattering process involving both elastic and inelastic processes. Since the reaction and its inverse involve a loss of particles to the inelastic channels, the two processes are clearly not time inverses, but they do obey reciprocity, i.e., the scattering matrix is symmetric. From this theorem it is evident that the analyzing power in the T(p,d)D reaction is identical to the proton polarization in the D(d,p)T reaction at the same c.m. energy.

B. Results and Fits to Data

Experimental Results. -- Angular distributions of the analyzing power in T(p,d)D were obtained at average proton bombarding energies (corrected for energy loss in the target) of 6.7, 7.4, 8.0, 9.4, 10.7, 12.0, 13.4, and 14.7 MeV. The values are listed in Table 2. In order to facilitate comparison with previous D(d,p)T polarization data and with the mirror reaction $D(d,n)^3He$, it is convenient to convert the proton bombarding energies for T(p,d)D to equivalent deuteron bombarding energies for D(d,p)T. The relation is:

$$E_d = 2.0\,(\,0.75\,E_p - 4.03\,) \qquad (23)$$

The headings in Table 2 also give the equivalent deuteron bombarding energies, and in the following discussion, the present analyzing power results will be referred to as D(d,p)T proton polarizations at these energies. Data were recorded for the forward hemisphere only since the identity of the deuterons requires the polarization to be antisymmetric about 90 degrees in the center of mass. The errors listed are statistical. There is an additional overall normalization error of 2 per cent as discussed in Chapter V.

The T(p,d)D analyzing powers are plotted in Figure 11 as proton polarizations at the equivalent deuteron bombarding energies. The lines through the data are derived from associated Legendre polynomial fits to the differential polarization and are discussed in the next section. Figure 12 compares these data (dark circles) at three energies with earlier proton polarization values (open circles) obtained by double scattering (Porter and Haeberli, 1967). In general, their data agrees well with the present results, although there is considerable scatter in the earlier data because of the poorer statistics. The recent

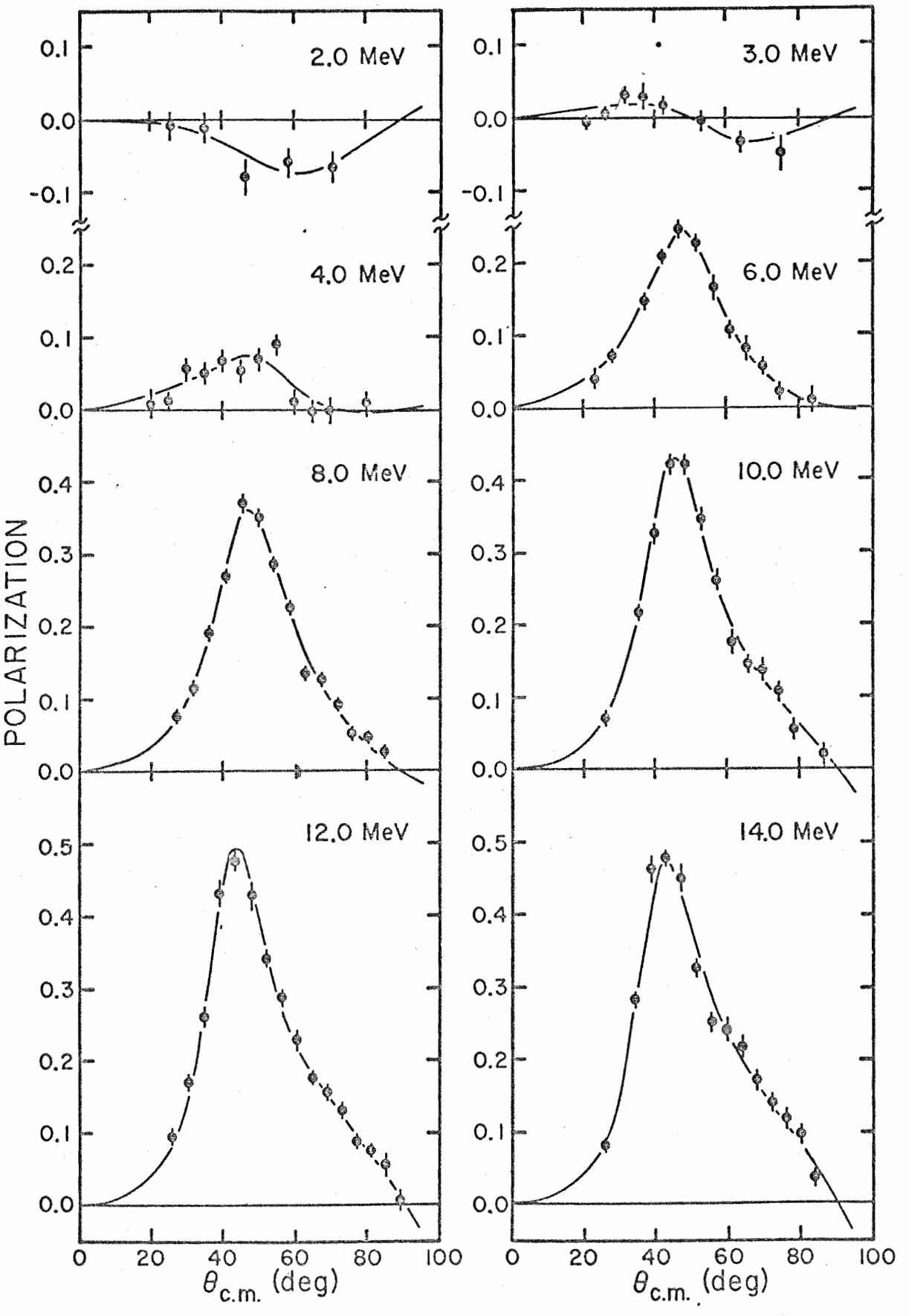

Figure 11. T(p,d)D Analyzing Power Data and Fits

TABLE 2

ANALYZING POWER DATA FOR T(P,D)D

T(P,D)D ANALYZING POWER 6.7 MEV
D(D,P)T POLARIZATION 2.Ø MEV

LAB ANGLE	C M ANGLE	ANALYZING POWER	ERROR
11.Ø	25.4	-Ø.ØØ9	Ø.Ø19
15.Ø	34.7	-Ø.Ø12	Ø.Ø19
2Ø.Ø	46.4	-Ø.Ø79	Ø.Ø25
25.Ø	58.4	-Ø.Ø58	Ø.Ø21
3Ø.Ø	7Ø.6	-Ø.Ø67	Ø.Ø18

T(P,D)D ANALYZING POWER 7.4 MEV
D(D,P)T POLARIZATION 3.Ø MEV

LAB ANGLE	C M ANGLE	ANALYZING POWER	ERROR
1Ø.Ø	21.2	-Ø.ØØ7	Ø.ØØ9
12.5	26.5	Ø.ØØ5	Ø.Ø12
15.Ø	31.8	Ø.Ø31	Ø.Ø13
17.5	37.1	Ø.Ø28	Ø.Ø18
2Ø.Ø	42.4	Ø.Ø16	Ø.Ø13
25.Ø	53.1	-Ø.ØØ6	Ø.Ø17
3Ø.Ø	63.8	-Ø.Ø33	Ø.Ø15
35.Ø	74.7	-Ø.Ø49	Ø.Ø25

T(P,D)D ANALYZING POWER 8.Ø MEV
D(D,P)T POLARIZATION 4.Ø MEV

LAB ANGLE	C M ANGLE	ANALYZING POWER	ERROR
1Ø.Ø	2Ø.1	Ø.ØØ8	Ø.Ø19
12.5	25.1	Ø.Ø12	Ø.Ø12
15.Ø	3Ø.1	Ø.Ø57	Ø.Ø14
17.5	35.1	Ø.Ø5Ø	Ø.Ø15
2Ø.Ø	4Ø.1	Ø.Ø67	Ø.Ø15
22.5	45.2	Ø.Ø53	Ø.Ø15
25.Ø	5Ø.2	Ø.Ø69	Ø.Ø17
27.5	55.2	Ø.Ø9Ø	Ø.Ø14
3Ø.Ø	6Ø.2	Ø.Ø1Ø	Ø.Ø17
32.5	65.2	-Ø.ØØ3	Ø.Ø16
35.Ø	7Ø.3	-Ø.ØØ2	Ø.Ø15
4Ø.Ø	8Ø.3	Ø.Ø67	Ø.Ø16

TABLE 2--CONTINUED

T(P,D)D ANALYZING POWER 9.4 MEV
D(D,P)T POLARIZATION 6.Ø MEV

LAB ANGLE	C M ANGLE	ANALYZING POWER	ERROR
12.5	23.6	Ø.Ø41	Ø.Ø15
15.Ø	28.3	Ø.Ø72	Ø.ØØ9
2Ø.Ø	37.7	Ø.145	Ø.Ø12
22.5	42.3	Ø.2Ø8	Ø.Ø1Ø
25.Ø	47.Ø	Ø.244	Ø.Ø12
27.5	51.7	Ø.226	Ø.Ø13
3Ø.Ø	56.3	Ø.165	Ø.Ø17
32.5	61.Ø	Ø.1Ø7	Ø.Ø12
35.Ø	65.6	Ø.Ø8Ø	Ø.Ø17
37.5	7Ø.2	Ø.Ø56	Ø.Ø13
4Ø.Ø	74.7	Ø.Ø18	Ø.Ø12
45.Ø	83.8	Ø.ØØ9	Ø.Ø18

T(P,D)D ANALYZING POWER 1Ø.7 MEV
D(D,P)T POLARIZATION 8.Ø MEV

LAB ANGLE	C M ANGLE	ANALYZING POWER	ERROR
15.Ø	27.3	Ø.Ø77	Ø.ØØ7
17.5	31.8	Ø.114	Ø.ØØ9
2Ø.Ø	36.3	Ø.192	Ø.Ø1Ø
22.5	4Ø.8	Ø.268	Ø.Ø1Ø
25.Ø	45.4	Ø.371	Ø.Ø12
27.5	49.8	Ø.348	Ø.Ø12
3Ø.Ø	54.3	Ø.284	Ø.Ø11
32.5	58.7	Ø.223	Ø.Ø1Ø
35.Ø	63.2	Ø.136	Ø.Ø1Ø
37.5	67.6	Ø.124	Ø.ØØ8
4Ø.Ø	71.9	Ø.Ø91	Ø.ØØ8
42.5	76.2	Ø.Ø52	Ø.ØØ8
45.Ø	8Ø.6	Ø.Ø47	Ø.ØØ8
47.5	84.8	Ø.Ø24	Ø.Ø1Ø

T(P,D)D ANALYZING POWER 12.Ø MEV
D(D,P)T POLARIZATION 1Ø.Ø MEV

LAB ANGLE	C M ANGLE	ANALYZING POWER	ERROR
15.Ø	26.7	Ø.Ø72	Ø.Ø1Ø
2Ø.Ø	35.5	Ø.216	Ø.Ø12
22.5	39.9	Ø.323	Ø.Ø14
25.Ø	44.3	Ø.42Ø	Ø.Ø16
27.5	48.6	Ø.421	Ø.Ø16
3Ø.Ø	53.Ø	Ø.347	Ø.Ø18

TABLE 2--CONTINUED

32.5	57.3	Ø.26Ø	Ø.Ø15
35.Ø	61.6	Ø.175	Ø.Ø17
37.5	65.9	Ø.146	Ø.Ø13
4Ø.Ø	7Ø.1	Ø.138	Ø.Ø16
42.5	74.4	Ø.1Ø7	Ø.Ø12
45.Ø	78.5	Ø.Ø53	Ø.Ø16
5Ø.Ø	86.7	Ø.Ø19	Ø.Ø15

T(P,D)D ANALYZING POWER 13.4 MEV
D(D,P)T POLARIZATION 12.Ø MEV

LAB ANGLE	C M ANGLE	ANALYZING POWER	ERROR
15.Ø	26.2	Ø.Ø94	Ø.Ø1Ø
17.5	3Ø.6	Ø.17Ø	Ø.Ø13
2Ø.Ø	34.9	Ø.259	Ø.Ø12
22.5	39.2	Ø.43Ø	Ø.Ø2Ø
25.Ø	43.5	Ø.473	Ø.Ø15
27.5	47.8	Ø.427	Ø.Ø21
3Ø.Ø	52.Ø	Ø.34Ø	Ø.Ø13
32.5	56.3	Ø.283	Ø.Ø12
35.Ø	6Ø.5	Ø.227	Ø.Ø14
37.5	64.7	Ø.174	Ø.Ø11
4Ø.Ø	68.8	Ø.154	Ø.Ø12
42.5	73.Ø	Ø.131	Ø.Ø11
45.Ø	77.Ø	Ø.Ø87	Ø.Ø09
47.5	81.1	Ø.Ø74	Ø.Ø11
5Ø.Ø	85.1	Ø.Ø56	Ø.Ø16
52.5	89.Ø	Ø.ØØ5	Ø.Ø14

T(P,D)D ANALYZING POWER 14.7 MEV
D(D,P)T POLARIZATION 14.Ø MEV

LAB ANGLE	C M ANGLE	ANALYZING POWER	ERROR
15.Ø	25.9	Ø.Ø8Ø	Ø.ØØ9
2Ø.Ø	34.4	Ø.279	Ø.Ø12
22.5	38.7	Ø.4ØØ	Ø.Ø19
25.Ø	43.Ø	Ø.474	Ø.Ø11
27.5	47.2	Ø.447	Ø.Ø2Ø
3Ø.Ø	51.4	Ø.326	Ø.Ø13
32.5	55.6	Ø.252	Ø.Ø16
35.Ø	59.7	Ø.24Ø	Ø.Ø17
37.5	63.8	Ø.217	Ø.Ø17
4Ø.Ø	68.Ø	Ø.169	Ø.Ø15
42.5	72.Ø	Ø.141	Ø.Ø13
45.Ø	76.Ø	Ø.118	Ø.Ø14
47.5	8Ø.Ø	Ø.Ø94	Ø.Ø13
5Ø.Ø	83.9	Ø.Ø36	Ø.Ø12

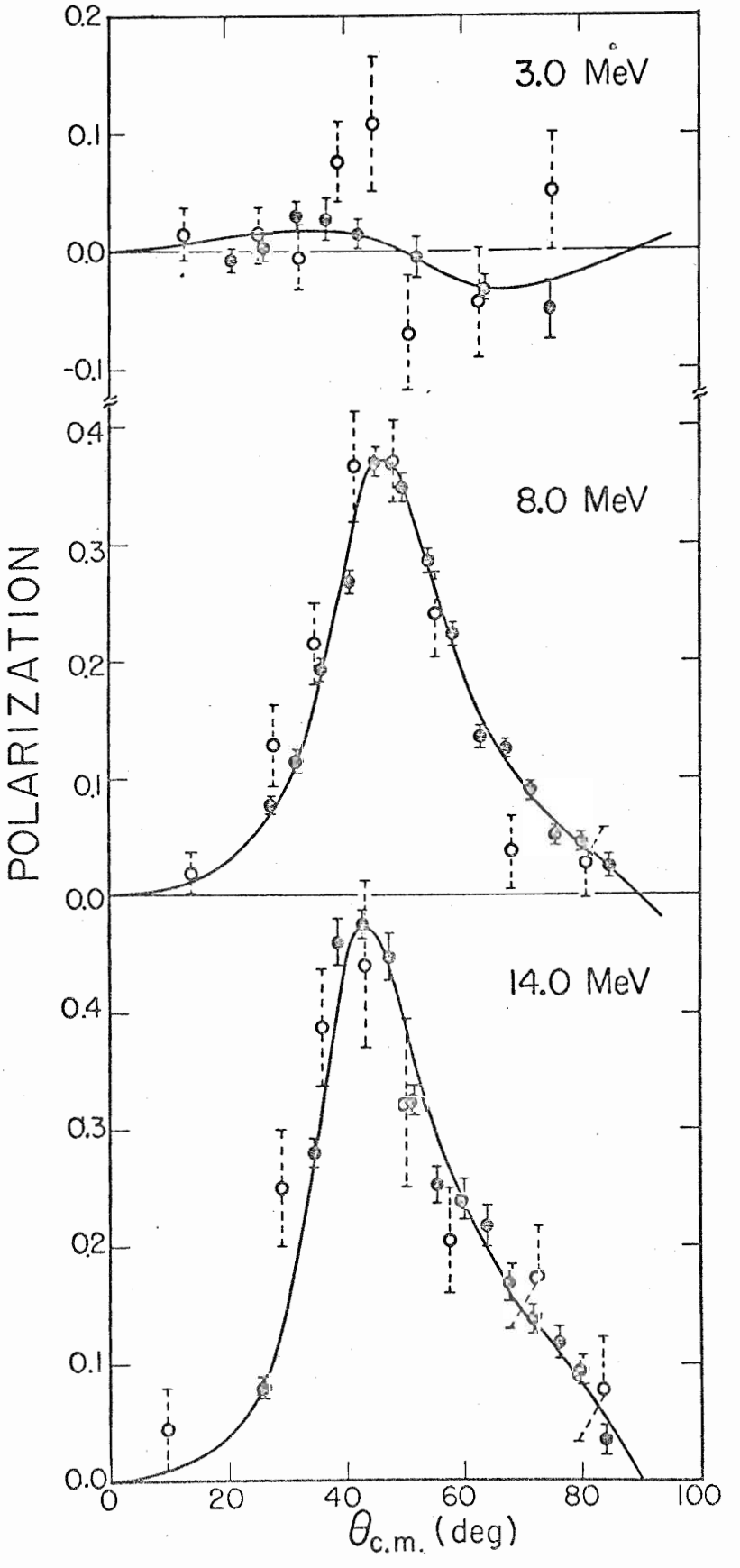

Figure 12. Comparisons of T(p,d)D and D(d,p)T Data

proton polarization data of Dietze and Lorenzen (1970), however, does not agree past 35 degrees c.m. at 2.0 MeV, the only energy of overlap between experiments.

Fits to the Data. -- The differential cross section for a reaction can be expressed by a sum of Legendre polynomials (Simon and Welton, 1953).

$$\sigma(\theta) = \sum_{L=0}^{L_{max}} c_L P_L(\cos\theta) \tag{24}$$

Similarly, the product of the differential cross section and the polarization, called the differential polarization $\pi(\theta)$, can be expressed as a series of associated Legendre polynomials.

$$\pi(\theta) = \sigma(\theta) P(\theta) = \sum_{L=1}^{L_{max}} a_L P_L^1(\cos\theta) \tag{25}$$

The coefficients in the above expressions are made up of rather complicated combinations of elements of the scattering matrix and angular momentum coefficients. The maximum value of L is related by the complexity rule to the highest value of angular momentum contributing to the reaction (Simon and Welton, 1953; Haeberli, 1963). The symmetry of $\sigma(\theta)$ and the antisymmetry of $P(\theta)$ about 90 degrees due to identical particles require that the odd coefficients in Equations (24) and (25) vanish.

The D(d,p)T differential cross sections from 6 to 14 MeV have been reported by Brolley et al. (1957). Legendre coefficients were obtained by these authors for data at deuteron bombarding energies from 1.4 to 14 MeV. Porter and Haeberli (1967) fitted both the existing cross section data and their own polarization data in an energy dependent analysis by expressing the energy dependence of the coefficients in a power series in E. Polarizations calculated with their π coefficients give an unsatisfactory fit to the present

data in view of the much smaller errors obtained here. It was desirable, therefore, to perform a new analysis in order to parameterize the present results and possibly deduce information on the complexity of the reaction.

The analysis was done using the TUNL computer and the code POLN originally written by Spalek (1971). Because of difficulties in determining the effect of changing search parameters, the code was rewritten for this analysis to provide on-line display of cross section, polarization, and differential polarization data and calculated values. In its present form, POLN also allows a set of calculations to be saved along with the experimental data for comparison with subsequent calculations. In addition, there is increased flexibility in the input and line printer output. The fit to the polarization at each energy was obtained in the following way:

The $\sigma(\theta)$ values were calculated at the experimental $P(\theta)$ angles from the σ Legendre coefficients of Porter and Haeberli (1967). Their energy dependent formula for σ coefficients is believed to be the best parameterization of cross section data in this energy range and was therefore used throughout the present analysis. The product of σ and P were taken and the resulting $\pi(\theta)$ values were fitted with a sum of associated Legendre polynomials. The resulting coefficients were then used to calculate π which was divided by σ at each angle to obtain the calculated value for P. It can be seen, therefore, that the calculated P is intimately connected to the σ values. Investigation showed that the quality of the fit to the polarization data was greatly influenced by the experimental σ values, the number of coefficients used to describe σ, and the errors assigned to these coefficients. In general, these quantities affected the fit to P as much as the number of π coefficients used. This made a determination of the complexity of the reaction subject to many ambiguities. Adding to this difficulty was the fact that neither

Brolley et al. nor Porter and Haeberli assigned errors to their coefficients for σ. In order to make reasonable assignments to these errors, POLN was used to fit the σ data of Brolley et al. at 12 MeV. The errors for the coefficients obtained from the $\sigma(\theta)$ fit at 12 MeV were used for the σ coefficient errors at all energies. These errors are used in the program to calculate errors in $\sigma(\theta)$ which contribute to the errors in $\pi(\theta)$. The fits to π and P were then calculated as described above for from 1 to 6 associated Legendre polynomials.

The following criteria were used to decide on the number of coefficients to use for the final fits:

(a) Chi-square per degree of freedom for $\pi(\theta)$

(b) Total chi-square and chi-square per degree of freedom for $P(\theta)$

(c) Errors assigned by the search routine to the coefficients

(d) Observed fit to the polarization

For the D(d,p)T differential polarization distributions from 2 to 10 MeV, the above criteria pointed to a need for only two coefficients. For the 12 and 14 MeV distributions, (a) and (b) indicated a preference for four coefficients. However, (c) and (d) did not seem to warrant this rather unphysical jump from two to four coefficients. The third and fourth coefficients were small, and there was no indication of a trend with increasing energy. The major change in the observed fit with their inclusion was a slightly better fit near the peak at 12 MeV and on the back slope at 14 MeV. Changes to the fit of similar proportions could be obtained, for example, by using different errors for the σ coefficients input for the fit. It is concluded, therefore, that two coefficients produce an acceptable fit to the present data from 2 to 14 MeV. Table 3 lists the associated Legendre coefficients obtained at each energy along with the values of chi-square per degree of freedom for both the differential polarization and the polarization. These

Table 3

Associated Legendre Coefficients for D(d,p)T

E_d	a_2	a_4	$\pi(\theta)$ χ^2/deg	$P(\theta)$ χ^2/deg
2.0	-0.202 ± 0.048	0.030 ± 0.036	1.2	1.2
3.0	0.002 ± 0.025	0.076 ± 0.022	1.5	1.5
4.0	0.187 ± 0.018	0.094 ± 0.018	1.7	1.7
6.0	0.470 ± 0.013	0.140 ± 0.014	0.4	0.4
8.0	0.589 ± 0.011	0.075 ± 0.009	1.1	1.3
10.0	0.615 ± 0.013	0.033 ± 0.012	0.8	1.0
12.0	0.673 ± 0.012	0.036 ± 0.010	0.7	0.9
14.0	0.720 ± 0.014	0.027 ± 0.012	1.5	2.1

coefficients are plotted in the next section (Figure 14) along with the coefficients for the $D(d,n)^3He$ reaction.

Discussion of results. -- The need for only two associated Legendre polynomials to describe the reaction up to 14 MeV is somewhat surprising in view of the increased accuracy of the present data over earlier results. Porter and Haeberli (1967) in their energy dependent analysis found a need for the third coefficient above about 8 MeV. Also, fits to the cross section for both D(d,p)T and $D(d,n)^3He$ require 5 or 6 Legendre coefficients over the same energy range. The cross sections, however, display sharper structure than the differential polarizations, and it is easy to see how more coefficients are needed to reproduce this structure. The opposite trends of the cross section and polarization yield a rather smooth angular dependence of $\pi(\theta)$. Plots of the differential

polarization for the $D(d,n)^3He$ reaction, which are similar in shape to those for the D(d,p)T reaction, are given by Purser et al. (1965) and by Spalek et al. (1971). Spalek et al. also found no need for more than two coefficients to describe the neutron data for energies below 14 MeV.

The complexity rule which limits the number of coefficients in the sum (Equation 25) states that L_{max} must be less than or equal to twice the value of the incoming or outgoing orbital angular momentum (ℓ, ℓ') and the total angular momentum J. The D(d,p)T reaction is expected to proceed mainly through singlet channel spin states (see Chapter VII); thus ℓ, ℓ', and J are equal. The need for two coefficients (a_2 and a_4 because only even values contribute) therefore implies that only partial waves up to $\ell = 2$ contribute to the reaction. The need for six coefficients to fit the cross sections, however, implies $\ell_{max} = 5$. The reason for this difference is not understood, but it may be caused by different sensitivities to higher order polynomials for the $\sigma(\theta)$ and $\pi(\theta)$ fits.

C. Comparison with $D(d,n)^3He$ Data and Conclusion

General remarks. -- On the basis of charge independence of nuclear forces, one expects the same cross sections and polarizations in mirror reactions after corrections are made for Coulomb effects. It was pointed out by Barschall (1966) that there were several cases in light nuclei where available data showed the proton polarizations to be larger than the neutron polarizations in the mirror reaction. Since that time, more accurate data have reduced the differences in some of these reactions, but many of the differences are still believed to be real (Taylor et al., 1970; Mutchler et al., 1971; R. K. Walter,

1970). All previous comparisons of the neutron and proton polarizations from the D(d,p)T and D(d,n)^{3}He reactions have consistently shown the proton polarizations to be larger by a factor of 1.4 to 1.15 (Barschall, 1966; Porter and Haeberli, 1967; Spalek et al., 1970).

Comparison at same bombarding energies. -- In Figure 13, the present data are compared to the most recent neutron polarization data in the D(d,n)^{3}He reaction from 6 to 14 MeV. The dark circles are the proton polarizations and the crosses are the neutron polarizations from Spalek et al. (1970). The lines are from associated Legendre fits to the proton data as in Figure 11. The comparison here is at the same deuteron bombarding energy, as is customarily done. It is seen that the differences in the two polarizations are real when compared in this manner, but are decreasing as the energy increases. In fact, at 14 MeV, all of the neutron data except the peak point are within one standard deviation of the fit to the proton data. The differences at lower energies, however, are too large to be attributed to experimental errors.

Vector and tensor analyzing powers. -- Recently, experimentors have been looking for similar differences in the vector and tensor analyzing powers in D($\vec{d}$,p)T and D($\vec{d}$,n)^{3}He. Vector analyzing power measurements at 10 MeV (Bernstein et al., 1969) and at 12.3 MeV (Blyth et al., 1971) showed no differences in the two reactions. Grüebler et al. (1971) performed accurate measurements of the vector and tensor analyzing powers at 10.0 and 11.5 MeV. They found a difference between D($\vec{d}$,p)T and D($\vec{d}$,n)^{3}He only in T_{20}. No differences outside the experimental errors existed for iT_{11}, T_{21}, or T_{22}. Recently, however, very accurate measurements of iT_{11} by Hilscher and Liers (1971) at 10 MeV showed a small but significant difference at back angles. No theoretical explanation or predictions for the behavior of these spin-dependent parameters have appeared as yet.

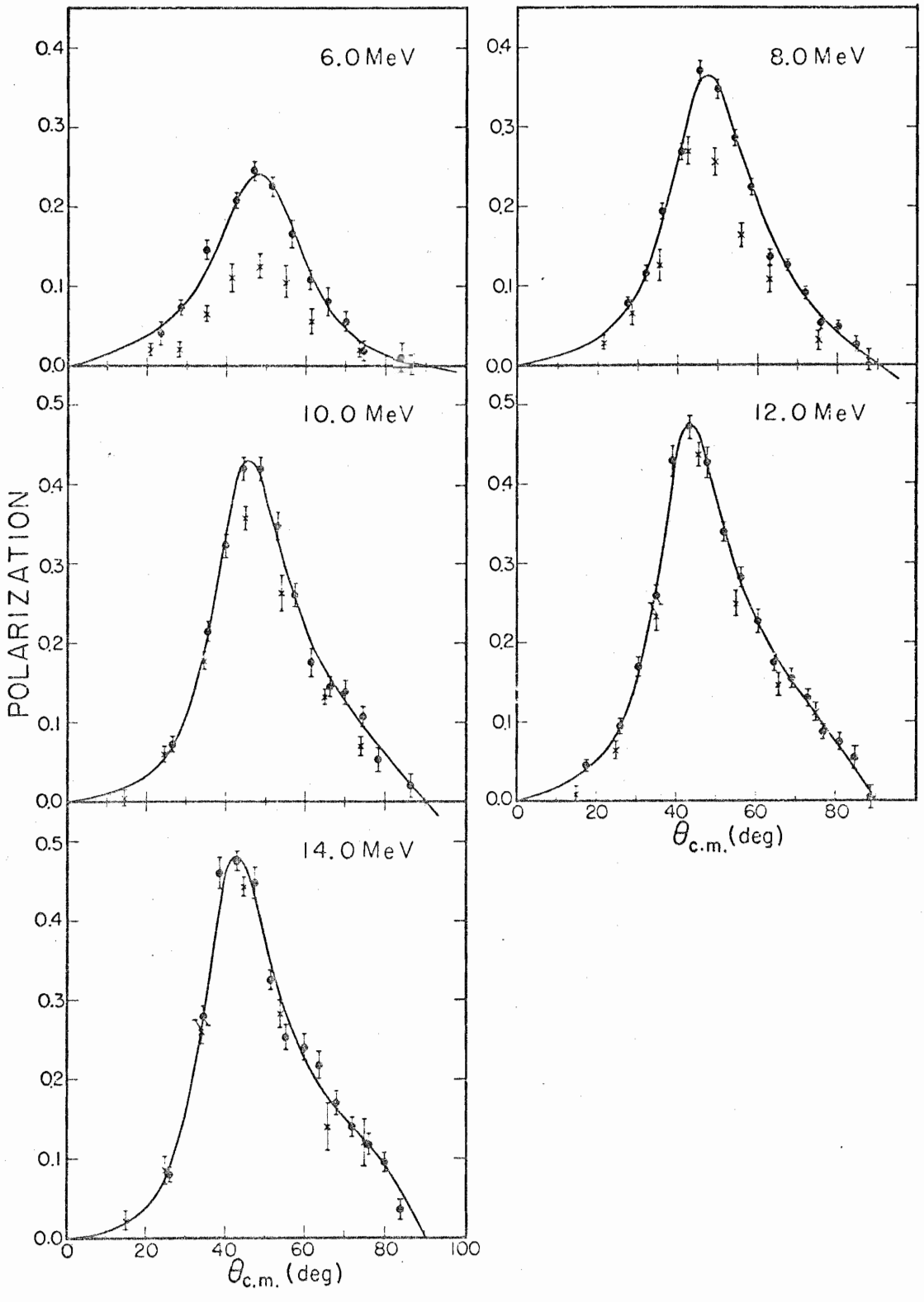

Figure 13. Comparisons of D(d,p)T and D(d,n)^{3}He Polarizations at Same Bombarding Energies

Comparison at same exit channel energies. -- In light nuclei, Coulomb effects are expected to be small. Indeed, the differential cross sections for D(d,p)T and D(d,n)^{3}He show identical shapes and differ in magnitude only slightly at forward angles (Brolley et al., 1957). The Coulomb energy of the two protons in ^{3}He, however, is responsible for a difference in Q-values for the two reactions. These Q-values are +3.269 MeV for D(d,n)^{3}He and +4.033 MeV for D(d,p)T. When the neutron and proton polarizations are compared at the same deuteron bombarding energies, one is neglecting the difference of 764 keV in the center of mass exit channel energies. When the kinematic factors are taken into account, it is seen that deuteron bombarding energies about 1.53 MeV lower in the D(d,p)T reaction give the same center of mass energies in the exit channels. In Figure 14, the two reactions are compared in this new way by plotting the associated Legendre coefficients obtained from fits to the differential polarizations. The dark circles are the D(d,p)T coefficients from Table 3. The open circles are D(d,n)^{3}He coefficients obtained by Purser et al. (1965) and Spalek et al. (1971) shifted in energy 1.53 MeV. The lines are drawn through the proton points for purposes of interpolation. Within the errors of the coefficients, the reactions are seen to be identical over the entire energy range measured when compared at the same exit channel energies.

To make the comparison more direct, the D(d,n)^{3}He polarization data from 3 to 14 MeV (Purser et al., 1965; Spalek et al., 1970) are shown in Figure 15 with calculated curves from the D(d,p)T coefficients. The coefficients for these curves were interpolated from the lines in Figure 14 at energies corresponding to the same exit channel energies as the D(d,n)^{3}He data. The excellent agreement between these curves and the neutron data demonstrates that the two mirror reactions do have identical polarizations when compared in this manner.

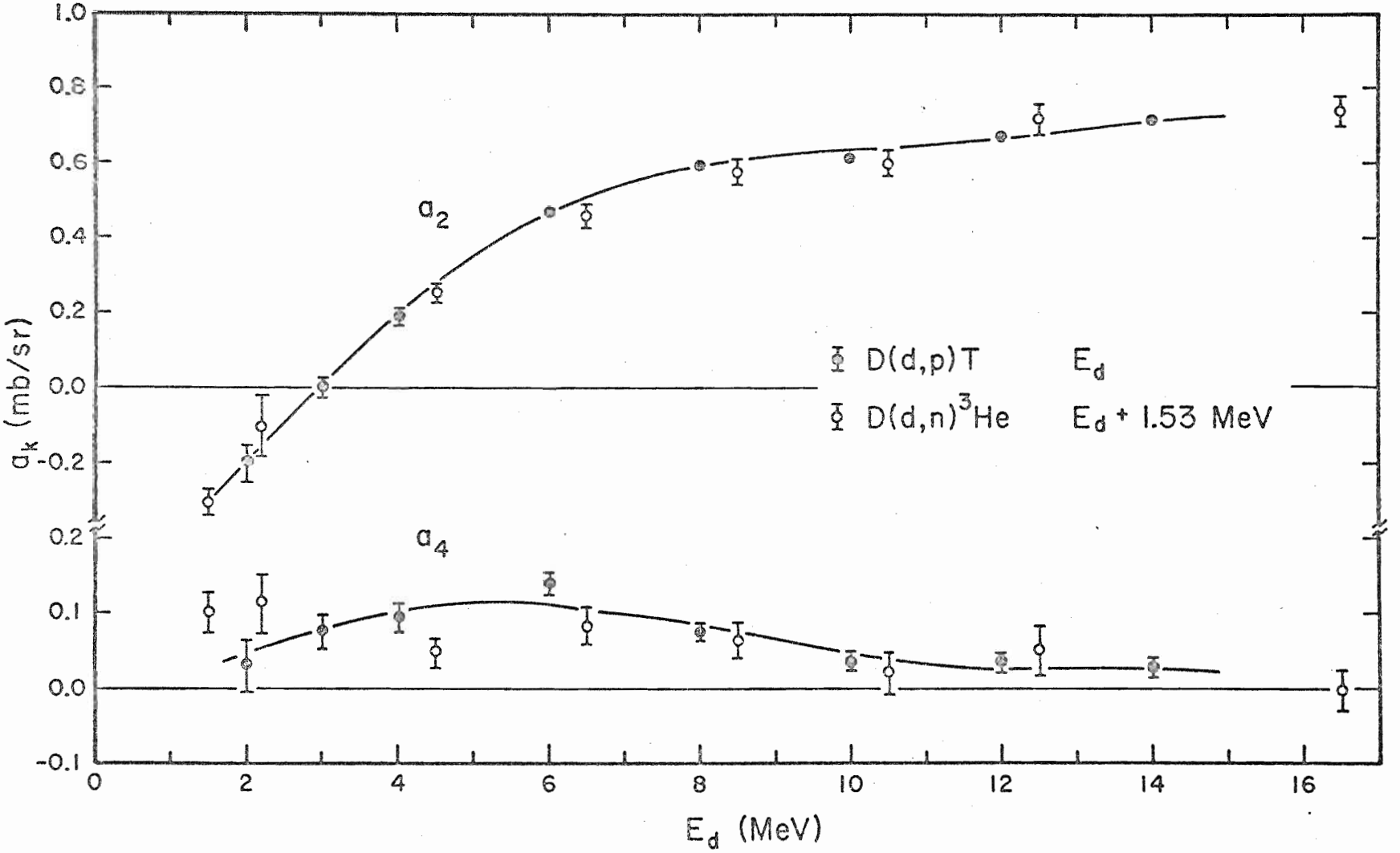

Figure 14. Comparisons of Associated Legendre Coefficients for D(d,p)T and D(d,n)^{3}He

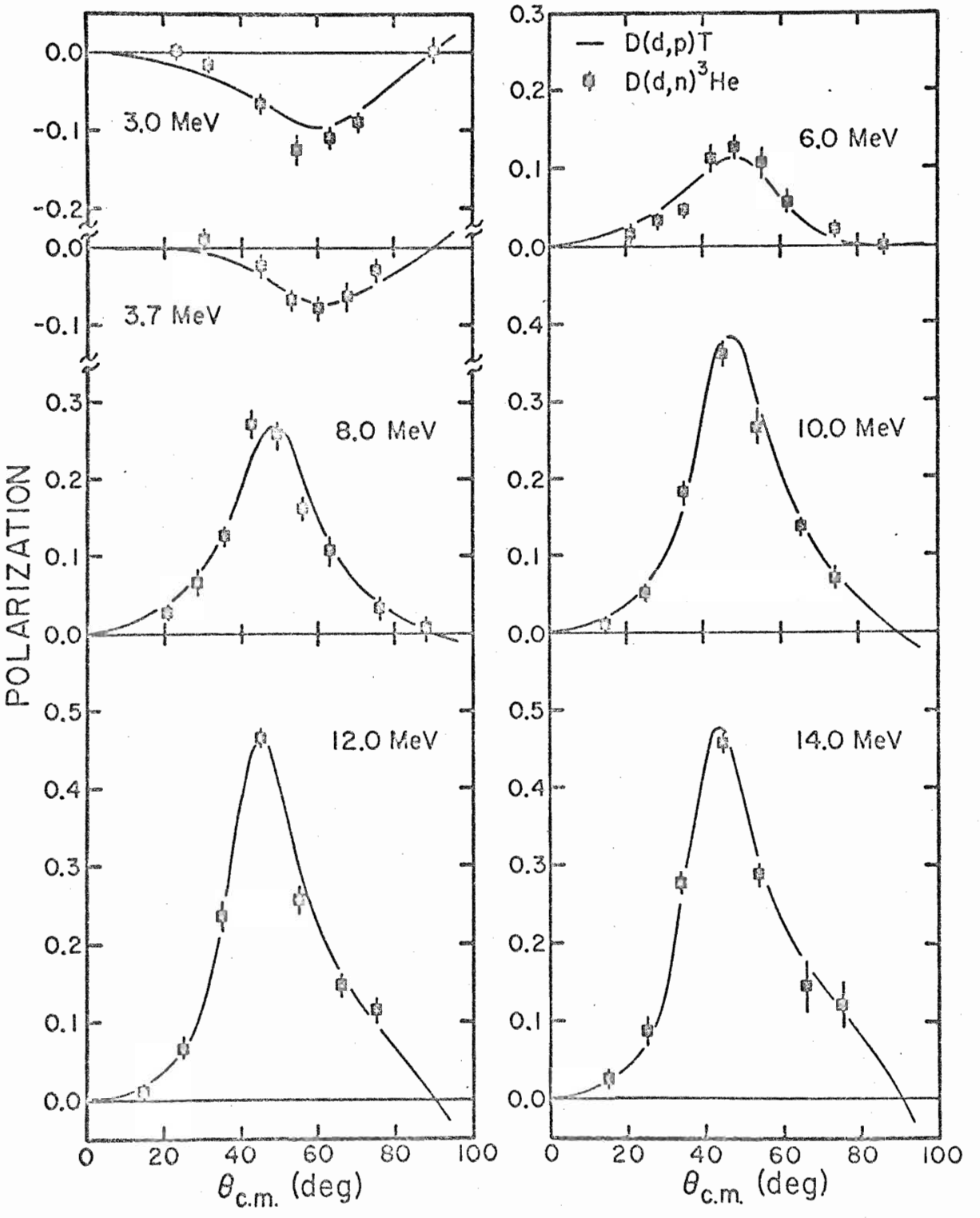

Figure 15. Comparisons of D(d,p)T and D(d,n)^{3}He Polarizations at Same Exit Channel Energies

Conclusion. -- There is some justification for comparing the two reactions at the same exit channel energies. If the reaction mechanism is primarily $\ell = 0$ stripping, direct reaction theory tells us that the polarizations result only from spin dependent distortions in the entrance and exit channels. The very low polarizations seen for d-d elastic scattering (Bernstein et al., 1969; Plattner and Keller, 1969; Arvieux et al., 1966) indicate that spin effects in the entrance channel are weak. Thus, the polarizations in the D(d,p)T and D(d,n)^{3}He reactions are most likely caused by spin dependent distortions in the exit channels. One would expect that these distortions are nearly the same for the same exit channel energies, and the D(d,p)T and D(d,n)^{3}He polarizations support this argument.

One might also expect, however, that the elastic scattering polarizations from T(p,p)T and ^{3}He(n,n)^{3}He should be identical. The T(p,p)T polarizations are known quite accurately (see Chapter VII), but ^{3}He(n,n)^{3}He polarization data are scarce and have fairly large statistical errors, i.e., on the order of ± 0.06. Figure 16 shows a comparison of the ^{3}He(n,n)^{3}He data at 8 MeV (Behof et al., 1966) and at 12 MeV (Büsser et al., 1969) with the T(p,p)T polarizations. The 8 MeV T(p,p)T data is from Erlangen (Kankowski et al., 1971) and the 12 MeV data is from the present work. The differences observed in these data could be experimental, but the quoted error bars do not even overlap at the peaks. Thus it seems that some differences in the elastic scattering polarizations do exist. Indeed, significant changes were observed in the polarizations calculated from the T(p,p)T phase shifts (Chapter VII) when the Coulomb interaction was removed. Perhaps these differences do not appear in the exit channel spin dependent distortions for D(d,p)T and D(d,n)^{3}He because the interaction radius is larger for a stripping type reaction than

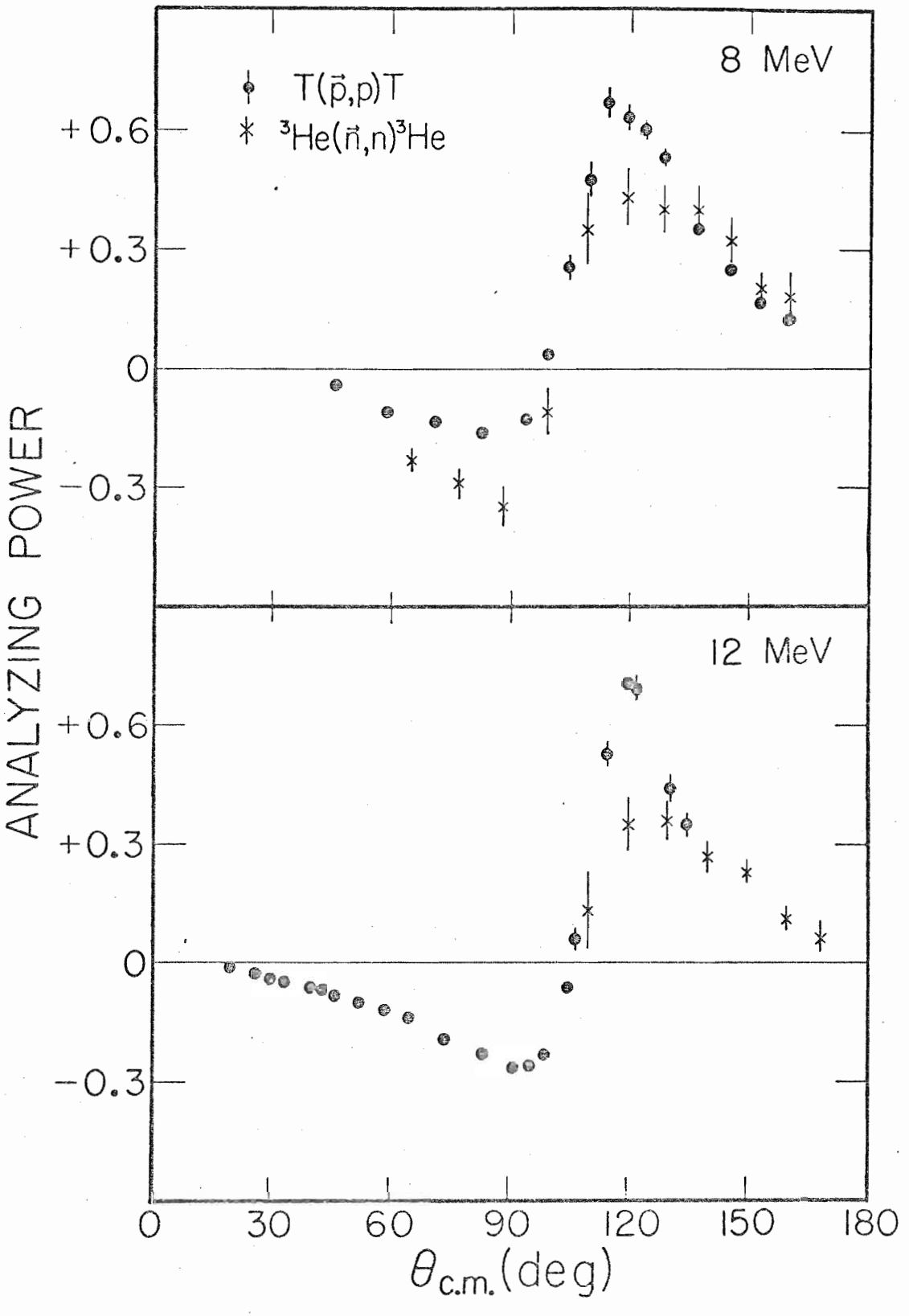

Figure 16. Comparisons of T(p,p)T and ^{3}He(n,n)^{3}He Polarization Data

for elastic scattering. Accurate $^{3}He(n,n)^{3}He$ polarization data would be useful in investigating this question further.

For comparisons of the vector and tensor analyzing powers, the situation is more complex. In this case the spin dependent distortions in the entrance channel can probably not be neglected. Also, the orientation of the deuterons may affect the average interaction radius and energy dependent effects may thus be different for the vector and various tensor polarizations. The present data of Gruebler et al. (1971) show differences between $D(\vec{d},p)T$ and $D(\vec{d},n)^{3}He$ only in T_{20} when compared at the same deuteron energies. Comparing their data at the same exit channel energies in the two reactions brings T_{20} into agreement but then the iT_{11} data do not agree. Accurate data over a broad energy range would be useful in helping to unravel this complex interaction. In any case, it seems premature to suggest that the differences observed in the mirror reactions $D(d,p)T$ and $D(d,n)^{3}He$ are an indication that charge independence is violated.

Chapter VII

T(p,p)T RESULTS AND ANALYSIS

A. Results and Comparison to Other Data

The values for the T(p,p)T analyzing power for incident proton energies of 6.7, 7.4, 8.0, 9.4, 10.7, 12.0, 13.4, and 14.7 MeV are listed in Table 4. Data were obtained by detecting either forward scattered protons or the tritons recoiling into the forward hemisphere. The data were recorded simultaneously with the T(p,d)D data and have very small statistical errors since the cross section for elastic scattering is about a factor of 10 larger than the reaction cross section. The errors listed in Table 4 are statistical only; the normalization error is discussed in Chapter V. These data are the most accurate T(p,p)T polarizations presently available. The three lower energy distributions are incomplete, and the values are included in Table 5 only for documentation. These partial distributions were not included in the analysis discussed later. Figure 17 shows the five higher energy angular distributions. The solid lines are phase shift fits which will be described in the next section. The principal features of the distributions are a relatively constant positive peak near 120 degrees c.m. and a negative peak near 90 degrees c.m. that is deepening with increasing energy.

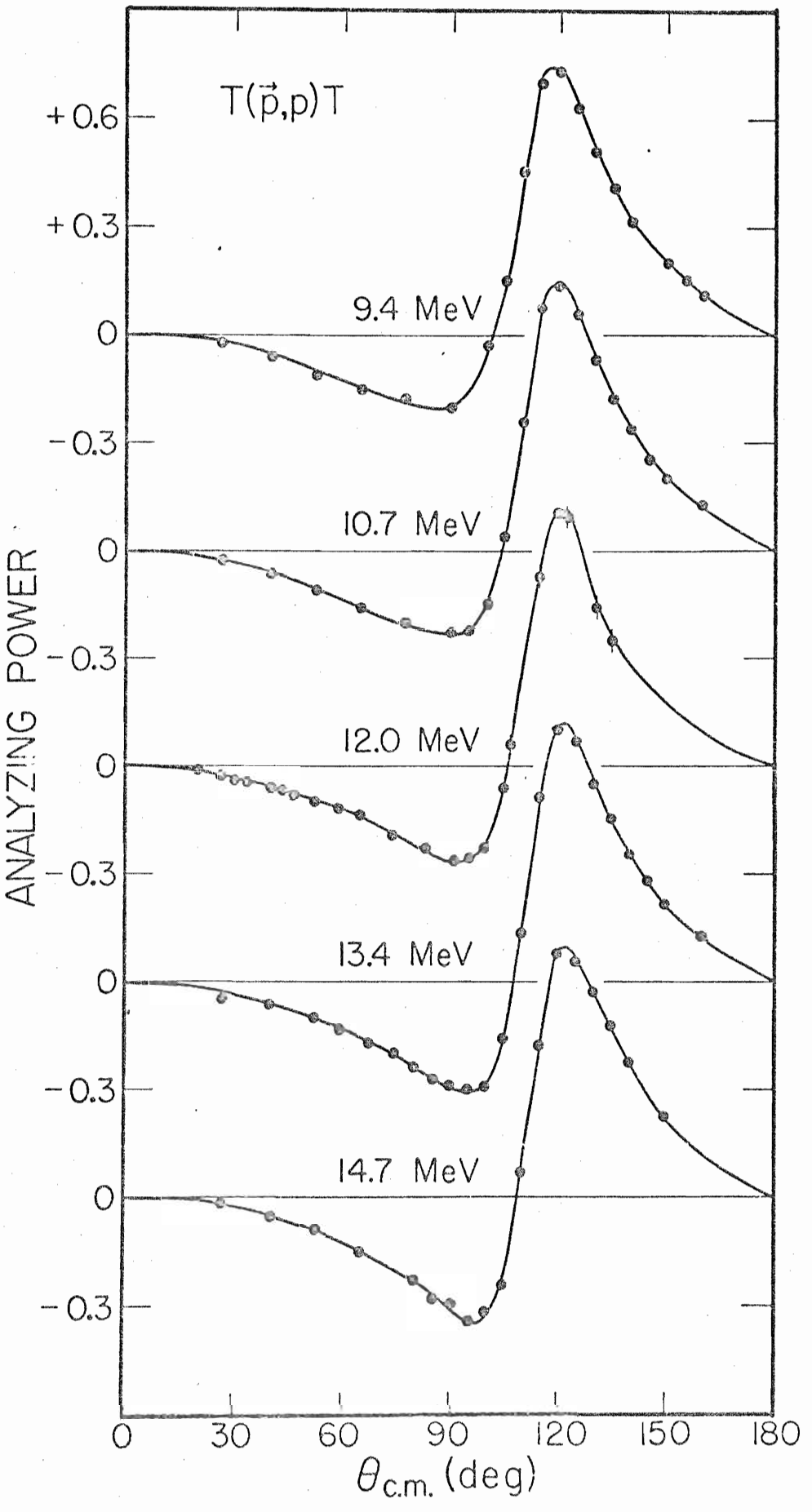

Figure 17. T(p,p)T Analyzing Power Data and Fits

TABLE 4

ANALYZING POWER DATA FOR T(P,P)T

T(P,P)T ANALYZING POWER 6.7 MEV

LAB ANGLE	C M ANGLE	ANALYZING POWER	ERROR
20.0	26.6	-0.017	0.005
25.0	33.2	-0.034	0.004
30.0	39.7	-0.056	0.004
30.0 *	120.0	0.624	0.006
25.0 *	135.0	0.523	0.006
20.0 *	140.3	0.295	0.006
15.0 *	150.0	0.193	0.005
11.0 *	158.0	0.127	0.006

T(P,P)T ANALYZING POWER 7.4 MEV

LAB ANGLE	C M ANGLE	ANALYZING POWER	ERROR
35.0 *	110.0	0.566	0.008
30.0 *	120.0	0.663	0.006
25.0 *	130.0	0.477	0.005
20.0 *	140.0	0.294	0.004
17.5 *	145.0	0.232	0.006
15.0 *	150.0	0.188	0.004
12.5 *	155.0	0.155	0.005
10.0 *	160.0	0.119	0.004

T(P,P)T ANALYZING POWER 8.0 MEV

LAB ANGLE	C M ANGLE	ANALYZING POWER	ERROR
40.0 *	100.0	0.667	0.008
35.0 *	110.0	0.529	0.008
32.5 *	115.0	0.682	0.007
30.0 *	120.0	0.677	0.007
27.5 *	125.0	0.586	0.005
25.0 *	130.0	0.470	0.006
22.5 *	135.0	0.379	0.005
20.0 *	140.0	0.298	0.005
17.5 *	145.0	0.240	0.005
15.0 *	150.0	0.176	0.005
12.5 *	155.0	0.158	0.005
10.0 *	160.0	0.105	0.008

* LAB ANGLE FOR RECOIL TRITON

TABLE 4--CONTINUED

T(P,P)T ANALYZING POWER 9.4 MEV

LAB ANGLE		C M ANGLE	ANALYZING POWER	ERROR
2Ø.Ø		26.6	-Ø.Ø22	Ø.Ø11
3Ø.Ø		39.7	-Ø.Ø61	Ø.Ø11
4Ø.Ø		52.5	-Ø.1Ø8	Ø.ØØ9
5Ø.Ø		64.9	-Ø.152	Ø.Ø1Ø
6Ø.Ø		76.9	-Ø.173	Ø.ØØ9
45.Ø	*	9Ø.Ø	-Ø.2Ø1	Ø.ØØ6
4Ø.Ø	*	1ØØ.Ø	-Ø.Ø31	Ø.ØØ7
37.5	*	1Ø5.Ø	Ø.152	Ø.ØØ9
35.Ø	*	11Ø.Ø	Ø.455	Ø.Ø12
32.5	*	115.Ø	Ø.7ØØ	Ø.ØØ7
3Ø.Ø	*	12Ø.Ø	Ø.732	Ø.ØØ8
27.5	*	125.Ø	Ø.63Ø	Ø.ØØ5
25.Ø	*	13Ø.Ø	Ø.51Ø	Ø.ØØ4
22.5	*	135.Ø	Ø.4Ø7	Ø.ØØ4
2Ø.Ø	*	14Ø.Ø	Ø.317	Ø.ØØ5
15.Ø	*	15Ø.Ø	Ø.2Ø4	Ø.ØØ4
12.5	*	155.Ø	Ø.154	Ø.ØØ7
1Ø.Ø	*	16Ø.Ø	Ø.1Ø9	Ø.ØØ6

T(P,P)T ANALYZING POWER 1Ø.7 MEV

LAB ANGLE		C M ANGLE	ANALYZING POWER	ERROR
2Ø.Ø		26.6	-Ø.Ø27	Ø.ØØ6
3Ø.Ø		39.7	-Ø.Ø63	Ø.ØØ4
4Ø.Ø		52.5	-Ø.1Ø7	Ø.ØØ5
5Ø.Ø		64.9	-Ø.157	Ø.ØØ7
6Ø.Ø		76.9	-Ø.2ØØ	Ø.ØØ6
45.Ø	*	9Ø.Ø	-Ø.223	Ø.ØØ4
42.5	*	95.Ø	-Ø.22Ø	Ø.ØØ5
4Ø.Ø	*	1ØØ.Ø	-Ø.149	Ø.ØØ5
37.5	*	1Ø5.Ø	Ø.Ø39	Ø.ØØ6
35.Ø	*	11Ø.Ø	Ø.357	Ø.ØØ8
32.5	*	115.Ø	Ø.675	Ø.ØØ7
3Ø.Ø	*	12Ø.Ø	Ø.738	Ø.ØØ6
27.5	*	125.Ø	Ø.659	Ø.ØØ5
25.Ø	*	13Ø.Ø	Ø.533	Ø.ØØ5
22.5	*	135.Ø	Ø.424	Ø.ØØ4
2Ø.Ø	*	14Ø.Ø	Ø.341	Ø.ØØ5
17.5	*	145.Ø	Ø.256	Ø.ØØ4
15.Ø	*	15Ø.Ø	Ø.2Ø4	Ø.ØØ4
1Ø.Ø	*	16Ø.Ø	Ø.127	Ø.ØØ4

* LAB ANGLE FOR RECOIL TRITON

TABLE 4--CONTINUED

T(P,P)T ANALYZING POWER 12.0 MEV

LAB ANGLE		C M ANGLE	ANALYZING POWER	ERROR
15.0		20.0	-0.011	0.003
20.0		26.6	-0.026	0.003
22.5		29.9	-0.039	0.003
25.0		33.2	-0.041	0.002
30.0		39.7	-0.057	0.003
32.5		42.9	-0.065	0.003
35.0		46.1	-0.081	0.004
40.0		52.5	-0.097	0.004
45.0		58.8	-0.116	0.005
50.0		65.0	-0.137	0.005
57.5		74.0	-0.193	0.006
65.0		82.8	-0.228	0.007
72.5		91.2	-0.262	0.011
42.5	*	95.0	-0.255	0.007
80.0		99.3	-0.228	0.015
37.5	*	105.0	-0.059	0.010
87.5		107.1	0.061	0.027
95.0		114.6	0.531	0.033
30.0	*	120.0	0.706	0.012
102.5		121.6	0.694	0.031
112.5		130.6	0.444	0.037
117.5		134.8	0.353	0.035

T(P,P)T ANALYZING POWER 13.4 MEV

LAB ANGLE		C M ANGLE	ANALYZING POWER	ERROR
20.0		26.6	-0.048	0.006
30.0		39.7	-0.061	0.006
40.0		52.5	-0.099	0.005
45.0		58.8	-0.133	0.006
52.0		67.4	-0.169	0.008
58.0		74.6	-0.194	0.009
50.0	*	80.0	-0.236	0.007
47.5	*	85.0	-0.270	0.005
45.0	*	90.0	-0.283	0.005
42.5	*	95.0	-0.298	0.006
40.0	*	100.0	-0.291	0.010
37.5	*	105.0	-0.155	0.009
35.0	*	110.0	0.135	0.013
32.5	*	115.0	0.513	0.011
30.0	*	120.0	0.700	0.011

* LAB ANGLE FOR RECOIL TRITON

TABLE 4--CONTINUED

LAB ANGLE		C M ANGLE	ANALYZING POWER	ERROR
27.5	*	125.0	0.670	0.013
25.0	*	130.0	0.549	0.008
22.5	*	135.0	0.457	0.009
20.0	*	140.0	0.354	0.006
17.5	*	145.0	0.280	0.007
15.0	*	150.0	0.217	0.006
10.0	*	160.0	0.127	0.005

T(P,P)T ANALYZING POWER 14.7 MEV

LAB ANGLE		C M ANGLE	ANALYZING POWER	ERROR
20.0		26.6	-0.016	0.005
30.0		39.7	-0.153	0.005
40.0		52.5	-0.088	0.006
50.0		65.8	-0.147	0.007
50.0	*	80.0	-0.231	0.005
47.5	*	85.0	-0.285	0.006
45.0	*	90.0	-0.294	0.007
42.5	*	95.0	-0.344	0.008
40.0	*	100.0	-0.317	0.015
37.5	*	105.0	-0.243	0.015
35.0	*	110.0	0.069	0.017
32.5	*	115.0	0.421	0.016
30.0	*	120.0	0.679	0.013
27.5	*	125.0	0.656	0.013
25.0	*	130.0	0.570	0.006
22.5	*	135.0	0.476	0.009
20.0	*	140.0	0.374	0.008
15.0	*	150.0	0.225	0.006

* LAB ANGLE FOR RECOIL TRITON

Figure 18 compares the distributions at two energies to those obtained at other laboratories. The lines are phase shift fits to the present data. The agreement with the Los Alamos data (Detch et al., 1971) is excellent. The agreement with the Erlangen results (Kankowski et al., 1971) is satisfactory, but it appears as though their normalization is lower than that for the present data. In addition to the comparisons shown, the Erlangen group has measured distributions of accuracy similar to the one shown in Figure 18 at energies from 4.15 to 12.0 MeV. There is also a distribution of Rosen and Leland (1962) obtained by double scattering at 14.5 MeV, but the errors are on the order of ±0.07.

B. Theory of Spin 1/2 on Spin 1/2 Scattering

General-- The general formulas for scattering and reaction cross sections in terms of the scattering matrix are given in the literature (Blatt and Biedenharn, 1952; Lane and Thomas, 1958). The discussion below will only outline the general features of the theory in order to clarify the relation between the phase shifts and the scattering problem for T(p,p)T.

For the general reaction $a + X = Y + b$, the system before the collision is described by three numbers: the channel index α, the channel spin s, and the orbital angular momentum ℓ. The channel spin is formed by vector addition of the intrinsic spin of the incoming particle and the spin of the target nucleus. After the collision the system is described by α', s', and ℓ'. The most general wave function in channel α, s with total angular momentum quantum numbers J,M consists of a superposition of an ingoing and outgoing spherical wave.

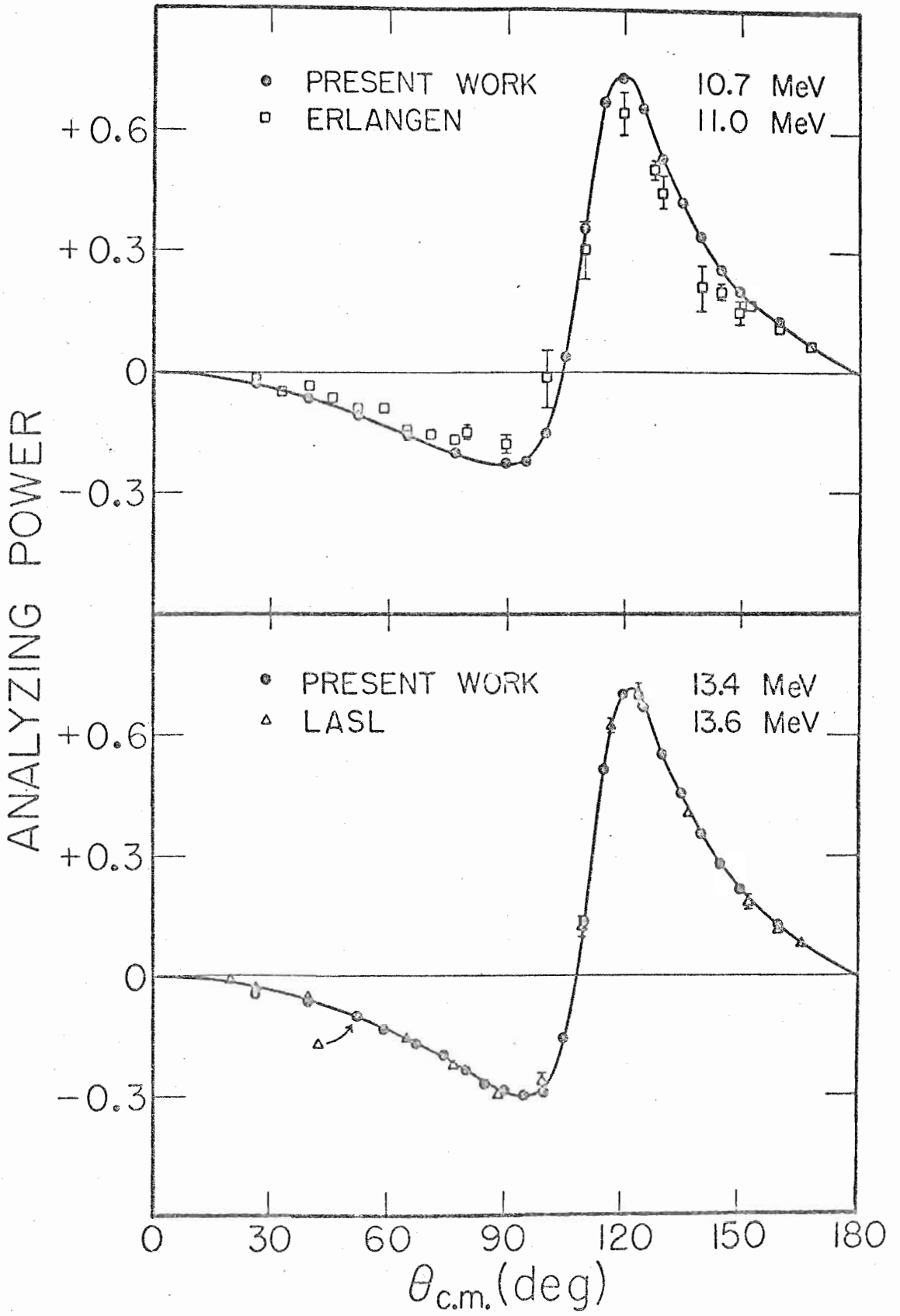

Figure 18. Comparisons with Other T(p,p)T Data Near 10.7 and 13.4 MeV

$$\Psi^{JM}_{\alpha ls} = A^{JM}_{\alpha ls} J^{JM}_{\alpha ls} - B^{JM}_{\alpha ls} O^{JM}_{\alpha ls} \tag{26}$$

Each of these waves $\Psi^{JM}_{\alpha ls}$ is an eigenfunction of the problem at sufficiently large distances, outside the region of nuclear interaction. The coefficients $A^{JM}_{\alpha ls}$ and $B^{JM}_{\alpha ls}$ are not independent of each other but are related by a scattering matrix which parameterizes the nuclear interaction.

$$B^{JM}_{\alpha' l' s'} = \sum_{\alpha ls} S^{J}_{\alpha' l' s'; \alpha ls} A^{JM}_{\alpha ls} \tag{27}$$

S is a unitary matrix (to conserve the normalization of the wave function in time) and is symmetric (due to time reversal invariance, or reciprocity). If we continue through the formalism, we find that the expression for the cross section for the process $\alpha s m_s \longrightarrow \alpha' s' m'_s$ contains this scattering matrix (Blatt and Biedenharn, 1952).

$$d\sigma_{\alpha' s' m'_s; \alpha s m_s} = \lambda^2 \left| \sum_{J=0}^{\infty} \sum_{l=|J-s|}^{J+s} \sum_{l'=|J-s'|}^{J+s'} i^{l-l'} \pi^{1/2} (2l+1)^{1/2} (ls0m_s | lsJM) \right.$$
$$\left. (l's'm_{s'} | l's'JM) (\delta_{\alpha\alpha'} \delta_{ss'} \delta_{ll'} - S^{J}_{\alpha' s' l'; \alpha s l}) Y_{l'm'}(\theta, \varphi) \right|^2 d\Omega \tag{28}$$

This cross section depends on the angle φ since the spin directions m_s and $m_{s'}$ are specified. From this basic formula, results for specific cases can be derived. For example, the cross section for the $\alpha s \longrightarrow \alpha' s'$ collision with an unpolarized beam is obtained by averaging over the incident spin directions m_s and summing over the final spin directions $m_{s'}$. Since the channel spins are not observed, we also average over the possible values of s and sum over the possible values of s'. Finally, if we restrict the reaction to elastic

scattering, $\alpha = \alpha'$. Resulting expressions can be simplified by using sum rules for the Clebsch-Gordan coefficients.

Spin zero on spin zero. --For a phase shift analysis of elastic scattering, we express the scattering matrix in terms of the eigen-phaseshifts of the problem. This is an exact quantum mechanical description in which, corresponding to each of the eigenfunctions Ψ^{JM}_{ls} there is a phase shift δ^{J}_{ls} to describe the nuclear contribution to the scattering. No assumption is made as to the nuclear interaction which gives rise to the phase shifts. For the simplest charged particle scattering problem, spinless particles on a spin zero target, the expression for the elastic cross section reduces to

$$\frac{d\sigma}{d\Omega} = \frac{1}{4k^2}\left| i\eta \csc^2\frac{\theta}{2}\, e^{i\eta \ln \csc^2\frac{\theta}{2}} + \sum_{l=0}^{\infty}(2l+1)\, e^{2i\alpha_l}\left(1 - S^{l}_{l0;l0}\right) \times P_l(\cos\theta)\right|^2 \qquad (29)$$

Here, the known Coulomb effects have been separated from the nuclear interaction and appear in the first term and in the Coulomb phase shifts α_l. The scattering matrix S has only one term of magnitude unity for each value of l. This may be expressed as $e^{2i\delta_l}$ where the phase shift δ_l is a real number.

Spin 1/2 on spin zero. --For the elastic scattering of spin 1/2 particles by spin zero nuclei, a given J value can be reached from two consecutive l values adding vectorially with the channel spin of 1/2. Since two consecutive l values indicate opposite parities for the incident waves, there is no mixing, and the scattering matrix is diagonal. For this case, Equation (27) reduces to

$$\begin{pmatrix} B^J_{J-1/2,\,1/2} \\ B^J_{J+1/2,\,1/2} \end{pmatrix} = \begin{pmatrix} S^J_{J-1/2,\,1/2;\,J-1/2,\,1/2} & 0 \\ 0 & S^J_{J+1/2,\,1/2;\,J+1/2,\,1/2} \end{pmatrix} \begin{pmatrix} A^J_{J-1/2,\,1/2} \\ A^J_{J+1/2,\,1/2} \end{pmatrix} \tag{30}$$

Again, unitarity requires that the two non-zero elements of the scattering matrix have unit magnitude. They may be expressed as $e^{2i\delta^J_{J-1/2}}$ and $e^{2i\delta^J_{J+1/2}}$ where the δ's are real. The elastic scattering cross section for this case is usually written as an expansion in ℓ-values, which leads to the familiar expression for spin 1/2 on spin zero scattering:

$$\frac{d\sigma(\theta)}{d\Omega} = |A(\theta)|^2 + |B(\theta)|^2 \tag{31}$$

The non-spin-flip amplitude $A(\theta)$ and the spin-flip amplitude $B(\theta)$ are given by

$$A(\theta) = -\frac{\eta}{2k}\csc^2\frac{\theta}{2}\, e^{i\eta\ln\csc^2\frac{\theta}{2}} + \frac{1}{k}\sum_{\ell=0}^{\infty}\Big\{e^{2i\sigma_\ell}\Big[(\ell+1)e^{i\delta_\ell^{\ell+1/2}}\sin\delta_\ell^{\ell+1/2} + \ell\, e^{i\delta_\ell^{\ell-1/2}}\sin\delta_\ell^{\ell-1/2}\Big]P_\ell(\cos\theta)\Big\} \tag{32}$$

$$B(\theta) = \frac{1}{k}\sum_{\ell=0}^{\infty}\Big\{e^{2i\sigma_\ell}\Big[e^{i\delta_\ell^{\ell-1/2}}\sin\delta_\ell^{\ell-1/2} - e^{i\delta_\ell^{\ell+1/2}}\sin\delta_\ell^{\ell+1/2}\Big]P_\ell'(\cos\theta)\Big\}$$

Spin 1/2 on spin 1/2. -- We now turn to the case which must be considered for the T(p,p)T analysis, the scattering of spin 1/2 particles from spin 1/2 nuclei. The channel spin can be either zero (singlet scattering) or one (triplet scattering). The elements of the scattering matrix can be expressed in terms of the following real phase shifts $\delta^J_{\ell s}$:

	Singlet	Triplet		
	$J = \ell$	$J = \ell+1$	$J = \ell$	$J = \ell - 1$
$\ell = 0$	δ_{00}^{0}	δ_{01}^{1}		
$\ell = 1$	δ_{10}^{1}	δ_{11}^{2}	δ_{11}^{1}	δ_{11}^{0}
$\ell = 2$	δ_{20}^{2}	δ_{21}^{3}	δ_{21}^{2}	δ_{21}^{1}
$\ell = 3$	δ_{30}^{3}	δ_{31}^{4}	δ_{31}^{3}	δ_{31}^{2}

If we neglect tensor forces which can cause transitions between states of the same J^{π} but different ℓ and s, we can write the scattering matrix equation (Equation 27) as follows:

$$\begin{pmatrix} B_{J0}^{J} \\ B_{J1}^{J} \\ B_{J-1,1}^{J} \\ B_{J+1,1}^{J} \end{pmatrix} = \begin{pmatrix} e^{2i\delta_{J0}^{J}} & & & \\ & e^{2i\delta_{J1}^{J}} & & \\ & & e^{2i\delta_{J-1,1}^{J}} & \\ & & & e^{2i\delta_{J+1,1}^{J}} \end{pmatrix} \begin{pmatrix} A_{J0}^{J} \\ A_{J1}^{J} \\ A_{J-1,1}^{J} \\ A_{J+1,1}^{J} \end{pmatrix} \tag{33}$$

The tensor interactions, however, will cause non-diagonal terms in the scattering matrix to be non-zero. These forces can mix states corresponding to ℓ-values differing by two (to conserve parity), e.g., δ_{01}^{1} and δ_{21}^{1}. Also, we have the possibility of spin-flip or transitions from the singlet to the triplet state with the same ℓ-value, e.g., δ_{10}^{1} and δ_{11}^{1}. Due to these spin dependent interactions there will now be some off-diagonal terms in the scattering matrix to account for the fact that part of an incident partial wave may emerge in a different channel. These mixing terms may be represented as 2 x 2 sub-matrices within the S matrix. Unitarity and reciprocity require these submatrices to be unitary and symmetric, as is the entire S matrix. This implies that each submatrix can be

characterized by three real parameters. A discussion of alternative methods of expressing these parameters is given by Stapp (1957) and by Detch (1970). In the Blatt-Biedenharn representation used in the present analysis, a unitary transformation is found which diagonalizes the upper 2 x 2 submatrix:

$$\begin{pmatrix} S_{11} & S_{12} \\ S_{21} & S_{22} \end{pmatrix} = \begin{pmatrix} \cos\epsilon & -\sin\epsilon \\ \sin\epsilon & \cos\epsilon \end{pmatrix} \begin{pmatrix} e^{2i\delta^J_{J0}} & \\ & e^{2i\delta^J_{J1}} \end{pmatrix} \begin{pmatrix} \cos\epsilon & \sin\epsilon \\ -\sin\epsilon & \cos\epsilon \end{pmatrix} \quad (34)$$

The resulting three parameters are called eigen-phaseshifts $\delta^J_{\ell s}$ and a mixing parameter ϵ. A similar transformation can be used for the lower 2 x 2 submatrix. It is expected from physical considerations that mixing between terms having ℓ-values differing by 2 should be small. Most phase shift analyses in the mass 4 system (see the following section) have neglected the corresponding mixing parameter. Only the channel spin mixing parameter was included in the present analysis. It is denoted by ϵ^{ℓ}.

The expression for the cross section for the spin 1/2 on spin 1/2 elastic scattering can be derived in terms of the scattering matrix from the general expression given earlier (Equation 28). It is a lengthy expression and will therefore not be reproduced here. It is given by Tombrello et al. (1962) in a form convenient for calculation (e.g., all of the Clebsch-Gordan algebra has been done). A subsequent paper by Tombrello (1965) gives the expression for the polarization.

Inelastic channels. -- Another complication in the present analysis is the presence of open reaction channels in addition to the elastic scattering. Although these channels can be accounted for explicitly in the general formalism (Equation 28), the resulting S matrix (now more properly called the collision matrix) is quite large and has many non-zero

terms. Dodder (1971) at Los Alamos has written a code to do simultaneous two and three channel analyses. Detch et al. (1971) have used this code in attempts to find solutions for the T + p problem. The two channel analysis has 43 parameters for ℓ-values only up to 2, and the three channel analysis has 87 parameters. With the data so far available, their results were inconclusive.

An alternative method to account for the open reaction channels is to allow the phase shifts to be complex.

$$e^{2i\delta_{\ell s}^{J}} \longrightarrow e^{2i(\delta_{\ell s}^{J} + i\nu_{\ell s}^{J})} = e^{-2\nu_{\ell s}^{J}} e^{2i\delta_{\ell s}^{J}} = \eta_{\ell s}^{J} e^{2i\delta_{\ell s}^{J}} \qquad (35)$$

The absorption parameter $\eta_{\ell s}^{J}$ defined above represents a flux loss from the entrance channel ℓsJ and can therefore account for inelastic processes in that channel. The parameter η can range from 1.0, corresponding to no absorption, to 0.0, corresponding to complete absorption of the partial wave. The S matrix is no longer unitary, the departure from unitarity being a measure of the total inelastic cross section. Accounting for the inelastic processes in this manner doubles the number of parameters in the analysis. It is clearly necessary, however, in the T + p problem where reaction cross sections are large.

C. Phase Shift Analysis

There are several analyses reported in the literature for elastic scattering of spin 1/2 on spin 1/2 in the mass 4 system. The $^{3}He(p,p)^{3}He$ reaction has been most thoroughly studied because of the large amount of data available and because inelastic channels may generally be neglected. (See, for examples, Tombrello et al., 1962; Tombrello, 1965;

Morrow and Haeberli, 1969; McSherry et al., 1969; Baker et al., 1971.) Phase shift analyses of T(n,n)T (Tombrello, 1966; R. K. Walter, 1970) and ^{3}He(n,n)^{3}He (Büsser and Niebergall, 1967) have also been reported at a few energies. No extensive phase shift analyses have been done on the T(p,p)T reaction until recently (Detch et al., 1971; Kankowski et al., 1971) because of the scarcity of data and the complications presented by the inelastic processes. The reaction channel T(p,n)^{3}He opens at a proton bombarding energy of 1.0 MeV and T(p,d)D at 5.4 MeV. In addition, the three and four nucleon final state reactions T(p,np)D and $T + p \longrightarrow 2n + 2p$ are open above 8.4 MeV and 11.3 MeV respectively, although their cross sections are expected to be small (Wilson et al., 1961).

A single energy phase shift analysis of T(p,p)T neglecting the inelastic channels was made at 13.6 MeV by Detch et al. (1971) using their accurate cross section and polarization values at this energy. Their purpose was to find starting phase shift sets for a multichannel analysis using the code of Dodder (1971). The most comprehensive analysis has been undertaken by Kankowski et al. (1971) at Erlangen. Their cross section and polarization data extend from 4.2 to 12.0 MeV, although their quoted errors are larger than those of Detch et al. or the present results. The Erlangen group have derived both real phase shifts and inelastic parameters from fitting their data.

For the present analysis, differential cross sections were obtained at the same energy and angles as the polarization data by interpolation of the Erlangen $\sigma(\theta)$ data at 9.0, 9.9, 11.0, and 12.0 MeV and the Los Alamos $\sigma(\theta)$ data at 13.6 and 16.2 MeV. The angular distributions were first quadratically interpolated to the polarization angles, then linearly interpolated in energy. For one case, the 13.6 MeV distribution of the Los

Alamos group, the energy was close enough to the present polarization energy that a first order correction in energy (13.6/13.4) was used instead of interpolation. (This correction comes from the fact that differential cross sections are inversely proportional to the square of the wave number.)

The reaction cross section for $T(p,n)^3He$ was obtained from Figure 7 in Wilson et al. (1961) and for T(p,d)D from the a_o Legendre coefficient for the D(d,p)T differential cross section. These coefficients were calculated from the energy dependent coefficients of Porter and Haeberli (1967) at the appropriate c.m. energies. The total reaction cross sections obtained in this fashion for D(d,p)T agreed with the earlier values found by Brolley et al. (1958). The D(d,p)T cross sections were then converted to T(p,d)D cross sections via detailed balance. The total inelastic cross section for T + p was taken as the sum of these two open channels, and a five per cent error was assigned. These values are lower limits due to the neglect of the three and four particle final state reactions. During the search, the inelastic cross section was given one-half the weight of a $\sigma(\theta)$ or $P(\theta)$ distribution.

The program CPHASE was written to do a phase shift analysis of the T(p,p)T elastic scattering. It uses a gradient search, calculating ditterential cross sections and polarizations for up to 30 experimental angles as well as the total inelastic cross section. It will handle complex phase shifts (δ and η) for s, p, d, and f waves, and the p and d wave channel-spin mixing parameters. In addition, there is an on-line oscilloscope display of all experimental and calculated distributions. The program and search procedure are described in Appendix B.

Although the program CPHASE will handle up through $\ell = 3$ (f waves), only s, p, and d waves were used for the present analysis. For the maximum proton bombarding energy of 14.7 MeV, the wave number k is 0.63 fm^{-1}. The proton radius is about 0.8 fm, and the triton radius is about 1.6 fm (Hofstadter, 1956). If it is assumed that the maximum distance of interaction may be approximated by the sum of the proton and triton radii, the maximum angular momentum contributing to the scattering at 14.7 MeV is 1.5$\hbar$. In this semi-classical approximation, a maximum ℓ-value of 2 seems reasonable for the analysis.

Table 5 lists phase shift sets used as starting values for preliminary calculations at 13.4 MeV. For all the starting sets except set 1, the phase shifts were real and thus predicted no absorption. Sets 1 and 4 included through d waves, but the triplet d wave

Table 5

Starting Phase Shift Sets for T(p,p)T Analysis

Set	Reaction	Energy (MeV)	Reference
1	T(p,p)T	12.0	Kankowski et al. (1971)
2	T(p,p)T	13.4	Detch et al. (1971, set T)
3	T(p,p)T	13.4	Detch et al. (1971, set α)
4	^{3}He(p,p)^{3}He	11.5	Tombrello (1965)
5	^{3}He(p,p)^{3}He	14.0	Reichstein et al. (1971)

phase was not split. Sets 2 and 3 included through f waves and had both channel-spin mixing and ℓ-value mixing terms. Set 5 was calculated from resonating group theory and had no triplet splitting, thus leading to zero polarization. In spite of these wide differences, the program converged for all starting sets in a reasonable period of time to an acceptable fit to the T(p,p)T data. (In fact, convergence to a good fit was also obtained starting with all phase shifts set equal to zero.) In most cases, however, few of the parameters varied far from the starting values. Chi-square values of 1.0 to 3.0 per point could be obtained if the search were allowed to continue long enough. The phase shifts and distributions obtained after about 15 minutes of searching (about 30 iterations) were very close to the final values. Chi-square could still be reduced by further iterations if desired, but convergence was slow, and changes to the phase shifts and calculated values were minimal.

From the results of these preliminary searches at 13.4 MeV, it was evident that the large number of parameters (a total of 22) allowed good fits to the data over a large volume of parameter space. In order to limit the analysis time, only two starting phase shift sets were chosen for the remaining energies. Set 1, from the complex phase shift analysis of the Erlangen T(p,p)T data, predicted starting distributions closest to the experimental values reported here. It was hoped that the more accurate polarization data obtained would help reduce the fluctuations of the Erlangen phases in this energy range. Set 4, obtained for the ^{3}He(p,p)^{3}He reaction, seemed an appropriate choice due to the extensive analysis of this reaction and its similarity to T(p,p)T. The searches at the other energies were therefore made for only starting sets 1 and 4. The results of the searches are listed in Table 6 and shown in Figures 19 and 20.

Table 6

Phase Shifts for T(p,p)T

	Starting phases (Set 1)	Energy (MeV)				
		9.4	10.7	12.0	13.4	14.7
Real phase shift (deg)						
singlet s	-54.0	-53.8	-53.7	-53.6	-52.8	-52.7
triplet s	-97.0	-92.1	-94.0	-95.6	-95.7	-95.8
singlet p	-25.0	-23.4	-24.1	-24.6	-26.4	-27.5
trip p (J=ℓ+1)	72.0	71.4	71.1	72.6	73.4	73.9
trip p (J=ℓ)	53.0	50.4	51.5	52.5	52.4	52.0
trip p (J=ℓ-1)	29.0	26.9	28.6	28.6	29.3	29.4
singlet d	10.0	11.5	11.4	10.5	14.0	13.5
trip d (J=ℓ+1)	1.0	-1.5	-2.6	-0.2	-4.0	-4.5
trip d (J=ℓ)	1.0	-1.3	-3.1	-1.3	-6.3	-6.5
trip d (J=ℓ-1)	1.0	1.0	-0.1	0.3	-1.6	-3.1
Inelastic parameters						
singlet s	0.56	0.55	0.56	0.56	0.59	0.62
triplet s	0.97	0.86	0.96	1.00	1.00	1.00
singlet p	0.92	0.88	0.83	0.82	0.74	0.69
trip p (J=ℓ+1)	0.94	0.94	0.98	0.90	1.00	1.00
trip p (J=ℓ)	0.95	0.86	0.84	0.85	0.79	0.78
trip p (J=ℓ-1)	0.96	0.96	0.95	0.94	0.93	0.94
singlet d	0.32	0.31	0.31	0.32	0.26	0.27
trip d (J=ℓ+1)	0.91	1.00	0.97	0.93	0.93	0.90
trip d (J=ℓ)	0.91	0.92	0.88	0.92	0.87	0.88
trip d (J=ℓ-1)	0.91	0.92	0.90	0.98	0.92	0.91
Mixing parameters (deg)						
p wave	-2.0	-3.7	-2.8	-3.1	-3.1	-4.3
d wave	2.0	1.3	0.4	2.0	-0.7	-0.4
Inelastic cross section (mb)						
experimental		305.0	290.0	272.0	248.0	226.0
calculated		295.0	261.9	239.9	229.4	220.4
Number of data points						
diff. cross section		17	19	20	22	18
polarization		18	19	22	22	18
Chi-square values						
diff. cross section		28.7	74.5	146.9	94.4	67.4
polarization		23.1	43.3	16.3	45.1	33.2
inelastic cross section		0.4	3.8	5.6	2.2	0.3
total chi-square		52.2	121.5	168.8	141.8	100.8

Table 6--Continued

	Starting phases (Set 4)	Energy (MeV) 9.4	10.7	12.0	13.4	14.7
Real phase shift (deg)						
singlet s	-84.6	-85.9	-88.0	-89.5	-90.8	-92.4
triplet s	-88.8	-90.9	-91.7	-94.7	-96.4	-96.1
singlet p	21.4	20.8	20.5	22.2	21.8	21.3
trip p (J=ℓ+1)	66.7	67.3	69.2	71.3	73.0	73.6
trip p (J=ℓ)	49.4	48.4	50.1	50.9	52.9	53.7
trip p (J=ℓ-1)	44.3	43.0	43.6	44.0	44.6	44.8
singlet d	-18.6	-20.7	-22.0	-16.7	-25.0	-26.6
trip d (J=ℓ+1)	2.5	0.9	-1.3	-0.2	1.7	1.8
trip d (J=ℓ)	2.5	0.6	0.3	1.3	1.3	1.3
trip d (J=ℓ-1)	2.5	1.5	-0.3	-0.8	-0.2	-1.3
Inelastic parameters						
singlet s	1.0	0.91	0.96	0.95	0.95	0.98
triplet s	1.0	0.95	1.00	1.00	1.00	1.00
singlet p	1.0	0.80	0.73	0.66	0.66	0.63
triplet p (J=ℓ+1)	1.0	0.83	0.85	0.83	0.87	0.84
triplet p (J=ℓ)	1.0	0.82	0.80	0.79	0.82	0.80
triplet p (J=ℓ-1)	1.0	0.91	0.88	0.91	0.93	0.91
singlet d	1.0	0.84	0.86	0.87	0.92	0.92
trip d (J=ℓ+1)	1.0	0.88	0.86	0.81	0.84	0.82
trip d (J=ℓ)	1.0	0.86	0.82	0.88	0.82	0.77
trip d (J=ℓ-1)	1.0	0.88	0.85	0.89	0.90	0.90
Mixing parameters (deg)						
p wave	-11.2	-15.5	-16.0	-14.3	-14.7	-15.3
d wave	0.0	0.0	-0.3	-2.4	-0.9	-0.7
Inelastic cross section (mb)						
experimental		305.0	290.0	272.0	248.0	226.0
calculated		284.6	262.4	241.3	197.4	201.3
Number of data points						
diff. cross section		17	19	20	22	18
polarization		18	19	22	22	18
Chi-square values						
diff. cross section		32.3	84.4	96.2	83.8	40.6
polarization		25.6	50.5	17.8	113.6	71.2
inelastic cross section		1.8	3.6	5.1	16.7	4.8
total chi-square		59.7	138.5	119.1	214.1	116.6

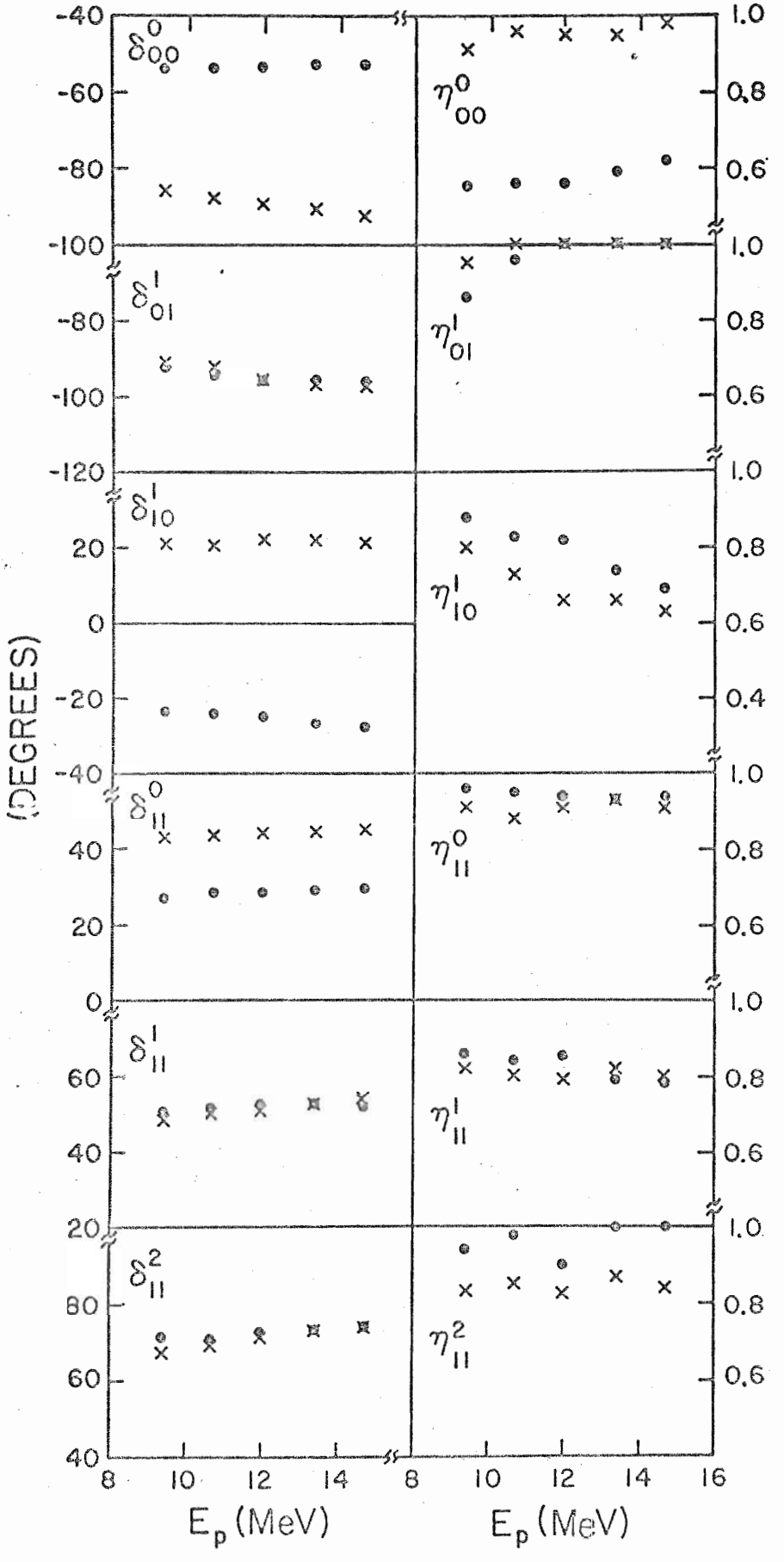

Figure 19. T(p,p)T Phase Shifts; S and P Waves

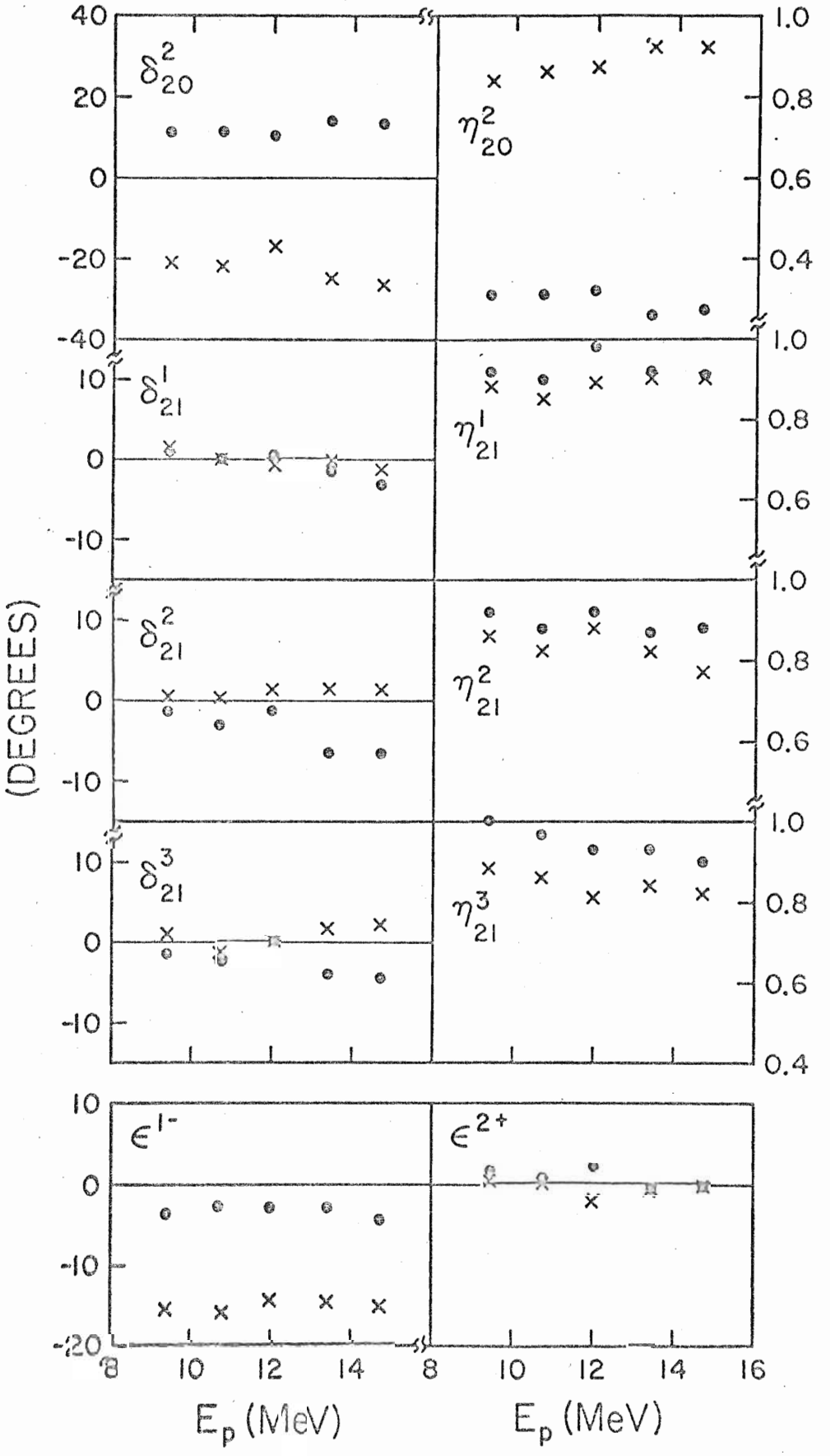

Figure 20. T(p,p)T Phase Shifts; D Waves and Mixing Parameters

The energy range investigated corresponds to excitation energies from 26.8 to 30.8 MeV in the compound nucleus ^{4}He. No resonant behavior is found for any of the phase shifts. All of the calculated fits gave total inelastic cross sections somewhat less than the experimental values input for the open two-body channels. This was probably caused by the low predictions of inelastic cross section using the starting phase shift sets. (The Erlangen phases predicted inelastic cross sections of about 70 per cent of the experimental values, while starting set 4 gave no absorption.) Increasing the weight given to the inelastic cross section during a search typically resulted in a poorer fit to the differential cross section.

Absorption in the triplet state to form the reaction products d-d or n-^{3}He can proceed only through a spin-flip of nuclei. Thus, one expects the absorption parameter to be near 1.0 for all triplet phase shifts. Also, the identical particles in the d-d reaction channel restrict the possible absorption parameters contributing to this channel. The large absorptions seen in the singlet phase shifts, particularly from starting set 1, are consistent with these expectations. This does not imply, however, that these solutions represent a unique set of phase shifts and absorption parameters. With proper constraints, other starting sets could also produce this result, and on the basis of quality of fit to the data, none of the phase shift sets could be eliminated.

Several conclusions may be reached from this analysis which may prove useful for future analyses of this type. First, allowing the phase shifts to be complex to account for inelastic processes greatly complicates the analysis by doubling the number of fitting parameters. The large number of parameters, even for only three partial waves, allows the program to converge to good fits from almost anywhere. Not all of the resulting phase

shifts and inelastic parameters are physically reasonable, however. If some of these parameters could be fixed from prior considerations, the search on the remaining phases would be more rapid, and perhaps the number of possible solutions would be reduced. Second, the gradient type search used in this analysis neglects correlations between phase shifts. A more sophisticated search would account for these correlations at least to first order, and convergence would be more rapid. It is unlikely, however, that this would reduce the large number of solutions obtained. This improvement could be added to the program CPHASE if more detailed analyses are attempted. Third, it is believed that different types of data (i.e., triple-scattering and spin-correlation parameters) are required to restrict the number of possible solutions. More accurate differential cross section and polarization data does not seem to be as useful in this respect as had been originally hoped. CPHASE could be easily modified to calculate other experimental observables as the data becomes available.

APPENDIXES

Appendix A

PROGRAMS FOR DATA ACQUISITION AND ANALYSIS IN POLARIZATION EXPERIMENTS

A. General

During the last two years, a library of polarization programs was developed by the author for data acquisition and analysis using the two TUNL computers. The purpose of this appendix is not to document these programs fully but to indicate what is available and state general capabilities. Complete documentation can be found on the numerous comment cards in the listings of the programs.

All of the programs are written in Fortran IV, but they make use of numerous assembly language (DAP) subroutines available in the TUNL systems library. These subroutines, which do such tasks as enabling data input through interrupts, writing binary data on magnetic tape, displaying an array on the oscilloscope, enabling the light pen, etc. are explained in the systems library documentation. A detailed knowledge of the programs described below requires a basic knowledge of these subroutines and their use.

Many of the 7.2 K words available for an on-line data taking program are used for storage of the data arrays. The number and length of these arrays determines how much additional space remains for programming the calculations, line printer and typewriter outputs, plots, etc. For the two neutron data programs, where array lengths and number of

detectors are small, analysis block arrays of the same length as the data arrays are used to store a previous run for extensive analysis while new data is being accumulated. Neutron experiments often require subtraction of background runs, and the analysis block is also useful for this purpose.

A brief description of the programs is given below. PPOL is described in some detail since it is the simplest of the polarization programs and forms a basis with which the others may be compared. NPOL is also described in more detail because of its automatic control features.

B. PPOL

PPOL is designed for vector analyzing power measurements with the polarized ion source. Data acquisition is through the parallel input channels (PIC) with no mass identification. The program stores pulses from 4 detectors in a symmetrical setup, i.e., two angles with a RIGHT and LEFT detector at each angle. These spectra are stored in four 512 channel arrays for incident spin UP and four 512 channel arrays for spin DOWN. A router is used with the ADC to route incoming data into the proper array corresponding to detector and spin direction. Another ADC and router is used for the two polarization monitor detectors. These are stored in four 128 channel spectra. The computer core used for data storage thus totals 4608 words. The automatic storage of spin UP and spin DOWN spectra in different arrays allows the experimenter to change the beam polarity frequently during a run if desired.

All of the spectra are displayed on the oscilloscope, and channels may be light-penned for summing the desired peaks. Sense switches are provided for transferring light-

penned channels from the UP spectra to the DOWN spectra or vice versa. Light penned channels are retained when data is cleared after a run. This is particularly useful for the monitor spectra where the peak positions may not change from run to run. The data dumped on magnetic tape also retains the light-penned (negative) channels so that off-line analysis can be done more rapidly.

The asymmetry calculations use the RIGHT and LEFT detectors at the same angles and the spin UP and spin DOWN sums to cancel instrumental asymmetries. The derivation of the equations used for the asymmetry and error calculation can be found in Chapter V along with a discussion of the errors involved. If the spin DOWN (UP) sums are zero, the program automatically calculates a simple L-R/L+R (or R-L/R+L) ratio to obtain the asymmetry. This result, of course, contains the instrumental asymmetry.

The typewriter is used for input of run number, magnetic tape file counter, tape label, number of detector pairs used, etc. Interrupt sense switches provide for starting and stopping a run, writing and reading runs on magnetic tape, calculating and typing the sums and asymmetries, incrementing run number, etc. A MASTER routine is included for sequencing sense switch operations at the end of a run. The following calculated quantities are output on the typewriter for each detector pair and for the monitor:

Asymmetry
Asymmetry error
Left/Right detector ratio
Counts in UP RIGHT peak
Counts in UP LEFT peak
Counts in DOWN RIGHT peak
Counts in DOWN LEFT peak
Sum of the above counts

The asymmetries calculated for the two detector pairs and the monitor may be displayed on the oscilloscope for continuous monitoring of beam polarization and experimental values.

The calculations are automatically updated about every 5 seconds.

C. POL8

POL8 stores three charged particle detector pairs (symmetrical setup) in 256 channel spectra. Because the third detector pair use the same ADC and router as the monitor, the monitor pair are also stored in 256 channels. As in PPOL, the routers are used to route the data into different spectra for incident spin UP and spin DOWN. This gives a total data storage of 4096 words (8 detectors, 256 channels each, spin UP and spin DOWN). All other features are similar to PPOL except that a background subtraction option is provided for the summed peaks. The background options are identical to those in program VPOL which is used for off-line analysis. They are described in detail in the listing for POL8.

D. APOL

APOL is used for vector analyzing power measurements with a polarized beam whenever mass identification is required. It will store four 512 channel particle spectra via the full buffered channel (FBC) using the DAP subroutine MFBC. The asymmetry calculations are set up for a symmetrical detector arrangement, i.e., two detector telescopes at equal RIGHT and LEFT angles, with two particles identified. Four telescopes may also be used if only one particle is identified. The mass identification electronics is shown in Figure (9) and a partial mass spectrum in Figure (10). Subroutine MFBC is described by

Nelson (1971) and on the comment cards in MFBC and APOL. In addition to the particle spectra, two 128 channel monitor spectra are stored via the parallel input channel as in PPOL. Only spin UP or spin DOWN runs are stored at one time, but the sums from the peaks of interest are saved between UP and DOWN runs so that the full asymmetry calculation may be done. The spin direction is automatically stored via an external sense line from the polarized ion source spin precession solenoid. Light-penned channels are saved between runs to facilitate the summing of peaks.

Calculations, asymmetry displays on the oscilloscope, and typewriter input and output are similar to PPOL. In addition, there are many input and display options provided for control of the mass identification. These are described in detail in the program listing. A particularly useful option during the setup of the electronics is the number display of the FBC buffer. The channel numbers of the first 20 data points in the buffer are averaged and displayed on the oscilloscope. When used in the ADC singles mode with a pulser, this allows amplifier gains to be matched precisely and quickly.

A subroutine is included in APOL to automatically quench the polarized beam, measure the quench ratio, and type out the calculated beam polarization. This subroutine uses the utility interrupt (L7) to count beam current integrator (BCI) pulses for a preset time, and it uses the external control line to provide a quenching signal to the polarized ion source. The length of the preset time in seconds, the delay time after changing quench modes, and the percent agreement required between first and last unquenched readings are typewriter inputs.

E. VPOL

VPOL is the off-line (alpha computer) analysis program used with data taken with either PPOL or APOL. Options are provided to read the magnetic tapes written by either of these programs, sum peaks with a linear background subtraction, output the sums and asymmetries, calculate beam polarization and analyzing powers, etc. Inputs include the analyzing power of the polarization monitor, background options desired, and tape handling commands.

In addition to display of all the data for a run (spin UP and spin DOWN runs are stored simultaneously), the calculated linear background may be superimposed under the peaks. This background is calculated by averaging an optional number of points on either side of the peak and drawing a line between the midpoints of the averaged channels. If four channels are light-penned in a spectrum, the averaging begins at the outer two points instead of the peak summing points. A more detailed discussion of the options available is given in the listing for VPOL. The asymmetry and error calculations are described in Chapter V. A sample output from VPOL appears below.

		ASYM	ERROR	L/R	SUM
DEUT		.2039	.0084	1.0576	13484
TRIT	-	.4177	.0062	1.0543	21373
MON		.5661	.0019	.8807	218742
BEAM		.5958	.0020		
DEUT		.3421	.0141		
TRIT	-	.7009	.0106		

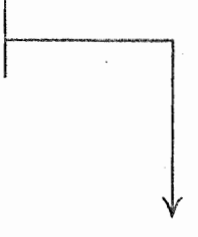

UR	UL	DR	DL	URB	ULB	DRB	DLB
2603	4164	3953	2764	11	12	14	14
7446	3224	3000	7703	18	18	12	13
24740	78649	92727	22626	3628	3951	3611	4088

F. NPOL

NPOL is the neutron polarization group data acquisition and control program for use with an unpolarized incident beam. The general method of data acquisition and a block diagram of the electronics showing the interaction with the computer is given in Chapter II and Figure 2. The coincidence spectra described there are stored in eight 128 channel arrays. The ungated recoil spectrum and the SUM spectrum (calculated from the 8 coincidence spectra) are also stored in 128 channel arrays. In addition, an ANALYSIS block stores these same 10 spectra from a previous run for detailed analysis during data acquisition. Thus a total of 2560 words are used for data storage in NPOL. This leaves a large amount of computer core available for analysis and control of experimental quantities. The automatic control of data acquisition provided in NPOL frees the experimenter from routine chores and allows him to concentrate on the experiment.

The oscilloscope display may be switched to any of the 20 arrays by combinations of the GROUP switch, BLOCK switch, and 1D-2D switch. When displaying the SUM spectrum in the DATA block, the program recalculates this spectrum about every 5 seconds. This is done by summing the 4 true coincidence spectra and subtracting the 4 accidental coincidence spectra channel by channel. A pair of points in the SUM spectrum may be light-penned and the corresponding channel numbers stored by a sense switch command. The two channel numbers, the net number of counts, and the asymmetry calculated between these channels can then be displayed on the oscilloscope. The sum and asymmetry value are updated about every 5 seconds. This provides a continuous monitor on the coincidence peak of interest. In addition, any number of pairs of channels may be light-penned in the SUM spectrum for typewriter output of the channel numbers, sums, asymmetries, and UP

detector to DOWN detector counting ratio for each window. The light penned channels are saved when the SUM spectrum is updated and also when the data is cleared. The control subroutine automatically types out these windows and their sums and asymmetries after each forward-reverse sequence in a sequential run. Windows may be set by typewriter input as well as by the light pen.

Figure 21 shows a flow diagram of the CONTRL subroutine. The subroutine is called on each pass through the display loop and frequently during any lengthy analysis routine. If a SEQUENTIAL RUN is not in progress, immediate return from the subroutine is provided. Automatic control of the solenoid and data acquisition is obtained by starting a SEQ. RUN, which sets the sequential run flag. The END OF SEQUENCE flag is set by the scaler read-in subroutine (DSCALE) when the master scaler has reached the preset number of BCI counts. The SOLENOID READY and POLARITY are checked via external sense lines from the solenoid control unit. A sense line from a beam current meter is also checked to see if the beam is within the variable high and low set points on this meter. Any fault condition during a SEQUENTIAL RUN will stop the data taking until the fault is corrected. When one of the FORWARD-REVERSE-REVERSE-FORWARD sequences is over, the data accumulation is stopped, the sequence number is incremented, and the scalers are typed out along with a notation of the sequence polarity. Depending on the sequence number, the polarity of the solenoid is reversed via an output control pulse (OCP) to the control unit, or the asymmetries are typed out. The scalers are reset automatically, and the next sequence begins.

At the end of the fourth sequence, the data is dumped on magnetic tape and the group number is incremented. The number of FRRF groups to be obtained in the sequential

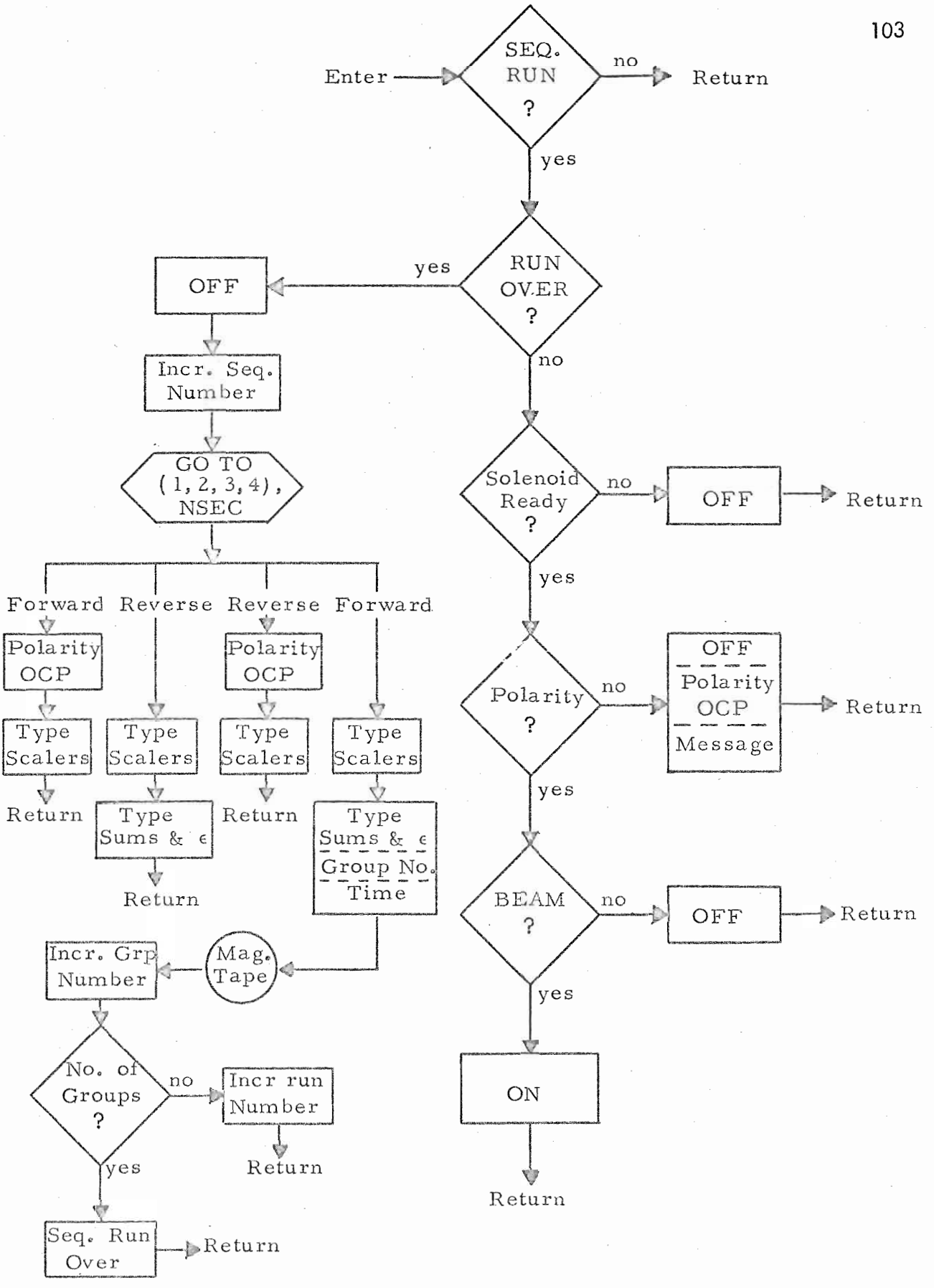

Figure 21. Flow Diagram of Control Subroutine for Neutron Polarization Data Acquisition

run has been previously set via a typewriter input. Note that the tape run number is not incremented after the final group in a sequential run. This is so that the correct run number will be transferred to the ANALYSIS BLOCK along with the data. The run number should be incremented after this transfer, e.g., as part of the MASTER sequence. The intermediate tape dumps after each FRRF group provide a fixed record of the progress of the run. They may be useful for recovering good data if a problem develops near the end of a long sequential run. Note that the tape dumps are from the DATA BLOCK.

The ANALYSIS BLOCK allows the operator to read previous runs from magnetic tape while taking data. Since the control subroutine may dump on tape while the tape is backspaced, the program automatically spaces out to the end of the last run dumped before writing on the tape. This is done by checking for a double file mark. A new tape must therefore have two file marks written at the beginning. Two file marks are written automatically after each dump, and one is backspaced over before the next dump.

All of the ANALYSIS BLOCK output is on the line printer. Light-penned (or typewriter input) windows in the analysis block SUM spectrum are cleared after each operation in contrast to the DATA BLOCK. ANALYSIS BLOCK operations include the following:

a) Print data

b) Plot any or all of the spectra. A scale factor may be entered via the typewriter, or the plots will be scaled automatically if no scale factor is input or if the command is from a sense switch. If PLOT ALL is selected, the individual coincidence spectra will be plotted to the same scale and the SUM and RECOIL spectra will be scaled individually. All automatic scaling ignores channels less than channel 30.

c) Calculated sums and asymmetries between pairs of light-penned points (or channels input on the typewriter).

d) Block asymmetry in increments (IBLOC) between a pair of light-penned channels. The increment size, e.g., 1 or 2 channels is a typewriter input.

e) HIGH END or LOW END FIXED asymmetries between light-penned channels. The low or high channel is incremented toward the fixed channel one channel at a time, and asymmetries are output at each step.

In addition, there are sense switches for clearing, adding, subtracting, transferring and exchanging the DATA and ANALYSIS blocks. At the beginning of a SEQUENTIAL RUN the oscilloscope display will be blanked out as a reminder to enter the new energy and/or angle into the computer via the typewriter. A sense switch will remove this blanking if these values have not changed. The energy and angle are output on printouts, plots, etc. to aid in identifying a run. They are also written on magnetic tape with the run for automatic input to the analysis programs (NPOL-α and ASP).

G. NPOL - α

This program is nearly identical to NPOL but runs on the alpha computer without the data acquisition. In addition to the previously described operations, there are provisions for a channel-by-channel asymmetry plot, correcting the backgrounds as discussed in Chapter III, reversing UP and DOWN spectra to allow addition of runs taken on opposite sides of the beam axis, smoothing the data, multiplying data for subtraction of partial runs,

etc. The data may also be dumped on paper tape in a format for (a) punching cards for input to PROMETHEUS or (b) direct input to ASP. The spectra formed in NPOL - α for input to ASP are discussed in Chapter III. To retain the information on data that was subtracted to form these final spectra, the array IACC must be formed in the proper way. This is discussed by Taylor (1971) and in the comment cards for NPOL - α.

H. NASM

NASM is designed for neutron asymmetry measurements with a polarized beam. It is similar to NPOL in that it has an ANALYSIS BLOCK with print and plot routines. The data input and calculations, however, are similar to PPOL or APOL (i.e., no backgrounds). At present, NASM will store two detectors (symmetric setup) in 256 channel spectra. It will store both incident spin UP and spin DOWN, providing four 256 channel arrays for the DATA BLOCK and the same for the ANALYSIS BLOCK. The total data storage is thus 2048 words. More data storage space is available for future expansion of this program.

The plot subroutine is similar to NPOL except that it averages adjacent channels to compress the spectrum to 128 channels in order to fit on one page of output. At present, no monitor detectors are provided for. The quench subroutine, as described under APOL, is included to determine beam polarization.

Appendix B

THE COMPUTER CODE CPHASE

The program CPHASE was written for the analysis of spin 1/2 on spin 1/2 elastic scattering data. The program, which runs on the TUNL 8K word computer, will minimize chi-square for differential cross sections and polarizations for up to 30 experimental angles, as well as the total inelastic cross section. It uses a simultaneous gradient search on complex phase shifts for s, p, d, and f waves (singlet and 3 triplet phases) and the p and d wave mixing parameters. In addition to the line printer output of search parameters and results, there is an oscilloscope display of all experimental and calculated distributions.

The formalism for spin 1/2 on spin 1/2 elastic scattering is discussed in Chapter VII. The formulae used for the differential cross sections and polarizations in CPHASE are from Tombrello et al. (1962) and Tombrello (1965). The mixing calculation and the total inelastic cross section formulae were derived from the equations of Blatt and Biedenharn (1952). Comparisons of the calculated results were made with published curves (see Chapter VII, section C for references to other analyses) and with tabulated results from codes at the University of Wisconsin and at Erlangen. Satisfactory agreement was found in all cases. In addition, many internal consistency checks were made (e.g.,

zero phase shifts give Rutherford cross section; real phase shifts give no absorption; no triplet splitting gives zero polarization, etc.). Unitarity checks are made during the search to prevent any inelastic parameter from becoming greater than 1.0.

The procedure followed in a typical search is briefly as follows: The kinematic information, experimental data, starting phase shifts, and search instructions are read into the computer on cards. After a single calculation with the starting phase shifts, the values are output on the line printer and the data and calculated distributions are displayed on the oscilloscope. These starting distributions can be saved in memory for visual comparison with later distributions calculated during the search. On starting the search, the program calculates a gradient by stepping each real and imaginary phase shift in turn by a small amount (typically one degree) and determining the change in chi-square. The gradient is calculated from these results, and all parameters are incremented simultaneously along this gradient until chi-square starts to increase. The minimum is then located by parabolic interpolation. The procedure is iterated by calculating a new gradient, etc. A single iteration takes about 30 seconds for 30 angles and 22 varied parameters. Convergence is rapid at first but slows as the minimum in chi-square is reached. After 15 to 20 iterations, chi-square is usually changing by less than one per cent.

Various sense switch options are provided for operating the program. The convergence of the search may be monitored, if desired, by having gradients, chi-square values, and phase shifts output on the line printer during the search. The search may be interrupted at any time to observe the oscilloscope display of the latest calculated distributions along with the experimental data and the saved distributions. As the minimum in chi-square is approached, the program will automatically decrease the step-size to permit a finer exam-

ination of the minimum. If desired, phase shifts for which the gradient becomes less than 0.05 degree will be automatically dropped from the search, thus speeding convergence of the remaining phase shifts. The search may be terminated at any time, and the program will output final values on the line printer and return to the display section. Termination will also occur if chi-square changes from one iteration to the next by less than one per cent (or whatever percentage is specified on input). A sense switch option provides for punching the phase shifts on cards. Other sense switches allow reading more data, changing search parameters, or continuing the search.

The program listing for CPHASE contains numerous comments which describe the options and card formats and outline the steps in the calculation. A description of the gradient search procedure is given by Bevington (1969).

LIST OF REFERENCES

LIST OF REFERENCES

N. V. Alekseev, U. R. Arifkhanov, N. A. Vlasov, V. V. Davydov, and L. N. Samoilov, Soviet Phys. JETP 18 (1964) 979

J. Arvieux, J. Goudergue, B. Mayer, and A Papineau, Phys. Lett. 22 (1966) 610

S. D. Baker, T. A. Cahill, P. Catillon, J. Durand, and D. Garreta, Nucl. Phys. A160 (1971) 428

H. H. Barschall, Proceedings of the 2nd International Symposium on Polarization Phenomena of Nucleons, Karlsruhe (1966) 393

Basel Convention, Proceedings of the International Symposium on Polarization Phenomena of Nucleons, Basel (1960)

A. F. Behof, J. M. Hevezi, and G. Spalek, Nucl. Phys. 84 (1966) 290

E. M. Bernstein, G. G. Ohlsen, V. S. Starkovich, and W. G. Simon, Nucl. Phys. A126 (1969) 641

P. R. Bevington, Data Reduction and Error Analysis for the Physical Sciences (McGraw-Hill, New York, N. Y., 1969)

L. C. Biedenharn, Nucl. Phys. 10 (1959) 620

J. M. Blatt and L. C. Biedenharn, Rev. Mod. Phys. 24 (1952) 258

C. O. Blyth, P. B. Dunscombe, J. S. C. McKee, and C. Pope, to be published (1971)

J. E. Brolley, Jr., T. M. Putnam, and Louis Rosen, Phys. Rev. 107 (1957) 820

W. B. Broste, G. S. Mutchler, J. E. Simmons, R. A. Arndt, and L. D. Roper, to be published (1971)

F. W. Büsser and F. Niebergall, Symposium on Few Body Problems, Light Nuclei, and Nuclear Interactions, Brela (1967) 469

F. W. Büsser, H. Dubenkropp, F. Niebergall, and K. Sinram, Nucl. Phys. A129 (1969) 666

A. Cesati, F. Cristofori, L. Milazzo Colli, and P. G. Sona, Prog. Nucl. Phys. 10 (1969) 119

J. L. Detch, Los Alamos Scientific Laboratory Report LA-4576 (1970)

J. L. Detch, R. L. Hutson, Nelson Jarmie, and J. H. Jett, Phys. Rev. C 4 (1971) 52

F. S. Dietrich, E. G. Adelberger, and W. E. Meyerhof, Bull. Am. Phys. Soc. 15 (1970) 495

G. Dietze and K. Lorenzen, Nucl. Phys. A158 (1970) 577

D. C. Dodder, private communication (1971)

B. L. Donnally, Proceedings of the Third International Symposium on Polarization Phenomena in Nuclear Reactions, Madison (1970) 295

P. S. Dubbledam and R. L. Walter, Nucl. Phys. 28 (1961) 414

J. C. Fritz, R. Kankowski, K. Kilian, A. W. Neufert, and D. Fick, Proceedings of the Third International Symposium on Polarization Phenomena in Nuclear Reactions, Madison (1970) 482

W. Grüebler, V. König, R. E. White, P. A. Schmelzbach, R. Risler, and P. Marmier, Phys. Lett. 36B (1971) 337

W. Haeberli, Fast Neutron Physics (Interscience Publishers, New York, 1963), Part II, p. 1379

W. Haeberli, Ann. Rev. Nucl. Sci. 17 (1967) 373

D. Hilscher and H. S. Liers, to be published (1971)

R. Hofstadter, Rev. Mod. Phys. 28 (1956) 214

B. Hoop and H. H. Barschall, Nucl. Phys. 83 (1966) 65

R. Kankowski, K. Kilian, and D. Fick, private communication (1971); see also Fritz et al. (1970)

W. E. Lamb and R. C. Retherford, Phys. Rev. 79 (1950) 549

W. E. Lamb and R. C. Retherford, Phys. Rev. 81 (1951) 222

A. M. Lane and R. G. Thomas, Rev. Mod. Phys. 30 (1958) 257

D. H. McSherry, S. D. Baker, G. R. Plattner, and T. B. Clegg, Nucl. Phys. A126 (1969) 233

M. M. Meier, (unpublished Ph.D. dissertation, Duke University, 1969)

G. L. Morgan and R. L. Walter, Nucl. Instr. Methods 58 (1968) 227

L. W. Morrow and W. Haeberli, Nucl. Phys. A126 (1969) 225

G. S. Mutchler, W. B. Broste, and J. E. Simmons, Phys. Rev. C 3 (1971) 1031

R. O. Nelson, (unpublished Ph.D. dissertation, Duke University, 1971)

G. G. Ohlsen and J. L. McKibben, Los Alamos Scientific Laboratory Report LA-3725 (1967)

G. G. Ohlsen, Los Alamos Scientific Laboratory Report LA-4451 (1970)

G. R. Plattner and A. D. Bacher, to be published (1971)

G. R. Plattner and L. G. Keller, Phys. Lett. 30B (1969) 327

L. E. Porter and W. Haeberli, Phys. Rev. 164 (1967) 1229

F. O. Purser, J. R. Sawers, and R. L. Walter, Phys. Rev. 140 (1965) B870

F. O. Purser, (unpublished Ph.D. dissertation, Duke University, 1966)

I. Reichstein, D. R. Thompson, and Y. C. Yang, Phys. Rev. C 3 (1971) 2139

T. C. Rhea, Th. Stammbach, and R. L. Walter, Proceedings of the Third International Symposium on Polarization Phenomena in Nuclear Reactions, Madison (1970) p. 556

L. Rosen and W. T. Leland, Phys. Rev. Lett. 8 (1962) 379

B. V. Rybakov, V. A. Sidorov, and N. A. Vlasov, Nucl. Phys. 23 (1961) 491

J. J. Sakurai, Advanced Quantum Mechanics (Addison-Wesley, 1967), p. 45

G. R. Satchler, Nucl. Phys. 8 (1958) 65

J. R. Sawers, (unpublished Ph. D. dissertation, Duke University, 1966)

D. G. Schuster and R. L. Hagengruber, Proceedings of the Third International Symposium on Polarization Phenomena in Nuclear Reactions, Madsion (1970) p. 865

P. Schwandt, T. B. Clegg, and W. Haeberli, Nucl. Phys. A163 (1971) 432

J. E. Simmons, W. B. Broste, G. P. Lawrence, J. L. McKibben, and G. G. Ohlsen, Phys. Rev. Lett. 27 (1971) 113

A. Simon and T. A. Welton, Phys. Rev. 90 (1953) 1036

G. Spalek, J. Taylor, R. A. Hardekopf, Th. Stammbach, and R. L. Walter, Proceedings of the Third International Symposium on Polarization Phenomena in Nuclear Reactions, Madison (1970) p. 462

G. Spalek, (unpublished Ph. D. dissertation, Duke University, 1971)

G. Spalek, J. Taylor, R. A. Hardekopf, Th. Stammbach, and R. L. Walter, to be published (1971)

Th. Stammbach, private communication (1970)

Th. Stammbach and R. L. Walter, to be published (1971)

H. P. Stapp, T. J. Ypsilantis, and N. Metropolis, Phys. Rev. 105 (1957) 302

J. Taylor, G. Spalek, Th. Stammbach, R. A. Hardekopf, and R. L. Walter, Phys. Rev. C 1 (1970) 803

J. Taylor, (unpublished Ph. D. dissertation, Duke University, 1971)

R. S. Thomason, (unpublished Ph. D. dissertation, Duke University, 1969)

T. A. Tombrello, C. Miller Jones, G. C. Phillips, and J. L. Weil, Nucl. Phys. 39 (1962) 541

T. A. Tombrello, Phys. Rev. 138 (1965) B40

T. A. Tombrello, Phys. Rev. 143 (1966) 772

R. K. Walter, Los Alamos Scientific Laboratory Report LA-4334 (1970)

R. L. Walter, Proceedings of the Third International Symposium on Polarization Phenomena in Nuclear Reactions, Madison (1970) p. 317

W. E. Wilson, R. L. Walter, and D. B. Fossan, Nucl. Phys. 27 (1961) 421

L. Wolfenstein, Ann. Rev. Nucl. Sci. 6 (1956) 43

BIOGRAPHY

Robert Allen Hardekopf

Born: October 14, 1940
St. Louis, Missouri

Education: B. S. Auburn University, 1962

Positions: Woodrow Wilson Fellow, Duke University, 1967 - 1969
Research Assistant, Duke University, 1969 - 1971

Publications:

Polarization in n-d Scattering at 7.8 MeV (with Taylor, Stammbach, Spalek, and Walter), Phys. Rev. C 1 (1970) 803

Polarization of Neutrons from the $D(d,n)^3He$ Reaction from 6 to 14 MeV (with Spalek, Taylor, Stammbach, and Walter), Proceedings of the Third International Symposium on Polarization Phenomena in Nuclear Reactions, Madison, 1970, p. 462

Remeasurement of the Neutron Polarization from the $^7Li(p,n)^7Be$ Reaction for 3 to 4 MeV Protons (with Joyce, Morgan, and Walter), ibid., p. 599

Polarization Produced in the $^9Be(d,n)$ Reactions at 3.0 and 3.5 MeV and a Comparison to DWBA Calculations (with Spalek, Taylor, Stammbach, and Walter), ibid., p. 749

Cross-Section and Polarization Measurements for the $^{11}B(d,n_0)$ and $^{11}B(d,n_1)$ Reactions from 7 to 12 MeV (with Taylor, Stammbach, Spalek, and Walter), ibid., p. 754

Remeasurement of the Neutron Polarization from the $^7Li(p,n)^7Be$ Reaction for 3 to 4 MeV Protons (with Hollandsworth, Walter, Joyce, and Morgan), Nuclear Physics A167 (1971) 49

Analyzing Power in the T(p,d)D Reaction (with Lisowski, Rhea, Walter, and Clegg), Symposium on the Nuclear Three Body Problem and Related Topics, Budapest, Hungary (1971) (to be published)

Abstracts:

Polarization of Neutrons from the $^{9}Be(d,n)^{10}B$ Reaction at 3.0 and 3.5 MeV (with Spalek, Taylor, Stammbach, and Walter), Bull. Am. Phys. Soc. 15 (1970) 482

Neutron Polarization Distributions from the $^{11}B(d,n_0)$ and $^{11}B(d,n_1)$ Reactions at 7.5 and 9.5 MeV (with Taylor, Stammbach, Spalek, and Walter), Bull. Am. Phys. Soc. 15 (1970) 483

Polarization of Neutrons from the $D(d,n)^{3}He$ Reaction from 12 to 22 MeV (with Rhea, Joyce, and Walter), Bull. Am. Phys. Soc. 16 (1971) 542

An Elastic Scattering Optical Model Code for Small Computers (with R. J. Eastgate), Bull. Am. Phys. Soc. 16 (1971) 646